UC Santa Cruz

UC Santa Cruz Electronic Theses and Dissertations

Title

Extremely Correlated Limit of the Hubbard Model

Permalink

https://escholarship.org/uc/item/9c53h0w6

Author

Perepelitsky, Edward

Publication Date

2014

Peer reviewed|Thesis/dissertation

eScholarship.org Powered by the California Digital Library
University of California

UNIVERSITY OF CALIFORNIA
UNIVERSITY OF CALIFORNIA SANTA CRUZ

EXTREMELY CORRELATED LIMIT OF THE HUBBARD MODEL

A dissertation submitted in partial satisfaction of the
requirements for the degree of

DOCTOR OF PHILOSOPHY

in

PHYSICS

by

Edward Perepelitsky

March 2014

The Dissertation of Edward Perepelitsky
is approved:

Professor Sriram Shastry, Chair

Professor Josh Deutsch

Professor Peter Young

Dean Tyrus Miller
Vice Provost and Dean of Graduate Studies

Copyright © by

Edward Perepelitsky

2014

Table of Contents

List of Figures

Abstract

Extremely Correlated Limit of the Hubbard Model

by

Edward Perepelitsky

In this work, we describe the simplifications to the Extremely Correlated Fermi Liquid Theory (ECFL) [3, 6] which occur in the limit of infinite spatial dimensions. In particular, we show that the single-particle electron Green's function $\mathcal{G}(k)$ ($k \equiv (\vec{k}, i\omega_k)$) can be written in terms of two momentum-independent self-energies $\Psi(i\omega_k)$ and $\chi(i\omega_k)$. Moreover, we elucidate the nature of the ECFL λ expansion in the limit of infinite dimensions and carry out this expansion explicitly to $O(\lambda^2)$. Additionally, we demonstrate the vanishing of vertex corrections to the optical conductivity in general and to each order in λ in the limit of infinite dimensions. We generalize the ECFL formalism to the infinite-U Anderson impurity model (AIM) , and demonstrate a Dynamical Mean-Field Theory (DMFT) like mapping between the ECFL objects of the infinite-dimensional t$-$J model and the infinite-U AIM, and show that this mapping holds to each order in λ. We compute the spectral function for the AIM to $O(\lambda^2)$ and make comparisons with results obtained through Numerical Renormalization Group (NRG) computations. Finally, we develop a novel formalism for the high-temperature expansion of dynamical correlation functions in the infinite-U Hubbard model which is more efficient than any used previously and gives results for an arbitrary number of spin species. We use it to calculate the single-particle Green's function $\mathcal{G}(k)$ to fourth order in (βt) for m spin-species on a d-dimensional hypercube.

I would like to thank my advisor, Sriram Shastry, for mentoring me, supporting me, and for his patience and kindness.

I would like to thank my family for their unconditional and never-ending love, caring, and support. Without them, nothing would be possible.

Part I

Introduction

The Hubbard model (HM) with the Hamiltonian:

$$H = -\sum_{ij\sigma} t_{ij} c^{\dagger}_{i\sigma} c_{j\sigma} + U \sum_{i} n_{i\uparrow} n_{i\downarrow} - \boldsymbol{\mu} \sum_{i} n_i, \tag{0.1}$$

has attracted great theoretical interest in condensed matter physics, and is also a fairly realistic model of strongly correlated materials such as the cuprates. While the small $\frac{U}{t}$ limit is well described by standard Fermi-Liquid theory[1, 2], the phase diagram of the Hubbard model for the large and intermediate $\frac{U}{t}$ (strongly correlated) cases, is much less well understood. This is due to the fact that there are very few exact results for this model. One of these is the classical result due to Nagaoka[27], that the ground of the infinite-U Hubbard model, doped with one hole away from half-filling, on the simple cubic or body-centered cubic lattice is a fully saturated ferromagnet, with all spins pointing in the same direction. He also shows that this is not the ground state for $U < WL$, where L is the number of sites on the lattice, and W is the bandwidth.

In [28], the authors consider the more realistic scenario of a thermodynamic concentration of holes δ. For the case of infinite-U, they construct a variational wave function whose energy is lower than that of the Nagaoka state in two and three dimensions for a large enough concentration of holes. However, their wave function has higher energy than the Nagaoka state in one dimension for all values of the doping. This is consistent with the exact result that the Nagaoka state must be the ground state in one dimensions for all values of the doping, due to the separation of spin and charge degrees of freedom. Finally, using their variational approach, they are able to determine the value of U below which the Nagaoka state becomes unstable for any value of the doping. Thus, in Fig.2 of [28], they

are able to map out the parameter-space in the $\delta - U$ plane in which the Nagaoka state becomes unstable, which generally happens for larger values of δ and smaller values of U.

For large but finite U, the low-energy physics of the Hubbard model is described by the t$-$J model [29, 30]. This model consists of taking the $U \to \infty$ limit of the Hubbard model (the t part of the model) and adding on a nearest neighbor anti-ferromagnetic coupling term (the J part of the model). It has been argued by Anderson[29] that the t-J model describes the physics of the cuprates. The $\delta - T$ phase diagram of the cuprates is well described in [31] (see Fig.1 of [31] or Fig.1 of [32]). For $\delta = 0$ (i.e. half-filling) and very small δ, up to very high temperatures, the cuprates are an anti-Ferromagnet. This anti-Ferromagnetism can be attributed to the J term in the Hamiltonian.

This anti-Ferromagnetism dies out very fast upon increasing δ, and for $\delta = .05$ at $T = 0$, the system enters into the superconducting phase. This phase exists within a superconducting dome, which extends between $\delta = .05$ and $\delta = .28$, and has doping-dependent transition temperature T_c. The highest point of the dome occurs for $\delta = .15$ and has $T_c \approx 90K$. Therefore, this is referred to as optimal doping. For $\delta < .15$, the under-doped regime, T_c increases with increasing doping, while for $\delta > .15$, the over-doped regime, T_c decreases with increasing doping. The superconducting phase can be understood through the standard BCS-theory for conventional superconductors, describing a condensate of Cooper-paired electrons with long-lived quasi-particles as excitations. The main difference is that while conventional superconductors have s-wave pairing between electrons, the cuprates have d-wave pairing.

In the over-doped regime, raising the temperature above T_c gives rise to the

strange-metal phase. This is the electron-liquid (normal) phase of the cuprates which contains no broken symmetries. However, it has many properties which distinguish it from the normal phase of ordinary metals (the Fermi-liquid phase). Amongst these are [30] the linear temperature dependence of the resistivity, the "Drude-like" tail of the mid-infrared conductivity, the T-dependent Hall effect, and the anomalous line-shapes of (ARPES) experiments (the line-shapes have been explained by the Extremely Correlated Fermi Liquid Theory [3, 6, 7, 13] described below). Upon increasing the doping, $\delta \to 1$, there is a crossover from strange-metal behavior to standard Fermi-liquid behavior. The fact that the Hubbard model is a Fermi-liquid for small densities even at large values of U is well known (see for example [34].)

In the under-doped regime, when the temperature is raised above T_c, the superconducting phase gives rise to the pseudogap phase. Upon further raising the temperature in the pseudogap phase to a temperature T^*, the system transitions from the pseudogap phase into the strange-metal phase. It has been a point of controversy whether this is a true phase transition or a crossover between different behaviors. However, there have been recent experimental studies [33] that give compelling thermodynamic evidence that it is indeed an actual phase transition. T^* decreases monotonically with increasing doping until it intersects $T = 0$ at a quantum critical point at around optimal doping.

The pseudogap phase is characterized by a reduction (from the normal phase) in the imaginary part of the low-frequency dynamic spin susceptibility [31]. This reduction is characteristic of gapped states such as the BCS superconducting state in which spin-singlet formation occurs. In the case of the cuprates, this reduction occurs only upon lowering

the temperature below T^* and there is no further reduction upon lowering the temperature below T_c. Therefore, one natural theory is that the Cooper pairs have already formed in the pseudogap state when $T_c < T < T^*$, but only condense in the superconducting state $T < T_c$ [31]. However, this is not the only possibility, as any symmetry-breaking phase would lead lead to an energy-gap and therefore a reduction in the density of states. Some other suggestions include anti-ferromagnetic order, charge-density waves, and loop-current electronic order [32].

It is our goal to understand the strange-metal phase of the cuprates, the philosophy being that a good understanding of the normal phase will lead to an understanding of the broken-symmetry phases. To do this, we study the liquid phase of the t−J model at all values of the doping, with the understanding that as $\delta \to 0$, it will be a meta-stable phase. In this model, the Hilbert space is Gutzwiller projected so that only single occupancy is allowed on each lattice site. The Hamiltonian for this model can be written in terms of the Hubbard X operators as[15]

$$\begin{aligned} H &= -\sum_{ij\sigma} t_{ij} X_i^{\sigma 0} X_j^{0\sigma} - \boldsymbol{\mu} \sum_{i\sigma} X_i^{\sigma\sigma} + \frac{1}{2} \sum_{ij\sigma} J_{ij} X_i^{\sigma\sigma} \\ &\quad + \frac{1}{4} \sum_{ij\sigma_1\sigma_2} J_{ij} \{ X_i^{\sigma_1\sigma_2} X_j^{\sigma_2\sigma_1} - X_i^{\sigma_1\sigma_1} X_j^{\sigma_2\sigma_2} \}. \end{aligned} \tag{0.2}$$

The operator $X_i^{ab} = |a\rangle\langle b|$ takes the electron at site i from the state $|b\rangle$ to the state $|a\rangle$, where $|a\rangle$ and $|b\rangle$ are one of the three allowed states $|\uparrow\rangle$, $|\downarrow\rangle$, or $|-\rangle$. In the over-doped regime of $n \leq .85$, where n is the electron density, the charge fluctuations dominate the spin fluctuations, and the physics is dominated by the t term in the Hamiltonian [30]. In addition, mathematically, this term already encapsulates much of the complexity of the

model. Therefore, we intend to study the t model, obtained by dropping the J term in Eq. (0.2), and which is identical to the $U = \infty$ limit of the HM. The Hamiltonian for this model is given by

$$H = -\sum_{ij\sigma} t_{ij} X_i^{\sigma 0} X_j^{0\sigma} - \mu \sum_{i\sigma} X_i^{\sigma\sigma}. \tag{0.3}$$

Our object of study is the Green's function written as

$$\mathcal{G}_{\sigma_1\sigma_2}(i,f) = -\langle T_\tau X_i^{0\sigma_1}(\tau_i) X_f^{\sigma_2 0}(\tau_f)\rangle, \tag{0.4}$$

where the angular brackets indicate the usual thermal average. Due to the non-canonical commutation relations of the X operators, the high frequency limit of the Green's function is $\frac{1-\frac{n}{2}}{i\omega_n}$ rather than $\frac{1}{i\omega_n}$ as in the canonical case. To avoid linear growth of the self-energy in the high frequency limit[15], the Dyson self-energy must be redefined to the Dyson-Mori self energy [4] as in:

$$\mathcal{G}(k) = \frac{1-\frac{n}{2}}{i\omega_k + \boldsymbol{\mu} - \epsilon_k(1-\frac{n}{2}) - \Sigma_{DM}(k)}. \tag{0.5}$$

Just as is the case for Σ_D in the finite-U Hubbard model, Σ_{DM} is finite as $i\omega \to \infty$ in the t-J model.

Shastry has recently introduced a novel and promising approach for calculating correlation functions within the t-J model based on Schwinger's formulation of field theory [15, 3, 6]. This has culminated in the theory of the Extremely Correlated Fermi Liquid (ECFL) [3, 6], which preserves the Fermi-surface volume of the ordinary Fermi-liquid, but

has large corrections to Fermi-liquid behavior due to the Gutzwiller projection . This theory has been successfully benchmarked against: line shapes from (ARPES) experiments[7, 13], high-temperature series[12] and the numerical renormalization group (NRG) calculations for the Anderson impurity model[11]. A recent theoretical benchmarking is the comparison with DMFT calculations for the large U Hubbard model[9]. In the ECFL theory, the physical Green's function $\mathcal{G}(k)$ is factored into a canonical auxiliary Green's function $\mathbf{g}(k)$ and an adaptive spectral $\mu(k)$, where $k = (\vec{k}, i\omega_k)$.

$$\mathcal{G}(k) = \mathbf{g}(k) \times \mu(k). \tag{0.6}$$

These two factors are in turn written in terms of two self-energies, $\Phi(k)$ and $\Psi(k)$.

$$\mathbf{g}^{-1}(k) = i\omega_k + \boldsymbol{\mu} - (1 - n/2)\epsilon_k - \Phi(k), \tag{0.7}$$

$$\mu(k) = 1 - \frac{n}{2} + \Psi(k). \tag{0.8}$$

Here $\Phi(k)$ plays the role of a Dyson self-energy for the canonical Green's function $\mathbf{g}(k)$, and $\Psi(k)$ is a frequency-dependent correction to $\mu(k)$ from its high frequency value of $1 - \frac{n}{2}$. Φ and Ψ are then given in terms of the vertices (i.e. functional derivatives w.r.t. the source of the $\mathbf{g}^{-1}$ and μ) as will be described below, leading to a closed set of Schwinger differential equations (the ECFL equations of motion). These equations are in general intractable since there is no obvious small parameter, and therefore to enable practical calculations, an expansion is carried out in a partial projection parameter λ. Here λ interpolates between

the free Fermi gas and the t-J model. The meaning of λ as a partial projection parameter is detailed in [6], and may be summarized in the mapping $X_i^{\sigma 0} \rightarrow f_{i\sigma}^{\dagger}(1 - \lambda\, n_{i\bar{\sigma}})$, where $f_{i\sigma}$ is a canonical electron operator. Thus at $\lambda = 0$ we have canonical electrons, whereas at $\lambda = 1$ we have the fully projected electrons.

The λ expansion is also argued to be a low density expansion[6]. Thus, at low enough densities of particles, the complete description of the system, including its dynamics is expected in *quantitative* terms, with just a few terms in the λ expansion. The theory to $O(\lambda^2)$ has been evaluated for the t-J model in Ref. ([8]), and higher order calculations in λ valid up to higher densities could be carried out in principle. Thus, one can envisage systematically cranking up the density from the dilute limit, until we hit singularities arising from phase transitions near $n \sim 1$ [35]. This represents a possible road map for solving one of the hard problems of condensed matter physics and is exciting for that reason.

Together Φ and Ψ must perform a delicate balancing act to ensure the simultaneous satisfaction of three sum rules:

- (a) $\lim_{i\omega_n \rightarrow \infty} \mathcal{G}(k) = \frac{1-\frac{n}{2}}{i\omega_n}$
- (b) The Luttinger-Ward volume of the Fermi-surface must be preserved[59].
- (c) $\sum_k \mathcal{G}(k) = \frac{n}{2}$

The first of these sum rules is enforced by the fact $\Psi(k)$ vanishes and $\Phi(k)$ remains finite in the high-frequency limit. The second one is enforced by requiring that the number of auxiliary Fermions be equal to the number of physical fermions, i.e. requiring that $\sum_k \mathbf{g}(k) = \frac{n}{2}$. This gives the auxiliary Green's function, described by a Fermi-liquid like self-energy $\Phi(k)$, the correct Fermi-surface volume. Furthermore, since $\Psi(k)$ is smooth

through the Fermi surface, the auxiliary-Fermions and the physical ones share the same Fermi-surface,which ensures that the Fermi-surface volume of the physical Green's function $\mathcal{G}(k)$, is the correct one. Finally, if $\Psi(k)$ were to vanish at all frequencies, the third sum rule would be violated, as the number of physical electrons would be depleted by a factor of $1-\frac{n}{2}$. Therefore, the third sum rule requires that $\Psi(k)$ be non-zero at small frequencies, and add enough weight to the spectral function to bring the number of physical Fermions up to the correct value.

Another feature of the ECFL formalism is the introduction of a second chemical potential u_0 [6]. This second chemical potential is motivated by the need to satisfy the shift-invariance of the model. By this we mean that, if one examines Eq. (0.3), it is clear that any shift of the kind $t_{i,j} \to t_{i,j} + u_t \delta_{i,j}$, where u_t is any constant, can be absorbed into the chemical potential μ leaving both the physical Green's function $\mathcal{G}(k)$ and the Dyson-Mori self-energy $\Sigma_{DM}(k)$ unchanged. u_0 ensures that such a shift can also be absorbed individually by the two ECFL self-energies $\Phi(k)$ and $\Psi(k)$. u_0 also serves the role of a Lagrange multiplier (as does the original chemical potential μ). Together, the two Lagrange multipliers μ and u_0 enable one to satisfy the number sum-rules for both the auxiliary and the physical Fermions.

A key physical idea that has emerged from the ECFL theory is the particle-hole asymmetry in the spectral density of the electron Green's function, and the spectral density of the Dyson-Mori self-energy, which becomes more pronounced as the density $n \to 1$[3, 4, 5]. This breaks a previous paradigm, in which the Fermi-liquid state was always believed to be particle-hole symmetric. This asymmetry is fundamentally a consequence of the Gutzwiller

projection in the extreme correlation limit. Within the ECFL theory, this asymmetry is generated by $\Psi(k)$, which adds spectral weight at low frequencies in an asymmetric fashion, leading to a skewing of the density of states towards the occupied states. Another key idea is that the two self-energies Φ and Ψ are Fermi-liquid like particle-hole symmetric self-energies [3, 4, 8], which, when combined through the ECFL functional form Eqs. (0.6) through (0.8), give rise to a Dyson-Mori self-energy with large corrections to Fermi-liquid behavior of the kind discussed above. These ideas have been corroborated in the work described here [9, 11, 12], as will be elaborated upon below.

In this thesis, we use the ECFL approach in three different contexts to gain a better understanding of the ECFL approach and what it reveals about the solution to this model. These three contexts are the limit of infinite spatial dimensions, the infinite-U Anderson Impurity Model (AIM), and the high-temperature series.

Considerable progress has been made by considering the HM in the limit of infinite dimensions [18, 19, 20, 21, 22, 23, 24, 25, 26]. One important result is that the Dyson self energy, defined by inverting the expression for the electron Green's function $\mathcal{G}$:

$$\mathcal{G}(k) = \frac{1}{i\omega_k + \boldsymbol{\mu} - \epsilon_k - \Sigma_D(k)}, \tag{0.9}$$

becomes momentum independent in this limit [18, 20, 21, 19]. Two other important results are the self-consistent mapping of the infinite dimensional HM onto the Anderson Impurity model (AIM), detailed in [23](Dynamical Mean Field Theory), and the vanishing of the vertex corrections in the optical conductivity[25, 26], so that the two particle response is obtainable from the single particle Green's function. The Dynamical Mean Field Theory

(DMFT) provides a means for doing reliable numerical calculations for the Hubbard model, at any value of U and has continued to provide new, and interesting results[16, 17].

In [10], we laid the foundation for the study of ECFL in the limit of infinite spatial dimensions. In this limit, $J \to 0$, and the Hamiltonian for the t$-$J model Eq. (0.2), automatically reduces to the one for the infinite-U Hubbard model Eq. (0.3) (see sec. 6A of Ref. ([9]) for a brief discussion of this). It is not clear a priori, whether or not the aforementioned results, valid for the infinite dimensional finite-U Hubbard model, carry over to the infinite dimensional t-J model. The possible conflict arises from the fact that in the case of the former, the ratio $\frac{U}{d} \to 0$, while in the case of the latter, $\frac{U}{d} \to \infty$. This question was raised in Ref. ([14]), pointing to the ECFL solution of the infinite dimensional t-J model as a source of resolution. Using the ECFL equations of motion, we were able to address this challenging task and to show that the two limits $U \to \infty$ and $d \to \infty$ do in fact commute. Moreover, we were able to determine the structure of the ECFL objects $\Phi(k)$ and $\Psi(k)$ in the limit of infinite dimensions. We were also able to elucidate the nature of the λ expansion, derive a DMFT-like mapping between the ECFL solutions of the infinite-U HM and infinite-U AIM, and demonstrate the vanishing of vertex corrections in the conductivity, in the large-d limit.

In [9], these results were put to use, in a comparative study between the DMFT and ECFL solutions of the infinite-dimensional t-J model. This work had several key findings:

- (a) Both ECFL and DMFT predict particle-hole asymmetry in the spectral density of the physical Green's function and the Dyson self-energy.

- (b) The rich frequency dependence of the momentum-independent Dyson self-energy $\Sigma(\omega)$ found through DMFT is reproduced by assuming standard Fermi-liquid forms (i.e. $\Psi''(\omega) \sim \{\omega^2 + (\pi k_B T)^2\}$) for each of two momentum-independent ECFL self-energies, which are then recombined through the ECFL functional form, giving rise to the exotic features of the Dyson-self energy. Thus, ECFL gives analytical insight into the exact numerical results provided by DMFT.

- (c) Even the leading order $O(\lambda^2)$ theory of ECFL is able to capture all of the main features of the exact DMFT spectral function. All of the error introduced in the truncation of the λ series at second order is reflected in Z, the quasiparticle weight, which when calculated through ECFL does not decay fast enough with increasing density as compared with the DMFT result.

It should be emphasized that while DMFT is a numerical technique which becomes exact in the limit of infinite dimensions, it does not provide sufficient analytical insight into the results for $\Sigma(\omega)$ which it produces. It is also not easily generalizable to lower dimensions, where the momentum-dependence of the self-energy becomes important. ECFL, on the other hand is an analytical theory which can be used in any number of spatial dimensions.

In [11], we generalized the ECFL theory to the infinite-U AIM. This problem, which describes a single correlated impurity site (with density n_d) coupled to a non-interacting bath, was introduced by Anderson Ref. ([36]) in 1961, and has been a fertile ground where several fruitful ideas and powerful techniques have been developed, and tested against experiments in Kondo, mixed valency and heavy Fermion systems. These include the renormalization group ideas- from the intuitive poor man scaling of Anderson [37, 38], to the

powerful numerical renormalization group (NRG) of Wilson [39], Krishnamurthy *et.al.* [40], and more recent work in [41, 42]. A comprehensive review of the AIM and many popular techniques used to study it, such as the large N expansion [43, 44], slave particles [45] and the Bethe *ansatz* [46] can be found in Ref. ([47]). In the AIM, the Wilson renormalization group method provides an essentially exact solution of the crossover from weak to strong coupling, without any intervening singularity in the coupling constant. As emphasized in [48, 49, 50], the ground state is asymptotically a Fermi liquid at all densities. This implies that as a function of the density n_d (at any U), the Fermi liquid ground state evolves smoothly without encountering any singularity, from the low density limit (the empty orbital limit) to the intermediate density limit (the mixed valent regime), and finally through to the very high density limit (Kondo regime). In view of the non singular evolution in density, the AIM provides us with an ideal problem to benchmark the basic ECFL ideas discussed above.

AIM studies of the spectral functions [51, 52, 53, 54] using NRG have become available in recent years. Therefore, in [11], we were able to conduct a comparative study between the ECFL and NRG techniques for the flat-band infinite-U AIM. The key findings of this study were the following:

- (a) The ECFL theory enforces the Friedel sum rule in the AIM model analogously to the way in which it enforces the Luttinger-Ward volume theorem in the t−J model.
- (b) The Dyson self-energy found through NRG for the flat-band (describing the bath electrons) AIM is very similar to the Dyson self-energy found through DMFT for the infinite-dimensional t−J model (which can also be viewed as an AIM with a much

more complicated band). In the case of the AIM, it is also reproduced by combining two Fermi-liquid like ECFL self-energies using the ECFL functional form.

- (c) The error introduced by truncating the λ expansion at second order is reflected in Z, the quasiparticle weight, which is overestimated by ECFL. Since the flat-band AIM has an exponentially decaying Z (as a function of n_d), as opposed to a linearly decaying one for the infinite-d t−J model, ECFL makes a greater error in the high density limit for the flat-band AIM as compared to the infinite-d t−J model.

- (d) After rescaling by Z, there is good quantitative agreement between the ECFL and NRG spectral functions at all values of the density, showing that the O(λ^2) ECFL theory captures the shape of the spectral function, but misses the scale in the high density limit.

Finally, we also study the Hamiltonian in Eq. (0.3) through the use of high-temperature series. In this series, all quantities are expanded in powers of $\left(\frac{t}{T}\right)$, where T is the temperature, and t is the magnitude of the hopping. In the regime $T > t$, the series converges nicely and gives reliable results. To obtain results for the case of $T < t$, one must use Padé approximations. One may also use this perturbation series to construct self-consistent approximations which sum infinite sub-classes of diagrams.

In [12], we used the high-temperature series for the single-particle Green's function, obtained by us to eighth order in $\left(\frac{t}{T}\right)$ in [69] to benchmark the ECFL $O(\lambda^2)$ results in the high-temperature limit. We found good quantitative agreement between the ECFL results, and the exact results of the series. Furthermore, using the aforementioned skew of the density of states towards the occupied states, we used a modified first moment of

the spectral function, which overestimates the contribution of the unoccupied states, as an estimate of the location of the quasi-particle peak. Since this moment was available to us from the series for any density, we were able to use it to study the evolution of the Fermi surface in the limit $n \to 1$, which is not directly accessible to the $O(\lambda^2)$ ECFL theory, for temperatures down to which the Padé approximations converged.

Finally, in this thesis, we develop a new formalism for the high-temperature series of the infinite-U HM model. This series has several advantages over those used previously:

- (a) A simple rule for the evaluation of the signature and spin sum of a diagram
- (b) The ability to calculate for an arbitrary number of m spin species without any additional computational difficulty.
- (c) A novel formula for the restricted lattice sum of a disconnected diagram consisting of several connected components.
- (d) The ability to go to at least ninth order for the single particle Green's function (the previous record is our eighth order result).
- (e) The ability to go to at least tenth order for any dynamic susceptibility (previously no results have been reported as this calculation has been deemed too hard [68]).

The computations alluded to in the last two points will be reported upon in a future publication which is currently a work in progress [70].

Part II

ECFL in the limit of infinite dimensions

Chapter 1

Introduction

1.1 Results in the limit of infinite dimensions

We show that in the large d limit, the two self energies $\Phi(k)$ and $\Psi(k)$ simplify in the following way.

$$\Psi(k) = \Psi(i\omega_k), \tag{1.1}$$

$$\Phi(k) = \chi(i\omega_k) + \epsilon_k \Psi(i\omega_k). \tag{1.2}$$

These in turn show that the Dyson-Mori self energy behaves as

$$\Sigma_{DM}(k) = \Sigma_{DM}(i\omega_k) = \frac{(i\omega_k + \boldsymbol{\mu})\Psi(i\omega_k) + (1 - \frac{n}{2})\chi(i\omega_k)}{1 - \frac{n}{2} + \Psi(i\omega_k)}, \tag{1.3}$$

and is therefore local in the limit of infinite dimensions. We show that to each order in the λ expansion, $\Psi(i\omega_k)$ and $\chi(i\omega_k)$ are each a product of an arbitrary number of factors, each of which take on the form $\sum_{\vec{p}} g(\vec{p}, i\omega_p)\epsilon_{\vec{p}}^m$, with m equal to zero or one, and with arbitrarily complex frequency dependence of the individual factors.

We show that just as in the finite U case[25, 26], the optical conductivity is given by the expression

$$\sigma^{\alpha\beta}(\omega) = \frac{2}{i\omega} \sum_{\vec{p}, i\omega_p} \mathcal{G}(\vec{p}, i\omega_p) v_{\vec{p}}^{\alpha} v_{\vec{p}}^{\beta} [\mathcal{G}(\vec{p}, \omega + i\eta + i\omega_p) - \mathcal{G}(\vec{p}, i\eta + i\omega_p)], \tag{1.4}$$

where $v_{\vec{p}}^{\alpha}$ is the component of the velocity in the α direction (Eq. (3.18)). We show that this formula can be applied at each order of the λ expansion.

We show that there is a self consistent mapping between the ECFL theory of the infinite-dimensional t-J model and the ECFL theory of the infinite-U AIM [11]. This mapping is similar in spirit to the mapping first discussed by Georges and Kotliar for the Hubbard model [23], but is made directly in the infinite U limit here. In this mapping, $\mathbf{g}_{i,i}[\tau_i, \tau_f]$ and $\mu_{i,i}[\tau_i, \tau_f]$ of the t-J model are mapped to the objects $\mathbf{g}[\tau_i, \tau_f]$ and $\mu[\tau_i, \tau_f]$ of the Anderson model, written with the same symbols, but without the spatial or momentum labels. This mapping is valid under the self-consistency condition

$$\sum_{\vec{k}} \epsilon_{\vec{k}} \mathbf{g}(k) = \sum_{\vec{k}} \frac{|V_{\vec{k}}|^2}{i\omega_n - \widetilde{\epsilon_{\vec{k}}}} \mathbf{g}(i\omega_k), \tag{1.5}$$

where $\epsilon_{\vec{k}}$ is the dispersion of the lattice in the t-J model, and $V_{\vec{k}}$ and $\widetilde{\epsilon_{\vec{k}}}$ are the hybridization and dispersion of the bath respectively in the Anderson impurity model. This

self-consistency condition is shown to be equivalent to the standard self-consistency condition from DMFT[23, 24]. We also show that the mapping holds to each order in λ under the same self-consistency condition. We note that this implies that ECFL computations for the infinite-dimensional t-J model can be done with a DMFT-like self-consistency loop involving ECFL computations for the AIM. However, since the λ expansion provides integral equations which are relatively straightforward to solve numerically, this is not necessary as the t-J model equations can be solved directly.

1.2 Outline of the chapter

This chapter is structured as follows. In section 2, some basic facts about lattice sums in the limit of large dimensions and the ECFL equations of motion as well as the λ expansion are reviewed. Additionally, the spatial dependence of various standard and ECFL specific objects in the limit of large dimensions is stated. Finally, we introduce a class of local functions denoted as class-L functions; these turn out to play a central role in the ECFL in the limit of large dimensions. In sections 3.1 and 3.2, Eqs. (1.1) and (1.2) are proven in general and to each order in λ, and the locality of the Dyson-Mori self energy is shown as a consequence. In section 3.3, Eq. (1.4) is shown to hold in general and to each order in λ. In section 3.4, the ECFL self-consistent integral equations are derived to $O(\lambda^2)$ in the large-d limit. Finally, in section 4, the ECFL of the infinite dimensional t-J model is mapped onto the ECFL of the infinite-U AIM under the self-consistency condition Eq. (1.5). This is done in general and to each order in λ.

Chapter 2

Preliminaries

2.1 Spatial dependence of lattice sums in large d dimensions

We take the hopping to nearest neighbor sites on the d-dimensional hypercube. In this case, it is well known [19] that $t_{ij} \to \frac{1}{\sqrt{2d}} t_0$ with t_0 of $O(1)$. We would like to exploit the smallness of individual t_{ij}'s, these can only contribute (after multiplying with another like object), if one of the indices is summed over the d-neighbors as in the simplest example $\sum_j t_{ij}^2 = t_0^2$. Extending this argument further, for a pair of sites (i, m) located at a (Manhattan metric) distance r_{im} on the hypercube, suppose there are two objects $W_{i,m}$ and $V_{i,m}$ who both have the dependence on r_{im}: $V_{i,m}; W_{i,m} \sim O\left(\frac{1}{(\sqrt{d})^{r_{im}}}\right)$. Then it follows that

$$W_{i,\mathbf{n}} V_{\mathbf{n},m} \sim O\left(\frac{1}{\left(\sqrt{d}\right)^{r_{im}}}\right). \tag{2.1}$$

Here, and in the rest of the paper, bold and repeated indices are summed and/or integrated over. This relation can be understood by first considering the case that the site $\mathbf{n}$ is on one of the shortest paths between i and m. In this case, $r_{i\mathbf{n}} + r_{\mathbf{n}m} = r_{im}$ proving the relation. If, $\mathbf{n}$ is a certain distance r_o off of a shortest path, then $r_{i\mathbf{n}} + r_{\mathbf{n}m} = r_{im} + 2r_o$. This introduces an extra factor of $\frac{1}{d^{r_o}}$ into the lattice sum in Eq. (2.1). However, this factor is exactly cancelled by the d^{r_0} choices for the site $\mathbf{n}$. In this argument, the number of shortest paths between i and m is taken to be $O(1)$.

2.2 ECFL Equations of Motion and the λ expansion

The ECFL equations of motion for the finite dimensional t-J model can be found in Ref. ([6]). There is some freedom in how these equations are written because one may add terms to them which vanish identically in the exact solution, but play a non-trivial role when implementing approximations (such as the λ expansion). We denote the version of these equations with no added terms the minimal theory, and the version containing the added terms the symmetrized theory (since the added terms make the resulting expressions symmetric in a certain sense). In Ref. ([6]), the ECFL equations of motion for the symmetrized theory are derived, and the added terms required to go from the minimal theory to the symmetrized theory are singled out. The ECFL equations for the minimal theory, which are the ones used in this paper and in Ref. ([9]), can therefore be obtained from those in Ref. ([6]) by dropping these extra terms.

Setting $J \to 0$ (as discussed in section I), we write the minimal theory ECFL

equations of motion in expanded form.

$$\begin{aligned}
\mathbf{g}^{-1}[i,m] &= (\boldsymbol{\mu} - \partial_{\tau_i} - \mathcal{V}_i)\ \delta[i,m] + t[i,m]\ (1-\lambda\gamma[i]) + \lambda t[i,\mathbf{j}]\ \xi^*.\mathbf{g}[\mathbf{j},\mathbf{n}].\Lambda_*[\mathbf{n},m;i], \\
\mu[i,m] &= (1-\lambda\gamma[i])\delta[i,m] - \lambda t[i,\mathbf{j}]\ \xi^*.\mathbf{g}[\mathbf{j},\mathbf{n}].\mathcal{U}_*[\mathbf{n},m;i],
\end{aligned} \tag{2.2}$$

where $\mathcal{V}_i \equiv \mathcal{V}_i(\tau_i)$ is the Bosonic Schwinger source function, and we have used the notation $\delta[i,m] = \delta_{i,m}\delta(\tau_i - \tau_m)$ and $t[i,m] = t_{i,m}\delta(\tau_i - \tau_m)$. These exact relations give the required objects $\mathbf{g}$ and μ in terms of the vertex functions. Here we also note that the local (in space and time) Green's function $\gamma[i]$, and the vertices $\Lambda[n,m;i]$ and $\mathcal{U}[n,m;i]$, are defined as

$$\gamma[i] = \mu^{(k)}[\mathbf{n},i^+].\mathbf{g}^{(k)}[i,\mathbf{n}]; \quad \Lambda[n,m;i] = -\frac{\delta}{\delta\mathcal{V}_i}\mathbf{g}^{-1}[n,m]; \quad \mathcal{U}[n,m;i] = \frac{\delta}{\delta\mathcal{V}_i}\mu[n,m], \tag{2.3}$$

where we have used the notation $M^{(k)}_{\sigma_1,\sigma_2} = \sigma_1\sigma_2 M_{\bar{\sigma}_2,\bar{\sigma}_1}$ to denote the time reversed matrix $M^{(k)}$ of an arbitrary matrix M. These exact relations give the vertex functions in terms of the objects $\mathbf{g}$ and μ. The vertices defined above (Λ and $\mathcal{U}$) have four spin indices, those of the object being differentiated and those of the source. For example, $\mathcal{U}^{\sigma_1\sigma_2}_{\sigma_a\sigma_b}[n,m;i] = \frac{\delta}{\delta\mathcal{V}_i^{\sigma_a\sigma_b}}\mu_{\sigma_1\sigma_2}[n,m]$. In Eq. (2.2), $\xi_{\sigma_a\sigma_b} = \sigma_a\sigma_b$, and the * indicates that these spin indices should also be carried over (after being flipped) to the bottom indices of the vertex, which is also marked with a $_*$. The top indices of the vertex are given by the usual matrix multiplication. An illustrative example is useful here: $(\xi^*.\mathbf{g}[j,\mathbf{n}].\mathcal{U}_*[\mathbf{n},m;i])_{\sigma_1\sigma_2} = \sigma_1\sigma_{\mathbf{a}}\ \mathbf{g}_{\sigma_{\mathbf{a}},\sigma_{\mathbf{b}}}[j,\mathbf{n}]\frac{\delta}{\delta\mathcal{V}_i^{\sigma_1\sigma_{\mathbf{a}}}}\mu_{\sigma_{\mathbf{b}},\sigma_2}[\mathbf{n},m]$. Finally, in order to ensure that the shift identities (Ref. ([6])) are satisfied, the substitution $t_{ij} \to t_{ij} + \frac{u_0}{2}\delta_{ij}$ is made, where u_0 is the second

chemical potential. For the sake of clarity, this substitution will be ignored in the proofs given below, although they are easily generalized to account for it. This generalization is discussed at the end of section 3.1.

The λ expansion is obtained by expanding Eq. (2.2) and Eq. (2.3) iteratively in the continuity parameter λ. The $\lambda = 0$ limit of these equations is the free Fermi gas. Therefore, a direct expansion in λ will lead to a series in λ in which each term is made up of the hopping t_{ij} and the free Fermi gas Green's function $\mathbf{g}_0[i, f]$. As is the case in the Feynman series, this can be reorganized into a skeleton expansion in which only the skeleton graphs are kept and $\mathbf{g}_0[i, f] \to \mathbf{g}[i, f]$. However, one can also obtain the skeleton expansion directly by expanding Eq. (2.2) and Eq. (2.3) in λ, but treating $\mathbf{g}[i, f]$ as a zeroth order (i.e. unexpanded) object in the expansion. This expansion is carried out to second order for the finite-dimensional case in Ref. ([6]). In doing this expansion, one must evaluate the functional derivative $\frac{\delta \mathbf{g}}{\delta \mathcal{V}}$. This is done with the help of the following useful formula which stems from the product rule for functional derivatives.

$$\frac{\delta \mathbf{g}[i, m]}{\delta \mathcal{V}_r} = \mathbf{g}[i, \mathbf{x}].\Lambda[\mathbf{x}, \mathbf{y}, r].\mathbf{g}[\mathbf{y}, m]. \tag{2.4}$$

This is an exact formula and will be used extensively in the arguments given below. Within the λ expansion, the LHS is evaluated to a certain order in λ by taking the vertex Λ on the RHS to be of that order in λ.

2.3 Leading order spatial dependence of various objects

All objects may be expanded in the inverse square root of the number of spatial dimensions d. The lowest order term in the physical Green's function $\mathcal{G}[i,f]$ must be at least $O\left(\frac{1}{(\sqrt{d})^{r_{if}}}\right)$. This must be so because it takes at least r_{if} hops to get from the site i to the site f. Any terms that contribute to $\mathcal{G}[i,f]$ at higher order than $O\left(\frac{1}{(\sqrt{d})^{r_{if}}}\right)$ are neglected in the large d limit. In a similar vein, the lowest order term in $\mathbf{g}[i,f]$, $\mathbf{g}^{-1}[i,f]$, $\mu[i,f]$, $\Lambda[i,f;r]$, and $\mathcal{U}[i,f;r]$ must be at least $O\left(\frac{1}{(\sqrt{d})^{r_{if}}}\right)$. Furthermore, using the real space version of Eq. (0.6) and Eq. (2.1), we see that any terms of higher order than this in $\mathbf{g}[i,f]$ and $\mu[i,f]$ will result in a higher order term in $\mathcal{G}[i,f]$ and may therefore be neglected as well. Finally, using matrix inversion in the space-time indices, we see that higher order terms may also be dropped from $\mathbf{g}^{-1}[i,f]$ as these will lead to higher order terms in $\mathbf{g}[i,f]$, and using Eq. (2.2), higher order terms may be dropped from $\Lambda[i,f;r]$, and $\mathcal{U}[i,f;r]$ as these will lead to higher order terms in $\mathbf{g}^{-1}[i,f]$ and $\mu[i,f]$ respectively. In summary, in all objects: $\mathcal{G}[i,f]$, $\mathbf{g}[i,f]$, $\mathbf{g}^{-1}[i,f]$, $\mu[i,f]$, $\Lambda[i,f;r]$, and $\mathcal{U}[i,f;r]$, terms of higher order than $O\left(\frac{1}{(\sqrt{d})^{r_{if}}}\right)$ may be neglected in the large d limit.

We also note that the correlation function $\Pi_{\alpha\beta}[i,f]$ appearing in Eq. (3.19) must be at least $O\left(\frac{1}{d^{r_{if}}}\right)$. This is due to the fact that unlike the creation and destruction operators which appear in the Green's function, the current operators appearing in this correlation function conserve particle number. Hence, one must hop from site i to site f and back, which takes $2 \times r_{if}$ hops. Any terms that contribute to $\Pi_{\alpha\beta}[i,f]$ at higher order than $O\left(\frac{1}{d^{r_{if}}}\right)$ are neglected in the large d limit.

2.4 Class L functions

For the arguments given below, we need to define a class of *localized functions*, denoted as class L functions. A class L function L_i has three properties.

- (a) $L_i \sim O\left(\frac{1}{d^0}\right)$.
- (b) L_i is a function of only one site i, and an arbitrary number of time variables. Upon turning off the sources, it becomes translationally invariant, but an arbitrary function of frequencies.
- (c) The $\mathcal{V}$ source derivative of L_i is also localized:

$$\frac{\delta}{\delta \mathcal{V}_i} L_j = \delta_{ij} L'_i, \tag{2.5}$$

  with L'_i again a Class-L function.

Our proofs deal with functions that turn out to be of this class. Iterating property (c), the following equation must hold for any positive integer s.

$$\frac{\delta}{\delta \mathcal{V}_{r_1}} \cdots \frac{\delta}{\delta \mathcal{V}_{r_s}} L_i = \delta_{ir_1} \ldots \delta_{ir_s} \frac{\delta}{\delta \mathcal{V}_i(\tau_{r_1})} \cdots \frac{\delta}{\delta \mathcal{V}_i(\tau_{r_s})} L_i. \tag{2.6}$$

In the presence of the current source κ (Eq. (3.21)), class L functions acquire one additional property (d): Consider a typical contribution to $\Pi_{\alpha\beta}[i, f]$ (Eq. (3.23)) denoted by O_{if}

$$O_{if} = W_{f,\mathbf{x}} \; \frac{\delta}{\delta \kappa_i^\alpha} \left(L_{\mathbf{x}}\right) \; V_{\mathbf{x},f}, \tag{2.7}$$

where the functions $V_{\mathbf{x},f}, W_{f,\mathbf{x}} \sim O\left(\frac{1}{(\sqrt{d})^{r_{\mathbf{x}f}}}\right)$. Then, neglecting terms of higher order than $O\left(\frac{1}{d^{r_{if}}}\right)$ in O_{if}, $\sum_{i-f} O_{if} \to 0$ as $\mathcal{A} \to 0$. Again iterating property (c) and using property (d), the following must hold for any nonnegative integer s:

$$\sum_{i-f}\left(W_{f,\mathbf{x}}\ \frac{\delta}{\delta\kappa_i^\alpha}\frac{\delta}{\delta\mathcal{V}_{\mathbf{x}}(\tau_{r_1})}\cdots\frac{\delta}{\delta\mathcal{V}_{\mathbf{x}}(\tau_{r_s})}\left(L_{\mathbf{x}}\right)\ V_{\mathbf{x},f}\right)_{\mathcal{A}\to 0} = 0. \tag{2.8}$$

Chapter 3

Limit of Large dimensionality through the ECFL equations of motion

3.1 Simplification of the ECFL self energies.

We use notation in which we indicate spatial dependence by subscripts, so that $\mathbf{g}[i,j] \rightarrow \mathbf{g}_{i,j}[\tau_i,\tau_j]$, and recall that $t[i,j] = t_{i,j}\ \delta(\tau_i - \tau_j)$, $\delta[i,j] = \delta_{i,j}\ \delta(\tau_i - \tau_j)$, and $\delta[\tau_i,\tau_j] = \delta(\tau_i - \tau_j)$ etc. After some inspection of Eq. (2.2) and Eq. (2.3) in the limit of high dimension, we make an Ansatz - to be proven below - namely

$$\begin{aligned}
\mathbf{g}^{-1}[i,m] &= (\boldsymbol{\mu} - \partial_{\tau_i} - \mathcal{V}_i)\ \delta[i,m] + \ t[i,m]\ (1 - \lambda\gamma[i]) - \lambda\ \delta_{i,m}\ \chi_i[\tau_i,\tau_m] + \lambda\ t_{i,m}\ \Psi_i[\tau_i,\tau_m], \\
\mu[i,m] &= \delta[i,m](1 - \lambda\gamma[i]) + \lambda\ \delta_{i,m}\ \Psi_i[\tau_i,\tau_m], \qquad (3.1)
\end{aligned}$$

where $\Psi_i[\tau_i, \tau_m]$, $\chi_i[\tau_i, \tau_m]$, and $\gamma[i]$ are class L functions. We will prove Eq. (3.1) by assuming that it is true, and then showing that this assumption is consistent with the equations of motion (Eqs. (2.2) and (2.3)). This argument will consist of a loop which begins with Eq. (3.1). Then, substituting this equation into Eq. (2.3), we will derive a certain form for Λ, $\mathcal{U}$, and γ. Finally, substituting these objects into Eq. (2.2), and using simplifications which occur in the large d limit, we will complete the loop and arrive back at Eq. (3.1).

Substituting Eq. (3.1) into Eq. (2.3), we find that the vertices and $\gamma[i]$ have the following form.

$$\begin{aligned}
\Lambda[n, m; i] &= \delta_{i,n}\delta_{i,m}\ A_i[\tau_n, \tau_m; \tau_i] + \delta_{i,n}t_{n,m}\ B_i[\tau_n, \tau_m; \tau_i], \\
\mathcal{U}[n, m; i] &= -\delta_{i,n}\delta_{i,m}\ B_i[\tau_n, \tau_m; \tau_i], \\
\gamma[i] &= \left(1 - \lambda\gamma^{(k)}[i]\right) \mathbf{g}^{(k)}[i, i] + \lambda\ \Psi_i^{(k)}[\tau_{\mathbf{j}}, \tau_i]\mathbf{g}_{ii}^{(k)}[\tau_i, \tau_{\mathbf{j}}],
\end{aligned} \tag{3.2}$$

where we defined two new functions:

$$\begin{aligned}
A_i[\tau_n, \tau_m; \tau_i] &= \delta[\tau_i, \tau_n]\delta[\tau_i, \tau_m]\ \mathbb{1} + \lambda\ \frac{\delta}{\delta\mathcal{V}_i}\chi_i[\tau_n, \tau_m], \\
B_i[\tau_n, \tau_m; \tau_i] &= \lambda\ \delta[\tau_n, \tau_m]\frac{\delta}{\delta\mathcal{V}_i}\gamma_i[\tau_n] - \lambda\ \frac{\delta}{\delta\mathcal{V}_i}\Psi_i[\tau_n, \tau_m].
\end{aligned} \tag{3.3}$$

Here A_i and B_i are class L functions since they inherit this property from Ψ_i, χ_i, and $\gamma[i]$ by functional differentiation. Substituting Eq. (3.2) into Eq. (2.2) and comparing with

Eq. (3.1),

$$\begin{aligned}\chi_i[\tau_i,\tau_m] &= -\,t_{i,\mathbf{j}}\;\xi^*.\;\mathbf{g}_{\mathbf{j},i}[\tau_i,\tau_{\mathbf{n}}].\;A_{i,*}[\tau_{\mathbf{n}},\tau_m;\tau_i],\\ \Psi_i[\tau_i,\tau_m] &= \;\;t_{i,\mathbf{j}}\;\xi^*.\;\mathbf{g}_{\mathbf{j},i}[\tau_i,\tau_{\mathbf{n}}].\;B_{i,*}[\tau_{\mathbf{n}},\tau_m;\tau_i].\end{aligned} \tag{3.4}$$

If we can now show that χ_i, Ψ_i, and $\gamma[i]$ as defined in Eq. (3.2) and Eq. (3.4) are Class L functions, we will have justified our Ansatz and therefore we will have proven all of the above equations. To do this, we must show that $\mathbf{g}_{ii}[\tau_i,\tau_m]$ and $t_{i,\mathbf{j}}\;\mathbf{g}_{\mathbf{j},i}[\tau_i,\tau_m]$ are Class L functions. Taking their functional derivatives we obtain:

$$\begin{aligned}\frac{\delta}{\delta\mathcal{V}_r}t_{i,\mathbf{j}}\;\mathbf{g}_{\mathbf{j},i}[\tau_i,\tau_m] &= t_{i,\mathbf{j}}\mathbf{g}_{\mathbf{j},r}[\tau_i,\tau_{\mathbf{k}}]\;A_r[\tau_{\mathbf{k}},\tau_{\mathbf{l}};\tau_r]\mathbf{g}_{r,i}[\tau_{\mathbf{l}},\tau_m]\\ &\quad + t_{i,\mathbf{j}}\mathbf{g}_{\mathbf{j},r}[\tau_i,\tau_{\mathbf{k}}]\;B_r[\tau_{\mathbf{k}},\tau_{\mathbf{l}};\tau_r]t_{r,\mathbf{l}}\mathbf{g}_{\mathbf{l},i}[\tau_{\mathbf{l}},\tau_m],\end{aligned} \tag{3.5}$$

and

$$\begin{aligned}\frac{\delta}{\delta\mathcal{V}_r}\mathbf{g}_{i,i}[\tau_i,\tau_m] &= \mathbf{g}_{i,r}[\tau_i,\tau_{\mathbf{k}}]\;A_r[\tau_{\mathbf{k}},\tau_{\mathbf{l}};\tau_r]\mathbf{g}_{r,i}[\tau_{\mathbf{l}},\tau_m]\\ &\quad + \mathbf{g}_{i,r}[\tau_i,\tau_{\mathbf{k}}]\;B_r[\tau_{\mathbf{k}},\tau_{\mathbf{l}};\tau_r]t_{r,\mathbf{l}}\mathbf{g}_{\mathbf{l},i}[\tau_{\mathbf{l}},\tau_m].\end{aligned} \tag{3.6}$$

Using Eq. (2.1), the terms on the RHS of Eq. (3.5) and Eq. (3.6) survive the large d limit if and only if $r = i$. Moreover, upon making the substitution $r \to i$, we see that the RHS is made up of the same objects that appear on the LHS of the equations (as well as the class L

functions A and B). Therefore, this argument can be iterated to any number of derivatives acting on $t_{i,\mathbf{j}}\ \mathbf{g}_{\mathbf{j},i}[\tau_i, \tau_m]$ or $\mathbf{g}_{i,i}[\tau_i, \tau_m]$ (as required by Eq. (2.6)), which are therefore class L functions. Thus, we have shown the self-consistency of our ansatz Eq. (3.1).

The above results hold for any value of λ, since the proof was done with λ present in all of the equations. In the bare expansion, this would imply that they also hold to each order in λ. However, this line of reasoning is not as straightforward in the skeleton expansion because each order in the skeleton expansion contains contributions from all orders in the bare expansion. Nonetheless, the above results do hold to each order in λ in the skeleton expansion. In proving this, we shall shed more light on the nature of the objects Ψ_i, χ_i, $\gamma[i]$, A_i, and B_i. In particular, we will show that they satisfy a certain explicit form stated below in Eq. (3.7). We will do this using an inductive argument, in which we will assume that they have this form through a certain order in λ, and then substituting this form into the equations of motion, will show that it must hold for the next order.

We now use the symbol R_i **as a proxy** for either of the two functions $\mathbf{g}_{i,i}[\tau_n, \tau_m]$ or $t_{i,\mathbf{j}}\mathbf{g}_{\mathbf{j},i}[\tau_n, \tau_m]$ where the time indices are arbitrary. **Inductive hypothesis**: Through n^{th} order in λ, Eq. (3.1) and Eq. (3.2) hold. Through $n-1^{st}$ order in λ, the objects Ψ_i, χ_i, and $\gamma[i]$, and through n^{th} order, the objects A_i and B_i, (all denoted below by the generic object L_i) can be written as the following product (multiplied by some delta functions in time variables):

$$(L_i)^{(n)} = \lambda^n (R_i)^m, \tag{3.7}$$

where m is arbitrary. We first examine the base case of zeroth order. In this case,

$$A_i^{(0)}[\tau_n, \tau_m; \tau_i] = \delta[\tau_i, \tau_n]\delta[\tau_i, \tau_m]; \quad B_i^{(0)}[\tau_n, \tau_m; \tau_i] = 0. \tag{3.8}$$

Clearly the hypothesis is satisfied. Now, we prove the inductive step. Explicitly displaying the order in λ of all objects, the equations for χ, Ψ, and γ (Eqs. (3.4) and (3.2)) become

$$\begin{aligned}
\chi_i^{(n)}[\tau_i, \tau_m] &= -\, t_{i,\mathbf{j}}\ \xi^*\cdot\ \mathbf{g}_{\mathbf{j},i}[\tau_i, \tau_\mathbf{n}].\ A_{i,*}^{(n)}[\tau_\mathbf{n}, \tau_m; \tau_i], \\
\Psi_i^{(n)}[\tau_i, \tau_m] &= \ \ t_{i,\mathbf{j}}\ \xi^*\cdot\ \mathbf{g}_{\mathbf{j},i}[\tau_i, \tau_\mathbf{n}].\ B_{i,*}^{(n)}[\tau_\mathbf{n}, \tau_m; \tau_i], \\
\gamma^{(n)}[i] &= -\lambda\ \gamma^{(k)(n-1)}[i]\mathbf{g}^{(k)}[i, i] + \lambda\ \Psi_i^{(k)(n-1)}[\tau_\mathbf{j}, \tau_i]\mathbf{g}_{ii}^{(k)}[\tau_i, \tau_\mathbf{j}].
\end{aligned} \tag{3.9}$$

By the inductive hypothesis, $\chi_i^{(n)}$, $\Psi_i^{(n)}$, and $\gamma^{(n)}[i]$ have the required form. The equations for A and B (Eq. (3.3)) become

$$\begin{aligned}
A_i^{(n+1)}[\tau_n, \tau_m; \tau_i] &= \lambda\ \left(\sum_{r\le n} \frac{\delta}{\delta\mathcal{V}_i}\chi_i^{(r)}[\tau_n, \tau_m]\right)^{(n)}, \\
B_i^{(n+1)}[\tau_n, \tau_m; \tau_i] &= \lambda\ \delta[\tau_n, \tau_m]\left(\sum_{r\le n} \frac{\delta}{\delta\mathcal{V}_i}\gamma_i^{(r)}[\tau_n]\right)^{(n)} - \lambda\ \left(\sum_{r\le n} \frac{\delta}{\delta\mathcal{V}_i}\Psi_i^{(r)}[\tau_n, \tau_m]\right)^{(n)}.
\end{aligned} \tag{3.10}$$

To see that $A^{(n+1)}$ and $B^{(n+1)}$ have the required form we note that for all $l \leq n$,

$$\begin{aligned}\left(\frac{\delta}{\delta \mathcal{V}_r} t_{i,\mathbf{j}}\ \mathbf{g}_{\mathbf{j},i}[\tau_i,\tau_m]\right)^{(l)} &= t_{i,\mathbf{j}}\mathbf{g}_{\mathbf{j},r}[\tau_i,\tau_{\mathbf{k}}]\ A_r^{(l)}[\tau_{\mathbf{k}},\tau_{\mathbf{l}};\tau_r]\mathbf{g}_{r,i}[\tau_{\mathbf{l}},\tau_m] \\ &\quad + t_{i,\mathbf{j}}\mathbf{g}_{\mathbf{j},r}[\tau_i,\tau_{\mathbf{k}}]\ B_r^{(l)}[\tau_{\mathbf{k}},\tau_{\mathbf{l}};\tau_r]t_{r,\mathbf{l}}\mathbf{g}_{\mathbf{l},i}[\tau_{\mathbf{l}},\tau_m], \qquad (3.11)\end{aligned}$$

and

$$\begin{aligned}\left(\frac{\delta}{\delta \mathcal{V}_r}\mathbf{g}_{i,i}[\tau_i,\tau_m]\right)^{(l)} &= \mathbf{g}_{i,r}[\tau_i,\tau_{\mathbf{k}}]\ A_r^{(l)}[\tau_{\mathbf{k}},\tau_{\mathbf{l}};\tau_r]\mathbf{g}_{r,i}[\tau_{\mathbf{l}},\tau_m] \\ &\quad + \mathbf{g}_{i,r}[\tau_i,\tau_{\mathbf{k}}]\ B_r^{(l)}[\tau_{\mathbf{k}},\tau_{\mathbf{l}};\tau_r]t_{r,\mathbf{l}}\mathbf{g}_{\mathbf{l},i}[\tau_{\mathbf{l}},\tau_m]. \qquad (3.12)\end{aligned}$$

In the limit of large dimensions, $r \to i$. We can therefore (using the inductive hypothesis) write the RHS of Eq. (3.11) and Eq. (3.12) as $\lambda^l (R_i)^m$. Applying Eq. (3.7) (which has been shown to hold for $\chi_i^{(n)}$, $\Psi_i^{(n)}$, and $\gamma^{(n)}[i]$) to Eq. (3.10), we may write

$$\begin{aligned}A_i^{(n+1)} &= \sum_{r=0}^{n} \lambda^{r+1}\left(\frac{\delta}{\delta \mathcal{V}_i}(R_i)^m\right)^{(n-r)}, \\ B_i^{(n+1)} &= \sum_{r=0}^{n} \lambda^{r+1}\left(\frac{\delta}{\delta \mathcal{V}_i}(R_i)^m\right)^{(n-r)}.\end{aligned} \qquad (3.13)$$

Eq. (3.13), in conjunction with Eq. (3.11) and Eq. (3.12), shows that $A_i^{(n+1)}$ and $B_i^{(n+1)}$ have the required form. This completes the proof.

Since $t_{i,j}$ is independent of the source, the substitution $t_{i,j} \to t_{i,j} + \frac{u_0}{2}\delta_{i,j}$ can be made directly into all of the above equations. The only problem that could potentially arise involves Eqs. (3.5) and (3.6), where the large d simplifications are actually used.

However, one can check that this substitution does not affect the simplifications. Therefore, this substitution merely adds the term $\lambda\frac{u_0}{2}\delta_{i,m}\Psi_i[\tau_i,\tau_m] - \lambda\frac{u_0}{2}\delta[i,m]\gamma[i]$ to $\mathbf{g}^{-1}[i,m]$, and everywhere replaces the local function $t_{i,\mathbf{j}}\mathbf{g}_{\mathbf{j},i}[\tau_n,\tau_m]$ with the local function $t_{i,\mathbf{j}}\mathbf{g}_{\mathbf{j},i}[\tau_n,\tau_m] + \frac{u_0}{2}\mathbf{g}_{i,i}[\tau_n,\tau_m]$. This can be seen explicitly in the $O(\lambda^2)$ equations in section 3.4, and does not change the general structure of the solution.

3.2 The zero source limit

Setting the sources to zero, the system becomes translationally invariant so that all objects can be written in momentum space. Additionally, $\gamma[i] \to \frac{n}{2}$. Then, the above results can be summed up in the following formulae (in which we set $\lambda = 1$):

$$\begin{aligned} \mathbf{g}^{-1}(k) &= i\omega_k + \boldsymbol{\mu} - \varepsilon_k(1-\frac{n}{2}) - \chi(i\omega_k) - \varepsilon_k\Psi(i\omega_k), \\ \mu(k) &= 1 - \frac{n}{2} + \Psi(i\omega_k), \end{aligned} \tag{3.14}$$

where $\Psi(i\omega_k)$ and $\chi(i\omega_k)$ are the two momentum independent self-energies of the ECFL in infinite dimensions. In terms of these self-energies, the physical Green's function is written as

$$\mathcal{G}(k) = \frac{1 - \frac{n}{2} + \Psi(i\omega_k)}{i\omega_k + \boldsymbol{\mu} - \varepsilon_k(1-\frac{n}{2}) - \chi(i\omega_k) - \varepsilon_k\Psi(i\omega_k)}. \tag{3.15}$$

Comparing with the standard form of the Green's function in terms of the Dyson-Mori self energy

$$\mathcal{G}(k) = \frac{1 - \frac{n}{2}}{i\omega_k + \boldsymbol{\mu} - \epsilon_k(1 - \frac{n}{2}) - \Sigma_{DM}(k)}, \tag{3.16}$$

we see the momentum independence of the Dyson-Mori self energy $\Sigma_{DM}(k) = \Sigma_{DM}(i\omega_k)$, and

$$\Sigma_{DM}(i\omega_k) = \frac{(i\omega_k + \boldsymbol{\mu})\Psi(i\omega_k) + (1 - \frac{n}{2})\chi(i\omega_k)}{1 - \frac{n}{2} + \Psi(i\omega_k)}. \tag{3.17}$$

3.3 Conductivity in the limit of large dimensions

It is well known that for the finite-U Hubbard model in the limit of large dimensions, for zero wave vector, vertex corrections can be neglected in the current current correlation function [25, 24]. This simple observation allows one to express the optical conductivity in terms of the single particle Green's function as in Eq. (3.29). We show that this is also the case for the infinite dimensional t-J model. Moreover, a question of practical importance for the purpose of calculating the optical conductivity within the framework of ECFL, is whether or not Eq. (3.29) can be applied at each order in the λ expansion (as is done in Ref. ([9])). We show that it can be applied and is the correct procedure. First, we define the relevant objects.

The Schrödinger picture current operator for site j in the direction α is defined as:

$$J_j^\alpha = i\sum_{k\sigma} v_{k,j}^\alpha X_k^{\sigma 0} X_j^{0\sigma}; \quad v_{k,j}^\alpha = t_{k,j}(\vec{R}_k - \vec{R}_j)_\alpha, \tag{3.18}$$

so that v is a velocity. Using the notation $J^\alpha[i] = J_i^\alpha(\tau_i)$; $\widetilde{J}^\alpha[i] = J^\alpha[i] - \langle J^\alpha[i]\rangle$, we define the correlation function $\Pi_{\alpha\beta}[i,f]$ and its Fourier transform as

$$\begin{aligned}
&\Pi_{\alpha\beta}[i,f] = \langle T_\tau \widetilde{J}^\alpha[i]\widetilde{J}^\beta[f]\rangle; \\
&\Pi_{\alpha\beta}(\vec{q}, i\Omega_n) = \int_0^\beta d(\tau_i - \tau_f)\; e^{i\Omega_n(\tau_i-\tau_f)} \sum_{i-f} e^{-i\vec{q}\cdot(\vec{R}_i - \vec{R}_f)} \Pi_{\alpha\beta}[i,f].
\end{aligned} \tag{3.19}$$

The optical conductivity can be given in terms of this object as

$$\sigma^{\alpha\beta}(\omega) = \frac{1}{i\omega - \eta}\left[\Pi_{\alpha\beta}(\vec{0}, \omega + i\eta) - \Pi_{\alpha\beta}(\vec{0}, i\eta)\right], \tag{3.20}$$

where $\eta = 0^+$. We would like to express the object $\Pi_{\alpha\beta}[i,f]$ as a functional derivative of the Green's function. To this end, we add a source which couples to the current operator

$$\mathcal{A} \to \mathcal{A} + \sum_{j\alpha}\int_0^\beta d\tau \kappa_j^\alpha(\tau) J_j^\alpha(\tau). \tag{3.21}$$

In terms of the κ source derivative of the Green's function, and using the definitions $v^\alpha[i,j] =$

$v^{\alpha}_{i,j}\delta(\tau_i - \tau_j); \kappa^{\alpha}_i = \kappa^{\alpha}_i(\tau_i)$, $\Pi_{\alpha\beta}[i,f]$ is given as

$$\Pi_{\alpha\beta}[i,f] = -i\ Tr\left(\frac{\delta}{\delta\kappa^{\alpha}_i}\mathcal{G}[f,\mathbf{j}]\ v^{\beta}[\mathbf{j},f^{+}]\right)_{\mathcal{A}\to 0}, \tag{3.22}$$

where the trace is over the spin degrees of freedom only. We expand the RHS of this equation using Eq. (2.4) (which holds equally well for the κ source derivative), finally obtaining an expression for $\Pi_{\alpha\beta}[i,f]$ in terms of the κ source derivatives of $\mathbf{g}^{-1}$ and μ.

$$\begin{aligned}\Pi_{\alpha\beta}[i,f] \;\; = \;\; & i\ Tr\left(\mathbf{g}[f,\mathbf{x}]\ \frac{\delta}{\delta\kappa^{\alpha}_i}\mathbf{g}^{-1}[\mathbf{x},\mathbf{y}]\ \mathbf{g}[\mathbf{y},\mathbf{k}]\mu[\mathbf{k},\mathbf{j}]\ v^{\beta}[\mathbf{j},f^{+}]\right)_{\mathcal{A}\to 0} \\ & -i\ Tr\left(\mathbf{g}[f,\mathbf{k}]\frac{\delta}{\delta\kappa^{\alpha}_i}\mu[\mathbf{k},\mathbf{j}]\ v^{\beta}[\mathbf{j},f^{+}]\right)_{\mathcal{A}\to 0}.\end{aligned} \tag{3.23}$$

We now consider how the additional source Eq. (3.21) affects the ECFL equations of motion (Eq. (2.2) and Eq. (2.3)). The source enters into the equations of motion in the same way as the Hamiltonian does, via its commutator with the destruction operator, $X^{0\sigma}_i$. Moreover, the source has the same form as the Hamiltonian, with the hopping in the kinetic energy replaced by the velocity in the current operator. Therefore, the additional source affects the equations of motion only through the substitution

$$t[i,f] \to t[i,f] - i\sum_{\alpha}\kappa^{\alpha}_f\ v^{\alpha}[i,f]. \tag{3.24}$$

Thus, the new equations of motion can be read off from Eq. (2.2) as

$$\begin{aligned}
\mathbf{g}^{-1}[i,m] &= (\boldsymbol{\mu} - \partial_{\tau_i} - \mathcal{V}_i)\ \delta[i,m] + (t[i,m] - i\sum_{\alpha} \kappa_m^{\alpha}\ v^{\alpha}[i,m])\ (1 - \lambda\gamma[i]) \\
&\quad + \lambda(t[i,\mathbf{j}] - i\sum_{\alpha} \kappa_{\mathbf{j}}^{\alpha}\ v^{\alpha}[i,\mathbf{j}])\ \xi^*.\mathbf{g}[\mathbf{j},\mathbf{n}].\Lambda_*[\mathbf{n},m;i], \\
\mu[i,m] &= (1 - \lambda\gamma[i])\delta[i,m] - \lambda(t[i,\mathbf{j}] - i\sum_{\alpha} \kappa_{\mathbf{j}}^{\alpha}\ v^{\alpha}[i,\mathbf{j}])\ \xi^*.\mathbf{g}[\mathbf{j},\mathbf{n}].\mathcal{U}_*[\mathbf{n},m;i].
\end{aligned} \tag{3.25}$$

Since there is no source derivative with respect to κ in the equations of motion and $v^{\alpha}[i,f]$ is of the same order in $\frac{1}{\sqrt{d}}$ as $t[i,f]$, all of the results derived in section 3.1 continue to hold after making the substitution in Eq. (3.24). In particular, we showed that $\mathbf{g}^{-1}[i,m]$ and $\mu[i,m]$ have the following form (Eq. (3.1)).

$$\begin{aligned}
\mathbf{g}^{-1}[i,m] &= (\boldsymbol{\mu} - \partial_{\tau_i} - \mathcal{V}_i)\ \delta[i,m] - \lambda\ \delta_{i,m}\ \chi_i[\tau_i,\tau_m] \\
&\quad + (t[i,m] - i\sum_{\alpha} \kappa_m^{\alpha}\ v^{\alpha}[i,m])\ (1 - \lambda\gamma[i]) \\
&\quad + \lambda\ (t_{i,m} - i\sum_{\alpha} \kappa_m^{\alpha}\ v_{i,m}^{\alpha})\ \Psi_i[\tau_i,\tau_m], \\
\mu[i,m] &= \delta[i,m](1 - \lambda\gamma[i]) + \lambda\ \delta_{i,m}\ \Psi_i[\tau_i,\tau_m],
\end{aligned} \tag{3.26}$$

where χ_i, Ψ_i, and $\gamma[i]$ have properties (a)-(c) of class L functions (sec.2.4), and are defined by Eqs. (3.1) through (3.4). We shall now further assume that they also satisfy property (d) (Eq. (2.8)) and show that this assumption is consistent with their definitions. This, in turn, will allow us to demonstrate the validity of Eq. (3.29).

Our task is then to show that χ_i, Ψ_i, and $\gamma[i]$, as defined in the last line of Eq. (3.2) and Eq. (3.4), satisfy Eq. (2.8). By Eq. (3.3), A_i and B_i satisfy Eq. (2.8) since

they inherit this property from χ_i, Ψ_i, and $\gamma[i]$. It remains to show that $\mathbf{g}_{x,x}[\tau_n,\tau_m]$ and $(t_{x,\mathbf{j}} - i\sum_\alpha \kappa^\alpha_{\mathbf{j}}(\tau_n)v^\alpha_{x,\mathbf{j}})\ \mathbf{g}_{\mathbf{j},x}[\tau_n,\tau_m]$ (the time indices are arbitrary) satisfy this equation.

Defining the notation $w_{i,f}(\tau_i) \equiv t_{i,f} - i\sum_\alpha \kappa^\alpha_f(\tau_i)\ v^\alpha_{i,f}$, and using (the κ source derivative version of) Eq. (2.4) as well as Eq. (3.26), we find that

$$\begin{aligned}
&\left(\frac{\delta}{\delta\kappa^\alpha_i} w_{x,\mathbf{j}}(\tau_n)\ \mathbf{g}_{\mathbf{j},x}[\tau_n,\tau_m]\right)_{\mathcal{A}\to 0} = -i\delta[\tau_i,\tau_n]v^\alpha_{x,i}\ \mathbf{g}_{i,x}[\tau_i,\tau_m] \\
&+it_{x,\mathbf{j}}\mathbf{g}_{\mathbf{j},\mathbf{a}}[\tau_n,\tau_\mathbf{a}](1-\lambda\gamma[\mathbf{a}]\delta[\tau_\mathbf{a},\tau_i]+\lambda\Psi_\mathbf{a}[\tau_\mathbf{a},\tau_i])v^\alpha_{\mathbf{a},i}g_{i,x}[\tau_i,\tau_m] \\
&+\lambda\ t_{x,\mathbf{j}}\mathbf{g}_{\mathbf{j},\mathbf{a}}[\tau_n,\tau_\mathbf{a}]\frac{\delta}{\delta\kappa^\alpha_i}\left(\gamma[\mathbf{a}]\delta[\tau_\mathbf{a},\tau_\mathbf{b}]-\Psi_\mathbf{a}[\tau_\mathbf{a},\tau_\mathbf{b}]\right)t_{\mathbf{a},\mathbf{b}}g_{\mathbf{b},x}[\tau_\mathbf{b},\tau_m] \\
&+\lambda\ t_{x,\mathbf{j}}\mathbf{g}_{\mathbf{j},\mathbf{a}}[\tau_n,\tau_\mathbf{a}]\frac{\delta}{\delta\kappa^\alpha_i}\left(\chi_\mathbf{a}[\tau_\mathbf{a},\tau_\mathbf{b}]\right)g_{\mathbf{a},x}[\tau_\mathbf{b},\tau_m],
\end{aligned} \tag{3.27}$$

where the RHS is also evaluated in the $\mathcal{A}\to 0$ limit. We now substitute this into Eq. (2.8) (with $s=0$). The last two terms must vanish by assumption (where $\mathbf{a}$ has taken the place of $\mathbf{x}$). The first term contains two paths from i to f, both via $\mathbf{x}$. Hence, this term must vanish in the large d limit unless $\mathbf{x}=i$ or $\mathbf{x}=f$. The former also vanishes since $v^\alpha_{i,i}=0$ while the latter must vanish due to the sum over $i-f$ and the odd parity of $v^\alpha_{i,f}$. The same reasoning applies to the second term except that in this term the $\mathbf{x}=i$ case vanishes by the odd parity of $v^\alpha_{i,f}$. Hence, we have shown that $(t_{x,\mathbf{j}} - i\sum_\alpha \kappa^\alpha_{\mathbf{j}}(\tau_n)v^\alpha_{x,\mathbf{j}})\ \mathbf{g}_{\mathbf{j},x}[\tau_n,\tau_m]$ satisfies Eq. (2.8) with $s=0$. A completely analogous argument shows that this is also the case for $\mathbf{g}_{x,x}[\tau_n,\tau_m]$. Using Eq. (3.5) and Eq. (3.6) (in particular the fact that the RHS is made up of the same objects as the LHS), the above argument can be used to show that the result holds for any value of s. Thus, we have demonstrated the self-consistency of our

ansatz (Eq. (2.8)).

Substituting Eq. (3.26) into Eq. (3.23), and using Eq. (2.8), we find that

$$\sum_{i-f} \Pi_{\alpha\beta}[i,f] = \sum_{i-f} Tr\left(\mathcal{G}[f,\mathbf{k}]v^{\alpha}[\mathbf{k},i]\mathcal{G}[i,\mathbf{j}]\ v^{\beta}[\mathbf{j},f^{+}]\right)_{\mathcal{A}\to 0}. \tag{3.28}$$

Substituting this equation into Eq. (3.20), the optical conductivity may be expressed as

$$\sigma^{\alpha\beta}(\omega) \;=\; \frac{2}{i\omega}\sum_{\vec{p},i\omega_p} \mathcal{G}(\vec{p},i\omega_p)v^{\alpha}_{\vec{p}}v^{\beta}_{\vec{p}}[\mathcal{G}(\vec{p},\omega+i\eta+i\omega_p)-\mathcal{G}(\vec{p},i\eta+i\omega_p)], \tag{3.29}$$

We now want to prove that this result holds to each order in λ. We do this via an inductive argument, in which we assume that through n^{th} order in λ, $\left(\frac{\delta}{\delta\kappa_i^{\alpha}}L_x\right)^{(n)}_{\mathcal{A}\to 0}$ (where L_i can be Ψ_i, χ_i, or $\gamma[i]$) satisfies a certain explicit form (Eq. (3.30)), and then show that this form holds for $n+1^{st}$ order. We then plug Eq. (3.26) into $\sum_{i-f}\Pi_{\alpha\beta}[i,f]$ (Eq. (3.23)), and use the explicit form of $\left(\frac{\delta}{\delta\kappa_i^{\alpha}}L_x\right)^{(n)}_{\mathcal{A}\to 0}$ to simplify the resulting expressions, thereby proving Eq. (3.28) and Eq. (3.29) to each order in λ.

For the reason given below Eq. (3.25), we are free to use any of the results from section 3.1, after making the substitution in Eq. (3.24). **We define** X_i to be a product of local functions of the type in Eq. (3.7) (i.e. $X_i = (R_i)^m$) **and** $Y_{i,f}$ to be a **proxy** for either $\mathbf{g}_{i,f}[\tau_n,\tau_m]$ or $t_{i,\mathbf{j}}\mathbf{g}_{\mathbf{j},f}[\tau_n,\tau_m]$ where the time indices are again arbitrary. **Inductive hypothesis**: Through n^{th} order in λ, the κ source derivative of the objects Ψ_i, χ_i, and $\gamma[i]$

(denoted below by the generic symbol L_i) can be written as

$$\left(\tfrac{\delta}{\delta\kappa_i^\alpha}L_x\right)^{(n)}_{\mathcal{A}\to 0} = \lambda^n\ X_x Y_{x,\mathbf{x}_1} X_{\mathbf{x}_1} Y_{\mathbf{x}_1,\mathbf{x}_2} X_{\mathbf{x}_2} \dots X_{\mathbf{x}_{m-1}} Y_{\mathbf{x}_{m-1},\mathbf{x}_m} X_{\mathbf{x}_m} v^\alpha_{\mathbf{x}_m,i}\ Y_{i,\mathbf{x}_{m-1}} X_{\mathbf{x}_{m-1}} \dots X_{\mathbf{x}_1} Y_{\mathbf{x}_1,x} X_x, \tag{3.30}$$

where the number m is arbitrary. In the base case of zeroth order, the objects Ψ_i, χ_i, and $\gamma[i]$ are

$$\begin{aligned}
&\Psi_i^{(0)}[\tau_i,\tau_m] = 0; \quad \gamma^{(0)}[i] = \mathbf{g}^{(k)}[i,i];\\
&\chi_i^{(0)}[\tau_i,\tau_m] = -(t_{i,\mathbf{j}} - i\sum_\alpha \kappa^\alpha_{\mathbf{j}}(\tau_i) v^\alpha_{i\mathbf{j}})\ \xi^*.\mathbf{g}_{\mathbf{j},i}[\tau_i,\tau_i]\delta[\tau_i,\tau_m].
\end{aligned} \tag{3.31}$$

We note that $\left(\tfrac{\delta}{\delta\kappa_i^\alpha} w_{x,\mathbf{j}}(\tau_n)\ \mathbf{g}_{\mathbf{j},x}[\tau_n,\tau_m]\right)^{(l)}_{\mathcal{A}\to 0}$ is given by Eq. (3.27) with the appropriate objects on the RHS evaluated to the appropriate order in λ. An analogous formula holds for $\left(\tfrac{\delta}{\delta\kappa_i^\alpha}\mathbf{g}_{x,x}[\tau_n,\tau_m]\right)^{(l)}_{\mathcal{A}\to 0}$. Using these formulas with $l = 0$ shows that the hypothesis is satisfied for the base case.

We now prove the inductive step. Eq. (3.7) continues to hold with $t_{i,\mathbf{j}} \to w_{i,\mathbf{j}}(\tau_n)$ (the time index is again arbitrary). Therefore, using the notation $\widetilde{R}_i = [R_i]_{t_{i,\mathbf{j}}\to w_{i,\mathbf{j}}(\tau_n)}$, we may write

$$\left(\frac{\delta}{\delta\kappa_i^\alpha}L_x\right)^{(n+1)}_{\mathcal{A}\to 0} = \sum_{r=0}^{n+1}\lambda^r \left(\frac{\delta}{\delta\kappa_i^\alpha}(\widetilde{R}_x)^m\right)^{(n+1-r)}_{\mathcal{A}\to 0}. \tag{3.32}$$

Substituting the formulas for $\left(\tfrac{\delta}{\delta\kappa_i^\alpha} w_{x,\mathbf{j}}(\tau_n)\ \mathbf{g}_{\mathbf{j},x}[\tau_n,\tau_m]\right)^{(l)}_{\mathcal{A}\to 0}$ and $\left(\tfrac{\delta}{\delta\kappa_i^\alpha}\mathbf{g}_{x,x}[\tau_n,\tau_m]\right)^{(l)}_{\mathcal{A}\to 0}$

(Eq. (3.27)) for $l \leq n+1$ into Eq. (3.32), and using the inductive hypothesis, shows that $\left(\frac{\delta}{\delta\kappa_i^\alpha}\Psi_x\right)^{(n+1)}_{\mathcal{A}\to 0}$, $\left(\frac{\delta}{\delta\kappa_i^\alpha}\chi_x\right)^{(n+1)}_{\mathcal{A}\to 0}$, and $\left(\frac{\delta}{\delta\kappa_i^\alpha}\gamma[x]\right)^{(n+1)}_{\mathcal{A}\to 0}$ all have the desired form (Eq. (3.30)). Thus, Eq. (3.30) holds to all orders in λ.

Substituting Eq. (3.26) into $\sum_{i-f}\Pi_{\alpha\beta}[i,f]$ (Eq. (3.23)), and using Eq. (3.30), the only non vanishing terms are those which involve a derivative of the explicit factor $(t_{\mathbf{x},\mathbf{y}} - i\sum_\alpha \kappa^\alpha_{\mathbf{y}}\, v^\alpha_{\mathbf{x},\mathbf{y}})$ from Eq. (3.26). The other terms vanish due to the following reasoning. Upon substituting Eq. (3.30), in each of these terms there are two paths from i to f, both of which pass through the point $\mathbf{x}$ as well as the points $\mathbf{x}_1 \ldots \mathbf{x}_{m-1}$ in Eq. (3.30). Hence, in the large d limit, all of these points must be chosen to be either i or f for these terms to be non vanishing. Then, if we choose $\mathbf{x}_{m-1} = i$, the term vanishes due to parity, while if we choose $\mathbf{x}_{m-1} = f$, the term vanishes due to parity combined with the sum $\sum_{i-f}$. Therefore, after making these simplifications, we find that Eq. (3.28) and consequently Eq. (3.29) hold to each order in λ.

3.4 $O\left(\lambda^2\right)$ theory in the limit of large dimensions

To obtain self-consistent integral equations to any order in λ for the objects $\mathbf{g}^{-1}[i,f]$ and $\mu[i,f]$, we expand Eqs. (3.1) through (3.4) iteratively in λ, and set the sources to zero. Once the sources are set to zero, the system becomes translationally invariant in both space and time and we may express the equations in momentum/frequency space. Using the definitions

$$\mathbf{g}_{loc,m}(i\omega_k) \equiv \sum_{\vec{k}} \mathbf{g}(k)\epsilon^m_{\vec{k}}, \tag{3.33}$$

$$I_{m_1m_2m_3}(i\omega_k) \equiv -\sum_{\omega_p,\omega_q} \mathbf{g}_{loc,m_1}(i\omega_q)\mathbf{g}_{loc,m_2}(i\omega_p)\mathbf{g}_{loc,m_3}(i\omega_q + i\omega_p - i\omega_k), \tag{3.34}$$

the resulting equations to $O\left(\lambda^2\right)$ are:

$$a_{\mathcal{G}} \equiv 1 - \lambda\frac{n}{2} + \lambda^2\frac{n^2}{4}, \tag{3.35}$$

$$\mathbf{g}^{-1}(k) = i\omega_k + \boldsymbol{\mu'} - a_{\mathcal{G}}\ (\varepsilon_k - \frac{u_0}{2}) - \lambda\left(\epsilon_{\vec{k}} - \frac{u_0}{2}\right)\Psi(i\omega_k) - \lambda\chi(i\omega_k), \tag{3.36}$$

$$\mu(i\omega_k) = a_{\mathcal{G}} + \lambda\Psi(i\omega_k), \tag{3.37}$$

$$\boldsymbol{\mu'} = \boldsymbol{\mu} - u_0(\lambda\frac{n}{2} - \lambda^2\frac{n^2}{8}) + \lambda\sum_p \varepsilon_p\mathbf{g}(p) - a_{\mathcal{G}}\frac{u_0}{2}, \tag{3.38}$$

$$\Psi(i\omega_k) = -\lambda u_0 I_{000}(i\omega_k) + 2\lambda I_{010}(i\omega_k), \tag{3.39}$$

$$\chi(i\omega_k) = -\frac{u_0}{2}\Psi(i\omega_k) - u_0\lambda I_{001}(i\omega_k) + 2\lambda I_{011}(i\omega_k). \tag{3.40}$$

Before solving the equations, one must set $\lambda = 1$. The two Lagrange multipliers $\boldsymbol{\mu}$ and u_0 are determined by the two sum rules:

$$\sum_k \mathbf{g}(k) = \frac{n}{2}; \quad \sum_k \mathcal{G}(k) = \frac{n}{2}. \tag{3.41}$$

The objects $\mathbf{g}_{loc,m}(i\omega_k)$ are given by an appropriate integral over the non-interacting density of states of a function composed of the two self energies $\chi(i\omega_k)$ and $\Psi(i\omega_k)$ and the energy ϵ (Eq. (3.36)). Therefore, these constitute a self-consistent set of equations for the two self energies. These equations have been solved numerically and compared to DMFT calculations in Ref. ([9]).

Chapter 4

Anderson Model

A word is needed at this point on the notation used, since similar looking symbols represent quite different objects in the t-J model and the AIM. We use the functions $\mathcal{G}(\{\tau_j\}), \mathbf{g}(\{\tau_j\}), \mu(\{\tau_j\})$ or $\mathcal{G}(\{i\omega_j\}), \mathbf{g}(\{i\omega_j\}), \mu(\{i\omega_j\})$ and the related vertex functions for the impurity site of the AIM as well, but distinguish them from the t-J model variables by dropping the spatial or momentum labels. Therefore in an equation such as Eq. (4.26), the object on the left (right) hand side corresponds to the t-J model (AIM).

4.1 Equations of Motion for Anderson Model

In DMFT[23, 24], the local Green's function of the infinite-dimensional finite-U Hubbard model is mapped onto the impurity Green's function of the finite-U AIM, with a self-consistently determined set of parameters. Using the ECFL equations of motion for both models, we show that the same mapping can be made between the infinite-dimensional t-J model and the infinite-U AIM. Further, we show that this mapping also extends to

the auxiliary Green's function $\mathbf{g}$, and the caparison factor μ individually. In this section, we briefly review the ECFL theory of the AIM[11], and we establish the mapping in the following section.

Consider the AIM in the limit $U \to \infty$ which has the following Hamiltonian.

$$H = \sum_{\sigma} \epsilon_d X^{\sigma\sigma} + \sum_{k\sigma} \widetilde{\epsilon}_k n_{k\sigma} + \sum_{k\sigma} (V_k \; X^{\sigma 0} \; c_{k\sigma} + V_k^* \; c_{k\sigma}^\dagger \; X^{0\sigma}), \tag{4.1}$$

where we have set the Fermi energy of the conduction electrons to be zero. The impurity Green's function is given by the following expression.

$$\mathcal{G}_{\sigma_i\sigma_f}[\tau_i, \tau_f] = -\langle\langle \; X^{0\sigma_i}(\tau_i) \; X^{\sigma_f 0}(\tau_f)\rangle\rangle. \tag{4.2}$$

The ECFL solution of the Anderson model is presented in Ref. ([11]). The impurity Green's function is factored into the auxiliary Green's function and the caparison factor.

$$\mathcal{G}[\tau_i, \tau_f] = \mathbf{g}[\tau_i, \tau_{\mathbf{j}}] \; .\mu[\tau_{\mathbf{j}}, \tau_f]. \tag{4.3}$$

The equations of motion for $\mathbf{g}$ and μ can be written as

$$\begin{aligned} (\partial_{\tau_i} + \epsilon_d + \mathcal{V}(\tau_i))\mathbf{g}[\tau_i, \tau_f] &= -\delta(\tau_i - \tau_f) - (1 - \lambda\gamma[\tau_i]).\Delta[\tau_i, \tau_{\mathbf{j}}].\mathbf{g}[\tau_{\mathbf{j}}, \tau_f] \\ &\quad -\lambda \; \xi^* \Delta[\tau_i, \tau_{\mathbf{j}}].\mathbf{g}[\tau_{\mathbf{j}}, \tau_{\mathbf{x}}].\Lambda_*[\tau_{\mathbf{x}}, \tau_{\mathbf{y}}; \tau_i].\mathbf{g}[\tau_{\mathbf{y}}, \tau_f], \end{aligned} \tag{4.4}$$

$$\mu[\tau_i,\tau_f] = \delta(\tau_i-\tau_f)(\mathbb{1}-\lambda\gamma[\tau_i]) + \lambda\ \xi^*.\Delta[\tau_i,\tau_{\mathbf{j}}].\mathbf{g}[\tau_{\mathbf{j}},\tau_{\mathbf{x}}].\mathcal{U}_*[\tau_{\mathbf{x}},\tau_f;\tau_i], \tag{4.5}$$

where the conduction band enters through the ($\mathcal{V}$ independent) function

$$\Delta[\tau_i,\tau_f] = -\mathbb{1}\sum_k |V_k|^2(\partial_{\tau_i}+\widetilde{\epsilon}_k)^{-1}\delta(\tau_i-\tau_f). \tag{4.6}$$

We have also made use of the following definitions:

$$\begin{aligned}
&\Lambda[\tau_n,\tau_m;\tau_i] = -\frac{\delta}{\delta\mathcal{V}(\tau_i)}\mathbf{g}^{-1}[\tau_n,\tau_m]; \quad \mathcal{U}[\tau_n,\tau_m;\tau_i] = \frac{\delta}{\delta\mathcal{V}(\tau_i)}\mu[\tau_n,\tau_m];\\
&\gamma[\tau_i] = \mu^{(k)}[\tau_{\mathbf{n}},\tau_i^+].\mathbf{g}^{(k)}[\tau_i,\tau_{\mathbf{n}}].
\end{aligned} \tag{4.7}$$

4.2 Mapping of t-J model onto Anderson model in infinite dimensions

Now let us consider the t-J model in the limit of infinite dimensions. Inverting Eq. (2.2), the equations of motion for $\mathbf{g}_{i,i}[\tau_i,\tau_f]$ and $\mu_{i,i}[\tau_i,\tau_f]$ are

$$\begin{aligned}
(\partial_{\tau_i}-\mu+\mathcal{V}_i(\tau_i))\ \mathbf{g}_{i,i}[\tau_i,\tau_f] \ &= \ -\delta(\tau_i-\tau_f) + (1-\lambda\gamma[i]).\ t_{i,\mathbf{j}}\ \mathbf{g}_{\mathbf{j},i}[\tau_i,\tau_f]\\
&\quad +\lambda\ t_{i,\mathbf{j}}\ \xi^*.\mathbf{g}_{\mathbf{j},i}[\tau_i,\tau_{\mathbf{x}}].A_{i,*}[\tau_{\mathbf{x}},\tau_{\mathbf{y}};\tau_i].\mathbf{g}_{i,i}[\tau_{\mathbf{y}},\tau_f]\\
&\quad +\ \lambda\ t_{i,\mathbf{j}}\ \xi^*.\mathbf{g}_{\mathbf{j},i}[\tau_i,\tau_{\mathbf{x}}].B_{i,*}[\tau_{\mathbf{x}},\tau_{\mathbf{y}};\tau_i].\ t_{i,\mathbf{y}}\ \mathbf{g}_{\mathbf{y},i}[\tau_{\mathbf{y}},\tau_f],
\end{aligned} \tag{4.8}$$

$$\mu_{i,i}[\tau_i,\tau_f] = (1-\lambda\gamma[i])\delta(\tau_i-\tau_f) + \lambda\ t_{i,\mathbf{j}}\ \xi^*.\mathbf{g}_{\mathbf{j},i}[\tau_i,\tau_{\mathbf{x}}].B_{i,*}[\tau_{\mathbf{x}},\tau_f;\tau_i]. \tag{4.9}$$

By mapping $\mathbf{g}_{i,i}[\tau_i,\tau_f]$ and $\mu_{i,i}[\tau_i,\tau_f]$ onto $\mathbf{g}[\tau_i,\tau_f]$ and $\mu[\tau_i,\tau_f]$ of the AIM, we would like to show that the equations of motion of the AIM (Eqs. (4.4) and (4.5)) and those of the infinite dimensional t-J model (Eqs. (4.8) and (4.9)) map onto each other. To do this, we need the analog of the object $\mathbf{g}^{-1}[\tau_i,\tau_f]$ of the AIM in the t-J model. We denote this new object by $\mathbf{g}^{-1}_{loc,i}[\tau_i,\tau_f]$ and define it to be the temporal inverse of the local auxiliary Green's function.

$$\mathbf{g}_{i,i}[\tau_i,\tau_{\mathbf{j}}].\mathbf{g}^{-1}_{loc,i}[\tau_{\mathbf{j}},\tau_f] = \delta(\tau_i-\tau_f). \tag{4.10}$$

Note that $\mathbf{g}^{-1}_{loc,i}[\tau_i,\tau_f] \neq \mathbf{g}^{-1}_{i,i}[\tau_i,\tau_f]$. We also define the corresponding vertex.

$$\Lambda_{loc,i}[\tau_n,\tau_m;\tau_i] = -\frac{\delta}{\delta\mathcal{V}_i(\tau_i)}\mathbf{g}^{-1}_{loc,i}[\tau_n,\tau_m]. \tag{4.11}$$

We now make use of the following identity.

$$\Lambda_{loc,i}[\tau_x,\tau_{\mathbf{y}};\tau_i].\mathbf{g}_{i,i}[\tau_{\mathbf{y}},\tau_f] = A_i[\tau_x,\tau_{\mathbf{y}};\tau_i].\mathbf{g}_{i,i}[\tau_{\mathbf{y}},\tau_f] + B_i[\tau_x,\tau_{\mathbf{y}};\tau_i].t_{i,\mathbf{y}}\ \mathbf{g}_{\mathbf{y},i}[\tau_{\mathbf{y}},\tau_f]. \tag{4.12}$$

This identity is easily proven by considering $\frac{\delta}{\delta\mathcal{V}_i(\tau_i)}\mathbf{g}_{i,i}[\tau_x,\tau_f]$.

$$\frac{\delta}{\delta\mathcal{V}_i(\tau_i)}\mathbf{g}_{i,i}[\tau_x,\tau_f] = \mathbf{g}_{i,i}[\tau_x,\tau_{\mathbf{j}}]\Lambda_{loc,i}[\tau_{\mathbf{j}},\tau_{\mathbf{y}};\tau_i]\mathbf{g}_{i,i}[\tau_{\mathbf{y}},\tau_f]. \tag{4.13}$$

The LHS can also be expressed as

$$\frac{\delta}{\delta \mathcal{V}_i(\tau_i)} \mathbf{g}_{i,i}[\tau_x, \tau_f] = \mathbf{g}_{i,i}[\tau_x, \tau_{\mathbf{j}}].(A_i[\tau_{\mathbf{j}}, \tau_{\mathbf{y}}; \tau_i].\mathbf{g}_{i,i}[\tau_{\mathbf{y}}, \tau_f] + B_i[\tau_{\mathbf{j}}, \tau_{\mathbf{y}}; \tau_i].t_{i,\mathbf{y}}\ \mathbf{g}_{\mathbf{y},i}[\tau_{\mathbf{y}}, \tau_f]). \tag{4.14}$$

Left multiplying the above 2 equations by $\mathbf{g}^{-1}_{loc,i}$, we recover the identity Eq. (4.12). Substituting this identity into Eq. (4.8), we obtain

$$\begin{aligned}(\partial_{\tau_i} - \mu + \mathcal{V}_i(\tau_i))\mathbf{g}_{i,i}[\tau_i, \tau_f] &= -\delta(\tau_i - \tau_f) + (1 - \lambda\gamma[i]).\ t_{i,\mathbf{j}}\mathbf{g}_{\mathbf{j},i}[\tau_i, \tau_f] \\ &\quad +\lambda\ t_{i,\mathbf{j}}\ \xi^*.\mathbf{g}_{\mathbf{j},i}[\tau_i, \tau_{\mathbf{x}}].\Lambda_{loc,i*}[\tau_{\mathbf{x}}, \tau_{\mathbf{y}}; \tau_i].\mathbf{g}_{i,i}[\tau_{\mathbf{y}}, \tau_f].\end{aligned} \tag{4.15}$$

We are now ready to map the t-J model onto the Anderson model. To do this, we map the local objects $\mathbf{g}_{i,i}[\tau_i, \tau_f]$ and $\mu_{i,i}[\tau_i, \tau_f]$ of the t-J model to the objects $\mathbf{g}[\tau_i, \tau_f]$ and $\mu[\tau_i, \tau_f]$ of the Anderson model. We also map μ to $-\epsilon_d$. The following mappings also follow as a consequence of these.

$$\gamma[i] \rightarrow \gamma[\tau_i]; \quad \Lambda_{loc,i}[\tau_n, \tau_m; \tau_i] \rightarrow \Lambda[\tau_n, \tau_m; \tau_i]; \quad B_i[\tau_n, \tau_m; \tau_i] \rightarrow -\mathcal{U}[\tau_n, \tau_m; \tau_i]. \tag{4.16}$$

Comparing Eq. (4.15) with Eq. (4.4) and Eq. (4.9) with Eq. (4.5), we see that the equations

of motion map onto each other if the following constraint is satisfied.

$$t_{i,\mathbf{j}}\ \mathbf{g}_{\mathbf{j},i}[\tau_i,\tau_f] = -\Delta[\tau_i,\tau_\mathbf{j}].\mathbf{g}[\tau_\mathbf{j},\tau_f]. \tag{4.17}$$

4.3 Mapping to each order in λ

The $O(\lambda^2)$ equations for the infinite-dimensional t-J model and infinite-U AIM are solved numerically in Ref. ([9]) and Ref. ([11]) respectively. This can in principle be done to higher orders in λ as well, and it is therefore interesting to know if the mapping from the previous section holds to each order in λ. We show that it does, and give a simple prescription for obtaining the ECFL integral equations for one model from those of the other one (Eq. (4.21)).

We review the λ expansion for the Anderson model from Ref. ([11]). There, Eq. (4.4) and Eq. (4.5) are written as

$$\begin{aligned}\mathbf{g}^{-1}[\tau_i,\tau_f] &= -(\partial_{\tau_i}+\epsilon_d+\mathcal{V}(\tau_i))\delta(\tau_i-\tau_f)-(1-\lambda\gamma[\tau_i]).\Delta[\tau_i,\tau_f] \\ &\quad -\lambda\xi^*\Delta[\tau_i,\tau_\mathbf{j}].\mathbf{g}[\tau_\mathbf{j},\tau_\mathbf{x}].\Lambda_*[\tau_\mathbf{x},\tau_f;\tau_i],\end{aligned} \tag{4.18}$$

$$\mu[\tau_i,\tau_f] = \delta(\tau_i-\tau_f)(\mathbb{1}-\lambda\gamma[\tau_i])+\lambda\xi^*.\Delta[\tau_i,\tau_\mathbf{j}].\mathbf{g}[\tau_\mathbf{j},\tau_\mathbf{x}].\mathcal{U}_*[\tau_\mathbf{x},\tau_f;\tau_i]. \tag{4.19}$$

The λ expansion is obtained in the same way as for the t-J model, by iterating the equations in $\mathbf{g}^{-1}$ and μ and keeping track of explicit powers of λ. The details to $O(\lambda^2)$

can be found in Ref. ([11]). To relate this to the λ expansion for the infinite-dimensional t-J model, recall from Eq. (3.7) that to each order in λ, Ψ_i, χ_i, $\gamma[i]$, A_i, and B_i can be written as a product of the functions $\mathbf{g}_{i,i}[\tau_n,\tau_m]$ and $t_{i,\mathbf{j}}\mathbf{g}_{\mathbf{j},i}[\tau_n,\tau_m]$. We can now state our **inductive hypothesis**: through n^{th} order in λ, the λ expansion for the Anderson model has the form

$$\begin{aligned}
\mathbf{g}^{-1}[\tau_i,\tau_m] &= -(\partial_{\tau_i}+\epsilon_d+\mathcal{V}(\tau_i))\ \delta[\tau_i,\tau_m]-\lambda\ \chi[\tau_i,\tau_m] \\
&\quad -(1-\lambda\gamma[\tau_i])\Delta[\tau_i,\tau_m]-\lambda\ \Psi[\tau_i,\tau_{\mathbf{j}}]\Delta[\tau_{\mathbf{j}},\tau_m], \\
\mu[\tau_i,\tau_m] &= \delta[\tau_i,\tau_m](1-\lambda\gamma[\tau_i])+\ \lambda\Psi[\tau_i,\tau_m], \\
\Lambda[\tau_n,\tau_m;\tau_i] &= \ A[\tau_n,\tau_m;\tau_i]-\ B[\tau_n,\tau_{\mathbf{j}};\tau_i]\Delta[\tau_{\mathbf{j}},\tau_m], \\
\mathcal{U}[\tau_n,\tau_m;\tau_i] &= -\ B[\tau_n,\tau_m;\tau_i],
\end{aligned} \tag{4.20}$$

where through n^{th} order in λ, the objects $A[\tau_n,\tau_m;\tau_i]$ and $B[\tau_n,\tau_m;\tau_i]$, and through $n-1^{st}$ order in λ, the objects $\gamma[\tau_i]$, $\chi[\tau_i,\tau_m]$, and $\Psi[\tau_i,\tau_m]$, can be obtained from their infinite dimensional t-J model counterparts via the substitution

$$\mathbf{g}_{i,i}[\tau_n,\tau_m]\to\mathbf{g}[\tau_n,\tau_m];\quad \boldsymbol{\mu}\to-\epsilon_d;\quad t_{i,\mathbf{j}}\mathbf{g}_{\mathbf{j}i}[\tau_n,\tau_m]\to-\Delta[\tau_n,\tau_{\mathbf{j}}].\mathbf{g}[\tau_{\mathbf{j}},\tau_m]. \tag{4.21}$$

We first examine the base case of zeroth order.

$$A^{(0)}[\tau_n,\tau_m;\tau_i]=\delta[\tau_i,\tau_n]\delta[\tau_i,\tau_m];\ B^{(0)}[\tau_n,\tau_m;\tau_i]=0. \tag{4.22}$$

Comparing with Eq. (3.8), the hypothesis clearly holds. We now prove the inductive step. Eq. (4.7) together with Eq. (4.18) through Eq. (4.20) implies the following:

$$\begin{aligned}
\chi^{(n)}[\tau_n,\tau_m] &= \xi^*\Delta[\tau_n,\tau_{\mathbf{j}}].\mathbf{g}[\tau_{\mathbf{j}},\tau_{\mathbf{x}}].A_*^{(n)}[\tau_{\mathbf{x}},\tau_m;\tau_n],\\
\Psi^{(n)}[\tau_n,\tau_m] &= -\xi^*\Delta[\tau_n,\tau_{\mathbf{j}}].\mathbf{g}[\tau_{\mathbf{j}},\tau_{\mathbf{x}}].B_*^{(n)}[\tau_{\mathbf{x}},\tau_m;\tau_n],\\
A^{(n+1)}[\tau_n,\tau_m;\tau_i] &= \lambda\left(\frac{\delta}{\delta\mathcal{V}(\tau_i)}\chi[\tau_n,\tau_m]\right)^{(n)},\\
B^{(n+1)}[\tau_n,\tau_m;\tau_i] &= \lambda\ \delta[\tau_n,\tau_m]\left(\frac{\delta}{\delta\mathcal{V}(\tau_i)}\gamma[\tau_n]\right)^{(n)} - \lambda\left(\frac{\delta}{\delta\mathcal{V}(\tau_i)}\Psi[\tau_n,\tau_m]\right)^{(n)},\\
\gamma^{(n)}[\tau_i] &= -\lambda\ \gamma^{(k)(n-1)}[\tau_i]\mathbf{g}^{(k)}[\tau_i,\tau_i] + \lambda\ \Psi^{(k)(n-1)}[\tau_{\mathbf{j}},\tau_i]\mathbf{g}^{(k)}[\tau_i,\tau_{\mathbf{j}}]. \quad (4.23)
\end{aligned}$$

Comparing with Eq. (3.9), we see that $\chi^{(n)}[\tau_n,\tau_m]$, $\Psi^{(n)}[\tau_n,\tau_m]$, and $\gamma^{(n)}[\tau_i]$ have the desired form. We also note that

$$\left(\frac{\delta}{\delta\mathcal{V}(\tau_r)}\mathbf{g}[\tau_i,\tau_m]\right)^{(l)} = \mathbf{g}[\tau_i,\tau_{\mathbf{x}}](A^{(l)}[\tau_{\mathbf{x}},\tau_{\mathbf{y}};\tau_r] - B^{(l)}[\tau_{\mathbf{x}},\tau_{\mathbf{j}};\tau_r]\Delta[\tau_{\mathbf{j}},\tau_{\mathbf{y}}])\mathbf{g}[\tau_{\mathbf{y}},\tau_m]. \quad (4.24)$$

Comparing this with Eq. (3.5) and Eq. (3.6), we see that by the inductive hypothesis, the mapping Eq. (4.21) continues to hold through order $l \leq n$ even after both sides have been acted on with a functional derivative. Furthermore, in evaluating $A^{(n+1)}[\tau_n,\tau_m;\tau_i]$ and $B^{(n+1)}[\tau_n,\tau_m;\tau_i]$ using Eq. (4.23), we will at most need to set $l = n$ in Eq. (4.24). Finally, comparing Eq. (4.23) with Eq. (3.10), we see that $A^{(n+1)}[\tau_n,\tau_m;\tau_i]$ and $B^{(n+1)}[\tau_n,\tau_m;\tau_i]$ have the desired form. Thus, we have proven our inductive hypothesis.

Setting the sources to zero, and Fourier transforming Eq. (4.20), we may write

$(\lambda \to 1,\, \gamma[\tau_i] \to \frac{n_d}{2} \equiv \frac{n}{2})$

$$\begin{aligned} \mathbf{g}^{-1}(i\omega_k) &= i\omega_k - \epsilon_d - (1-\frac{n}{2})\Delta(i\omega_k) - \chi(i\omega_k) - \Delta(i\omega_k)\Psi(i\omega_k), \\ \mu(i\omega_k) &= 1 - \frac{n}{2} + \Psi(i\omega_k). \end{aligned} \tag{4.25}$$

Comparing with Eq. (3.14), it immediately follows that under the mapping Eq. (4.21), $\mu_{i,i}(i\omega_k) \to \mu(i\omega_k)$. Furthermore, multiplying both sides of the equation for $\mathbf{g}^{-1}(k)$ by $\mathbf{g}(k)$, summing over $\vec{k}$, and using the mapping Eq. (4.21), it follows that $\mathbf{g}_{i,i}(i\omega_k) \to \mathbf{g}(i\omega_k)$. Therefore, the ECFL solution of the infinite dimensional t-J model maps onto the ECFL solution of the AIM to each order in λ as long as the following self-consistency condition is satisfied.

$$\sum_{\vec{k}} \epsilon_{\vec{k}} \mathbf{g}(k) = \sum_{\vec{k}} \frac{|V_{\vec{k}}|^2}{i\omega_n - \widetilde{\epsilon_{\vec{k}}}} \mathbf{g}(i\omega_k). \tag{4.26}$$

This mapping and self-consistency condition can be understood by referring back to DMFT. In DMFT[24], the physical Green's function $\mathcal{G}_{i,f}(i\omega_k)$ is determined for any separation of i and f by the local green's function $G_{i,i}(i\omega_k)$ or equivalently the local self energy $\Sigma(i\omega_k)$. The impurity Green's function of the Anderson model $\mathcal{G}(i\omega_k)$ can be set equal to $G_{i,i}(i\omega_k)$ as long as $\widetilde{\varepsilon_k}$ and V_k satisfy a self-consistency condition relating them to $\mathcal{G}(i\omega_k)$ (See Eqs.(13) and (15) of Ref. ([24])). In the ECFL mapping, the auxiliary Green's function $\mathbf{g}_{i,f}(i\omega_k)$ is determined for any separation of i and f by the local auxiliary green's function $\mathbf{g}_{i,i}(i\omega_k)$ and by the local caparison factor $\mu_{i,i}(i\omega_k)$, or equivalently by the two local self energies $\Psi(i\omega_k)$ and $\chi(i\omega_k)$. $\mu_{i,f}(i\omega_k)$ is itself local and related simply to $\Psi(i\omega_k)$. The impurity

auxiliary Green's function of the Anderson model $\mathbf{g}(i\omega_k)$ can be set equal to $\mathbf{g}_{i,i}(i\omega_k)$ and the caparison factor of the Anderson model $\mu(i\omega_k)$ set equal to $\mu_{i,i}(i\omega_k)$ as long as $\widetilde{\varepsilon_k}$ and V_k satisfy the self-consistency condition Eq. (4.26). We now show that Eq. (4.26) can be put into the form of Eqs. (13) and (15) of Ref. ([24]). Using Eq. (3.14) the LHS can be written as

$$\sum_{\vec{k}} \epsilon_{\vec{k}} \mathbf{g}(k) = \frac{-1}{1 - \frac{n}{2} + \Psi(i\omega_k)} [1 - (i\omega_k + \boldsymbol{\mu} - \chi(i\omega_k))\mathbf{g}(i\omega_k)]. \tag{4.27}$$

Using Eqs. (0.9), (0.5), (3.14), (3.17) and the relation $\mathcal{G}(i\omega_k) = \mathbf{g}(i\omega_k).\mu(i\omega_k)$, the above equation becomes

$$\Sigma_D(i\omega_k) + \frac{1}{\mathcal{G}(i\omega_k)} - (i\omega_k + \boldsymbol{\mu}) = -\sum_{\vec{k}} \epsilon_{\vec{k}} \mathbf{g}(k) \frac{1}{\mathbf{g}(i\omega_k)}. \tag{4.28}$$

Substituting Eq. (4.26) into the RHS of the above equation, we recover Eqs.(13) and (15) from Ref. ([24]).

Chapter 5

Conclusion

In this chapter, we provide a detailed analysis of the simplifications arising from the large dimensionality limit of the t-J model, and have given the first few terms in the λ series that leads to practically usable results. It is clear that the formal result of a local Dysonian self energy is already implied by the large d results for the Hubbard model reviewed in Ref. ([24]), if we take the limit of infinite U; that is indeed another description of the model studied here. However it must be kept in mind that the present calculation starts with the infinite U limit already taken, and thus provides a non trivial check on the uniqueness of the limit of $U \to \infty$ and $d \to \infty$, i.e. its independence on the order of these two limits. Also the present work uses the novel ECFL methodology that rests on a different set of tools from the ones usually used to study the Hubbard model and its large dimensional limit. We use the Schwinger equations of motion, as opposed to the usual Feynman-Wick theory, and we have obtained analytical results that do not rely on the Wick's theorem.

Summarizing, we have considered the ECFL theory for the t-J model ($J = 0$)

by establishing the simplifications that arise in the equations of motion in the limit of large dimensions. The auxiliary Green's function $\mathbf{g}(k)$ and the caparison factor $\mu(k)$ can be written in terms of two local self energies $\Psi(i\omega_k)$ and $\chi(i\omega_k)$ as in Eq. (3.14). This insight into the structural form of the physical Green's function $\mathcal{G}(k)$ has been used in Ref. ([9]), to benchmark and compare the ECFL and DMFT calculations. The ECFL integral equations in the large d limit, derived here to $O(\lambda^2)$, have been solved numerically in Ref. ([9]), and their solution compares favorably with DMFT results. It can be seen explicitly from these equations that Eq. (3.14) holds to second order in λ, with $\Psi(i\omega_k)$ and $\chi(i\omega_k)$ written as a product of the functions $\mathbf{g}_{loc,m}(i\omega_k)$ (Eq. (3.33)) with $m = 0$ or $m = 1$. This continues to hold to each order in λ. We have analyzed the optical conductivity and have shown that it is given by Eq. (3.29) in general and to each order in λ. We have separately also studied the ECFL theory of the infinite-U AIM[11], and have shown that there is a mapping between the ECFL of the infinite dimensional t-J model and the ECFL of the AIM with a self-consistently determined set of parameters (Eq. (4.26)). This mapping holds to each order in λ and there is a simple prescription for obtaining the ECFL integral equations for one model from those of the other (Eq. (4.21)).

In conclusion, this provides a solid foundation for the study of the t-J model, and in particular for the ECFL formalism, in the limit of infinite dimensions, by providing exact statements about the k dependence of the self energies, the absence of vertex corrections in computing the conductivity, and finally in yielding a systematic expansion in the parameter λ that enables a quantitative comparison with other methods as in Ref. ([9]).

Part III

ECFL Theory of Anderson Impurity Model

Chapter 6

ECFL equations for the Anderson Impurity Model

6.1 Model and Equations for the Green's Function

We consider the Anderson impurity model in the limit $U \to \infty$ given by the following Hamiltonian:

$$\begin{aligned} H &= \sum_{\sigma} \epsilon_d X^{\sigma\sigma} + \sum_{k\sigma} \epsilon_k n_{k\sigma} \\ &\quad + \frac{1}{\sqrt{\Omega}} \sum_{k\sigma} (V_k \; X^{\sigma 0} \; c_{k\sigma} + V_k^* \; c_{k\sigma}^\dagger \; X^{0\sigma}), \end{aligned} \tag{6.1}$$

where Ω is the box volume, and we have set the Fermi energy of the conduction electrons to zero. Here $X^{ab} = |a\rangle\langle b|$ is the Hubbard projected electron operator with $|a\rangle$ describing the empty orbital, and the two singly occupied states $a = 0, \pm\sigma$. We study the impurity

Green's function:

$$\mathcal{G}_{\sigma_i\sigma_f}(\tau_i,\tau_f) = -\langle\langle\ X^{0\sigma_i}(\tau_i)\ X^{\sigma_f 0}(\tau_f)\rangle\rangle, \tag{6.2}$$

with T_τ the imaginary time ordering symbol, the definition for an arbitrary time dependent operator Q: $\langle\langle Q\rangle\rangle = \langle Tr\ T_\tau\ e^{-\mathcal{A}}Q\rangle/\langle Tr\ T_\tau\ e^{-\mathcal{A}}\rangle$, and with the Schwinger source term $\mathcal{A} = \int_0^\beta\ d\tau\ \mathcal{V}^{\sigma_1\sigma_2}(\tau)\ X^{\sigma_1\sigma_2}(\tau)$, involving a Bosonic time dependent potential $\mathcal{V}$. Often we abbreviate $\mathcal{V}(\tau_i) \to \mathcal{V}_i$. As usual this potential is set to zero at the end of the calculation. In this paper expressions such as $\mathcal{G}(\tau_i,\tau_f)$ and $\mathcal{V}$ are understood as 2×2 matrices in spin space. We assume a constant hybridization $V_k = V_0$, and a (flat) band of half-width D with constant density of states $\rho(\epsilon) = \rho_0\ \theta(D-|\epsilon|)$ with $\rho_0 = \frac{1}{2D}$.

Taking the time derivative of Eq. (6.2) we obtain the Schwinger equation of motion (EOM)

$$\begin{aligned}\{(\partial_{\tau_i}+\epsilon_d)\mathbb{1} + \mathcal{V}_i\}\mathcal{G}(\tau_i,\tau_f) &= -\delta(\tau_i-\tau_f)\times(\mathbb{1}-\gamma(\tau_i)) \\ -\frac{1}{\sqrt{\Omega}}\left[\mathbb{1}-\gamma(\tau_i)+\mathcal{D}_i\right].\sum_k V_k\ G(k,\tau_i;\tau_f),\end{aligned} \tag{6.3}$$

where $\gamma(\tau_i) = \mathcal{G}^{(k)}(\tau_i^-,\tau_i)$ following Ref. ([3]) Eq. (35), or more explicitly in terms of spin indices as $\gamma_{\sigma_i\sigma_f}(\tau_i) = \sigma_i\sigma_f\mathcal{G}_{\bar\sigma_f\bar\sigma_i}(\tau_i,\tau_i^+)$, and with $\bar\sigma = -\sigma$. In the following, we abbreviate $\gamma(\tau_i)\to\gamma_i$. Here we introduced the mixed Green's function $G_{\sigma_i\sigma_f}(k,\tau_i;\tau_f) = -\langle\langle c_{k\sigma_i}(\tau_i)X^{\sigma_f 0}(\tau_f)\rangle\rangle$, and a functional derivative operator $(\mathcal{D}_i)_{\sigma_i\sigma_j} = (\sigma_i\sigma_j)\ \delta/\delta\mathcal{V}^{\bar\sigma_i\bar\sigma_j}(\tau_i)$. In the ECFL formalism Ref. ([3]), Eq. (6.3) and similar equations are to be understood as matrix equations in spin space. Following the Schwinger technique, the higher order Green's

functions have been expressed in terms of the source functional derivatives of the basic ones; an example illustrates this: $\sigma_i\sigma_j\langle\langle X^{\bar{\sigma}_i\bar{\sigma}_j}Q\rangle\rangle = (\gamma_i - \mathcal{D}_i)\langle\langle Q\rangle\rangle$. Proceeding further, we take a time derivative of the mixed Greens function to find

$$(\partial_{\tau_i} + \epsilon_k)G(k,\tau_i;\tau_f) = -\frac{1}{\sqrt{\Omega}}V_k^*\ \mathcal{G}(\tau_i,\tau_f), \tag{6.4}$$

so combining with Eq. (6.3) we find the exact EOM for the localized electron Green's function:

$$\begin{aligned}\{(\partial_{\tau_i} + \epsilon_d)\mathbb{1} + \mathcal{V}_i\}\mathcal{G}(\tau_i,\tau_f) &= -\delta(\tau_i - \tau_f) \times (\mathbb{1} - \gamma_i) \\ -(\mathbb{1} - \gamma_i + \mathcal{D}_i)\,.\,\Delta(\tau_i - \tau_{\mathbf{j}}).\ \mathcal{G}(\tau_{\mathbf{j}},\tau_f),\end{aligned} \tag{6.5}$$

with the convention that the time label in bold letters $\tau_{\mathbf{j}}$ is to be integrated over $\in [0,\beta]$. The conduction band enters through the usual ($\mathcal{V}$ independent) function

$$\Delta(\tau_i - \tau_j) = -\frac{\mathbb{1}}{\Omega}\sum_k |V_k|^2(\partial_{\tau_i} + \epsilon_k)^{-1}\delta(\tau_i - \tau_j), \tag{6.6}$$

with a Fourier transform

$$\Delta(i\omega_n) = \frac{1}{\Omega}\sum_k \frac{|V_k|^2}{i\omega_n - \epsilon_k} = V_0^2\int \frac{\rho(\epsilon)\ d\epsilon}{i\omega_n - \epsilon}. \tag{6.7}$$

We will require below its analytic continuation $i\omega_n \to \omega + i\eta$:

$$\Delta(\omega + i\eta) = \Delta_R(\omega) - i\ \Gamma(\omega); \tag{6.8}$$

$$\Gamma(\omega) = \pi\ V_0^2\ \rho(\omega);\ \ \Delta_R(\omega) = \frac{\Gamma_0}{\pi} \log \frac{|\omega + D|}{|\omega - D|}. \tag{6.9}$$

Here $\Gamma_0 = \pi V_0^2 \rho_0$. We now use the non-interacting Green's function

$$\mathbf{g}_0^{-1}(\tau_i, \tau_f) = -(\partial_{\tau_i} + \epsilon_d + \mathcal{V}(\tau_i))\delta(\tau_i - \tau_f) - \ \Delta(\tau_i, \tau_f), \tag{6.10}$$

and rewrite the fundamental equation of motion Eq. (6.5) as

$$\{\mathbf{g}_0^{-1}(\tau_i, \tau_{\mathbf{j}}) + (\gamma_i - \mathcal{D}_i).\Delta(\tau_i - \tau_{\mathbf{j}})\}.\mathcal{G}(\tau_{\mathbf{j}}, \tau_f) = (\mathbb{1} - \gamma_i)\delta(\tau_i - \tau_f). \tag{6.11}$$

Let us note an important *shift invariance* of Eq. (6.11) and Eq. (6.10). If we consider a transformation $\Delta(\tau) \to \Delta(\tau) + u_t \times \delta(\tau)$ with an arbitrary u_t, it is possible to show that Eq. (6.11) is unchanged, except for a shift of ϵ_d by $-u_t$. The added term $u_t \times (\gamma_i - \mathcal{D}_i).\mathcal{G}(\tau_i, \tau_f)$ vanishes upon using the Pauli principle and the Gutzwiller projection applicable to operators *at the same time instant*. We use this shift invariance below, to introduce a second chemical potential. In the ECFL theory, we use a product *ansatz*

$$\mathcal{G}(\tau_i, \tau_f) = \mathbf{g}(\tau_i, \tau_{\mathbf{j}})\ .\ \mu(\tau_{\mathbf{j}}, \tau_f) \tag{6.12}$$

where $\mu(\tau_i, \tau_j)$ is the caparison factor, and use this in Eq. (6.11). It is useful to introduce two vertex functions $\Lambda^{\sigma_1\sigma_2}_{\sigma_3\sigma_4}(\tau_n, \tau_m; \tau_i) = -\frac{\delta}{\delta \mathcal{V}_i^{\sigma_3\sigma_4}} \mathbf{g}^{-1}_{\sigma_1\sigma_2}(\tau_n, \tau_m)$, and $\mathcal{U}^{\sigma_1\sigma_2}_{\sigma_3\sigma_4}(\tau_n, \tau_m; \tau_i) = \frac{\delta}{\delta \mathcal{V}_i^{\sigma_3\sigma_4}} \mu_{\sigma_1\sigma_2}(\tau_n, \tau_m)$ as usual, and suppressing the time indices, we note $\frac{\delta}{\delta \mathcal{V}}.\mathbf{g} = \mathbf{g}.\Lambda.\mathbf{g}$. We now use the chain rule and Eq. (6.12) to write $\mathcal{D}.\Delta.\mathcal{G} = \mathcal{D}.\Delta.\mathbf{g}.\mu = \xi^*.\Delta.\mathbf{g}.\Lambda_*.\mathbf{g}.\mu + \xi^*.\Delta.\mathbf{g}.\mathcal{U}_*$, with the matrix $\xi_{\sigma\sigma'} = \sigma\sigma'$. The $*$ symbol from Ref. ([3]) is illustrated in component form by an example: $\cdots \xi^*_{\sigma_a\sigma_b} \cdots \delta/\delta\mathcal{V}^* = \cdots \sigma_a\sigma_b \cdots \delta/\delta\mathcal{V}^{\bar{\sigma}_a\bar{\sigma}_b}$, or in terms of the vertex functions $\cdots \xi^*_{\sigma_a\sigma_b} \cdots \Lambda_*^{\sigma'\sigma''} \cdots = \cdots \sigma_a\sigma_b \cdots \Lambda^{\sigma'\sigma''}_{\bar{\sigma}_a\bar{\sigma}_b} \cdots$, with the upper indices of Λ governed by the rules of the matrix multiplication. Following Ref. ([3]) we define the linear operator $\mathbf{L}(i,j) = \xi^*.\Delta(i,\mathbf{j}).\mathbf{g}(\mathbf{j},j).\frac{\delta}{\delta\mathcal{V}_i^*}$. We can now collect these definitions to rewrite $\mathcal{D}.\Delta.\mathcal{G} = \xi^*.\Delta.\mathbf{g}.\Lambda_*.\mathbf{g}.\mu + \xi^*.\Delta.\mathbf{g}.\mathcal{U}_* = \Phi.\mathbf{g}.\mu + \Psi$, and define the two self-energies:

$$\begin{aligned}
\Phi(i,j) &= -\mathbf{L}(i,\mathbf{r}).\mathbf{g}^{-1}(\mathbf{r},j) = \xi^*.\Delta(i,\mathbf{j}).\mathbf{g}(\mathbf{j},\mathbf{k}).\Lambda_*(\mathbf{k},j;i); \\
\Psi(i,j) &= \mathbf{L}(i,\mathbf{r}).\mu(\mathbf{r},j) = \xi^*.\Delta(i,\mathbf{j}).\mathbf{g}(\mathbf{j},\mathbf{k}).\mathcal{U}_*(\mathbf{k},j;i).
\end{aligned} \tag{6.13}$$

Summarizing, we may rewrite the exact EOM Eq. (6.11) symbolically:

$$\{\mathbf{g}_0^{-1} + \gamma.\Delta - \Phi\}.\mathbf{g}.\mu = (\mathbb{1} - \gamma)\delta + \Psi. \tag{6.14}$$

This equation is split into two parts by requiring $\mathbf{g}$ to be canonical:

$$\mathbf{g}^{-1} = \{\mathbf{g}_0^{-1} + \gamma.\Delta - \Phi\}, \text{ and } \mu = (\mathbb{1} - \gamma)\delta + \Psi, \tag{6.15}$$

bringing it into the standard form in the ECFL theory Ref. ([3]). Using Eq. (6.13), we note that the formal solutions of Eq. (6.15) are: $\mathbf{g}^{-1} = (\mathbb{1} - \mathbf{L})^{-1}.\left(\mathbf{g}_0^{-1} + \gamma.\Delta\right)$ and $\mu = (\mathbb{1} - \mathbf{L})^{-1}.(\mathbb{1} - \gamma)\,\delta$. We introduce the resolvent kernel $\mathcal{L}$ using the identity $(\mathbb{1} - \mathbf{L})^{-1} = \mathbb{1} + \mathcal{L}$ where $\mathcal{L} = (\mathbb{1} - \mathbf{L})^{-1}.\mathbf{L}$. In terms of the resolvent, we see that

$$\Phi = \mathcal{L}.(-\mathbf{g}_0^{-1} - \gamma.\Delta), \text{ and } \Psi = -\mathcal{L}.\gamma.\delta. \tag{6.16}$$

Therefore distributing the action of $\mathcal{L}$ over the two terms, we can rewrite

$$\Phi = \chi + \Psi.\Delta, \tag{6.17}$$

$$\text{with } \chi = \mathcal{L}.(-\mathbf{g}_0^{-1}). \tag{6.18}$$

Therefore the self-energy Φ breaks up into two parts, as in Eq. (6.17). Note that in Eq. (6.16), the expressions $\gamma.\Delta$ and $\gamma.\delta$ involve multiplication at equal times, whereas in Eq. (6.17), $\Psi.\Delta$ implies a convolution in time. The two Green's functions satisfy the pair of sum rules

$$\mathbf{g}(\tau, \tau^+) = \frac{n_d}{2}; \quad \mathcal{G}(\tau, \tau^+) = \frac{n_d}{2}, \tag{6.19}$$

where n_d is the number of electrons on the d-orbital $n_d = \sum_\sigma \langle X^{\sigma\sigma} \rangle$.

In the context of the t-J model in Ref. ([6]), the sum rule for $\mathbf{g}$ is necessary to satisfy the Luttinger-Ward theorem. If we use the representation $\hat{f}_\sigma^\dagger(\lambda) = (1 - \lambda f_{\bar{\sigma}}^\dagger f_{\bar{\sigma}}) f_\sigma^\dagger$ for the correlated electrons, this constraint is understandable as the constraint on the number of

"uncorrelated" Fermions $\langle f_\sigma^\dagger f_\sigma \rangle$, which must agree with the number of physical (correlated) electrons $\langle \hat{f}_\sigma^\dagger \hat{f}_\sigma \rangle$. Similarly, in the present case, this constraint is needed to fulfill the Friedel sum rule. We also remark that the self-energy Ψ, unlike its counterpart Φ, is dimensionless, and thus interpreted as an adaptive spectral weight [6].

6.2 Zero Source Limit

Upon turning off the sources, all objects become functions of only $\tau_i - \tau_f$ and may therefore be Fourier transformed to Matsubara frequency space. By Fourier transforming Eq. (6.12), Eq. (6.15) and Eq. (6.17) and using $\gamma \to \frac{n_d}{2}$ we obtain the following expressions in frequency space:

$$\begin{aligned} \mathcal{G}(i\omega_n) &= \mathbf{g}(i\omega_n) \,.\, \mu(i\omega_n), \\ \mu(i\omega_n) &= 1 - \frac{n_d}{2} \;+\; \Psi(i\omega_n), \\ \mathbf{g}^{-1}(i\omega_n) &= i\omega_n - \epsilon_d - \Delta(i\omega_n)\mu(i\omega_n) - \chi(i\omega_n). \end{aligned} \tag{6.20}$$

Alternately this result can be rewritten in terms of the Dyson-Mori self-energy representation as

$$\mathcal{G}(i\omega_n) = \frac{1 - \frac{n_d}{2}}{i\omega_n - \epsilon_d - (1 - \frac{n_d}{2})\Delta(i\omega_n) - \Sigma_{DM}(i\omega_n)} \tag{6.21}$$

and

$$\Sigma_{DM}(i\omega_n) + \epsilon_d - i\omega_n = \frac{1 - \frac{n_d}{2}}{1 - \frac{n_d}{2} + \Psi(i\omega_n)} \left(\chi(i\omega_n) + \epsilon_d - i\omega_n\right). \tag{6.22}$$

The sum rules Eq. (6.19) are:

$$\sum_{i\omega_n} \mathcal{G}(i\omega_n) e^{i\omega_n \eta} = \frac{n_d}{2}; \quad \sum_{i\omega_n} \mathbf{g}(i\omega_n) e^{i\omega_n \eta} = \frac{n_d}{2}. \tag{6.23}$$

These are satisfied at a fixed n_d using two Lagrange multipliers, the localized state energy ϵ_d and the second chemical potential u_0 introduced below in Eq. (6.25). We observe that the usual Dysonian self-energy $\Sigma_{AM}(i\omega_n)$ defined through the usual Dyson equation (valid for finite U) $G^{-1} = i\omega_n - \epsilon_d - \Delta(i\omega_n) - \Sigma_{AM}(i\omega_n)$ in the infinite U limit can be obtained from

$$\Sigma_{AM}(i\omega_n) = \frac{2}{2 - n_d} \Sigma_{DM}(i\omega_n) + \frac{n_d}{2 - n_d} (\epsilon_d - i\omega_n). \tag{6.24}$$

The unlimited growth with ω_n makes this self-energy somewhat inconvenient to deal with, and therefore motivated the introduction of the Dyson Mori object, which is better behaved in this regard. After analytic continuation $i\omega_n \to \omega + i0^+$, the imaginary part of Σ_{AM} is well behaved and finite as $\omega \to \infty$. It is obtained from the NRG method and compared with the relevant ECFL functions after scaling by $1 - \frac{n_d}{2}$ as in Eq. (6.24). We notice that the density n_d appears explicitly in the expressions for the Green's functions, and must

therefore be calculated self-consistently, from Eq. (6.23). This feature is quite natural in the present approach, since Eq. (6.3) for the Green's function contains γ and therefore n_d explicitly.

6.3 Introducing λ and u_0 into the equations.

Summarizing the work so far: Eq. (6.15), Eq. (6.16) and Eq. (6.17) follow from Eq. (6.11) upon using the product ansatz Eq. (6.12), and are exact equations. In order to get concrete results, we proceed by introducing two parameters into the equations. (I) The parameter $\lambda \in [0, 1]$ multiplies certain terms shown in Eq. (6.25), allowing a density type expansion, and continuously connects the uncorrelated Fermi system $\lambda = 0$ to the extremely correlated case $\lambda = 1$. (II) The second parameter u_0 is introduced as shown in Eq. (6.25). It is the second chemical potential used to enforce the shift identities of the exact equation Eq. (6.11). Eq. (6.11) now becomes

$$\{\mathbf{g}_0^{-1} + \lambda(\gamma - \mathcal{D}).(\Delta - \frac{u_0}{2}\delta)\}.\mathcal{G} = (\mathbb{1} - \lambda\gamma)\delta. \tag{6.25}$$

As a consequence, in Eq. (6.14) to Eq. (6.18) we set $\gamma \to \lambda\gamma$, $\Psi \to \lambda\Psi$, and $\Phi \to \lambda\Phi$, or $\chi \to \lambda\chi$. Secondly in Eq. (6.14) to Eq. (6.18) we set $\Delta(\tau_i, \tau_f) \to \Delta(\tau_i, \tau_f) - \frac{u_0}{2}\ \delta(\tau_i - \tau_f)$. Note that there is no shift of Eq. (6.10) implied in Eq. (6.25).

We write Eq. (6.15) with λ inserted explicitly and the understanding that $\Delta(\tau_i, \tau_f)$

has been shifted as (Ref. ([55])):

$$\begin{aligned} \mathbf{g}^{-1}(\tau_i,\tau_f) &= \mathbf{g}_0^{-1}(\tau_i,\tau_f) + \lambda\gamma(\tau_i).\Delta(\tau_i,\tau_f) - \lambda\ \Phi(\tau_i,\tau_f), \\ \mu(\tau_i,\tau_f) &= \delta(\tau_i-\tau_f)(\mathbb{1}-\lambda\gamma(\tau_i)) + \lambda\ \Psi(\tau_i,\tau_f), \end{aligned} \tag{6.26}$$

where the two self-energies are given in terms of the vertex functions as

$$\begin{aligned} \Phi(\tau_i,\tau_f) &= \xi^*.\Delta(\tau_i,\tau_{\mathbf{j}}).\mathbf{g}(\tau_{\mathbf{j}},\tau_{\mathbf{k}}).\Lambda_*(\tau_{\mathbf{k}},\tau_f;\tau_i) \\ \Psi(\tau_i,\tau_f) &= \xi^*.\Delta(\tau_i,\tau_{\mathbf{j}}).\mathbf{g}(\tau_{\mathbf{j}},\tau_{\mathbf{k}}).\mathcal{U}_*(\tau_{\mathbf{k}},\tau_f;\tau_i). \end{aligned} \tag{6.27}$$

On switching off the sources, these expressions can be spin resolved and expressed as $\Phi = \Delta\ \mathbf{g}\ \Lambda^{(a)}$ and $\Psi = \Delta\ \mathbf{g}\ \mathcal{U}^{(a)}$, with the same time labels as above, and with the usual spin decomposition $\Lambda^{(a)} = \Lambda^{\sigma\sigma}_{\bar{\sigma}\bar{\sigma}} - \Lambda^{\sigma\bar{\sigma}}_{\sigma\bar{\sigma}}$.

λ Expansion

We note that we can obtain the equations of motion for the Anderson model from the equations of motion for the t$-$J model by making the following substitutions and replacing all space-time variables with just time[10].

$$t[i,f] \to -\Delta(\tau_i,\tau_f);\ \varepsilon_k \to \Delta(i\omega_k),\ J\to 0,\ \boldsymbol{\mu}\to -\epsilon_d. \tag{6.28}$$

The λ expansion for the Anderson model is therefore analogous to the one for the t-J model in Ref. ([6]) and the large-d t-J model in Ref. ([10]), and can be obtained from them by making the substitutions in Eq. (6.28) and changing all frequency momentum four

vectors to just frequency. For completeness, Appendix A provides a brief derivation (in time domain) of the following equations. Denoting

$$a_{\mathcal{G}} = 1 - \lambda\frac{n_d}{2} + \lambda^2\frac{n_d^2}{4}, \tag{6.29}$$

and the frequently occurring object

$$\mathcal{R} = \mathbf{g}(i\omega_p)\mathbf{g}(i\omega_q)\mathbf{g}(i\omega_p + i\omega_q - i\omega_n),$$

we obtain to $O(\lambda^2)$ the expressions :

$$\begin{aligned}
\mathcal{G}(i\omega_n) &= \mathbf{g}(i\omega_n)\mu(i\omega_n), \mu(i\omega_n) = a_{\mathcal{G}} + \lambda\Psi(i\omega_n), && (6.30)\\
\mathbf{g}^{-1}(i\omega_n) &= i\omega_n - \epsilon'_d - (\Delta(i\omega_n) - \frac{u_0}{2})\mu(i\omega_n) \\
&\quad -\lambda\chi(i\omega_n), && (6.31)\\
\chi(i\omega_n) &= -\lambda\sum_{p,q}[2\Delta(i\omega_p) - u_0] \\
&\quad \times[\Delta(i\omega_p + i\omega_q - i\omega_n) - \frac{u_0}{2}]\mathcal{R}, && (6.32)\\
\Psi(i\omega_n) &= -\lambda\sum_{p,q}[2\Delta(i\omega_p) - u_0]\mathcal{R}. && (6.33)
\end{aligned}$$

The energy ϵ'_d is given by collecting the static terms in Φ as

$$\epsilon'_d = \epsilon_d + u_0(\lambda\frac{n_d}{2} - \lambda^2\frac{n_d^2}{8}) + \frac{u_0}{2}a_{\mathcal{G}} - \lambda\sum_{i\omega_p}\Delta(i\omega_p)\mathbf{g}(i\omega_p). \tag{6.34}$$

The shift-theorem is satisfied by all the terms separately- since we have taken care to form expressions of the type $\Delta - \frac{u_0}{2}$. As discussed in Ref. ([6]), the shift theorems mandate the introduction of u_0, and its availability, in addition to ϵ_d, enables us to fix the pair of sum rules Eq. (6.19). As explained, we must set $\lambda \to 1$ before using these expressions.

Within the $O(\lambda^2)$ theory, the total spectral weight of the Green's function is $a_{\mathcal{G}}$ rather than the exact value $1 - \frac{n_d}{2}$. This is understood as the incomplete projection to singly occupancy leading to an excess in the total number of states available to the system. In order to ensure that $\Sigma_{DM}(\omega)$ retain the feature of being finite as $\omega \to \infty$, it must be slightly redefined (to $\hat{\Sigma}_{DM}$) in the $O(\lambda^2)$ theory.

$$G(\omega) = \frac{a_{\mathcal{G}}}{\omega - \epsilon_d'' - a_{\mathcal{G}}\Delta(\omega) - \hat{\Sigma}_{DM}(\omega)} \tag{6.35}$$

where

$$\epsilon_d'' \equiv \epsilon_d' - \frac{u_0}{2} a_{\mathcal{G}} \tag{6.36}$$

Using Eq. (6.30) and Eq. (6.31), we can relate $\hat{\Sigma}_{DM}(\omega)$ to $\chi(\omega)$ and $\Psi(\omega)$.

$$\hat{\Sigma}_{DM}(\omega) + \epsilon_d' - \omega = \frac{a_{\mathcal{G}}}{a_{\mathcal{G}} + \Psi(\omega)}(\chi(\omega) + \epsilon_d' - \omega) \tag{6.37}$$

Since $\Psi(\omega)$,$\chi(\omega) \to 0$ as $\omega \to \infty$, we see explicitly that $\hat{\Sigma}_{DM}(\omega)$ remains finite in this limit. Just as in the case of $\Im m\, \Sigma_{DM}(\omega)$, $\Im m\, \hat{\Sigma}_{DM}(\omega)$ is related to $\Im m\, \Sigma_{AM}(\omega)$ by a multiplicative constant ($1 - \frac{n_d}{2}$ and $a_{\mathcal{G}}$ respectively), and therefore their spectra are identical apart from this multiplicative constant. Comparing Eq. (6.21) and Eq. (6.35), we see that the latter is

obtained from the former with the substitutions

$$\Sigma_{DM}(\omega) \to \hat{\Sigma}_{DM}(\omega);\ \epsilon_d \to \epsilon_d'';\ 1 - \frac{n_d}{2} \to a_{\mathcal{G}}. \tag{6.38}$$

Keeping these substitutions in mind, we will now only use $\Sigma_{DM}(\omega)$ from the exact theory, with the understanding that the same expressions hold for $\hat{\Sigma}_{DM}(\omega)$ in the $O(\lambda^2)$ theory as long as the substitutions in Eq. (6.38) are made.

6.4 Friedel Sum Rule at $T = 0$

At $T = 0$, the Friedel sum rule [56, 57, 58] plays an important role in the AIM, parallel to that of the Luttinger-Ward volume theorem in Fermi liquids. In Ref. ([58]), the original form of the Friedel sum rule is written in terms of $\eta_\sigma(\omega)$, the phase shift of the conduction electron with spin σ at energy ω:

$$\eta_\sigma(\omega) \quad = \quad \frac{1}{2i} \log \left[\mathcal{G}_\sigma(\omega + i0^+) \mathcal{G}_\sigma^{-1}(\omega - i0^+) \right], \tag{6.39}$$

where the logarithm is chosen with a branch cut along the positive real axis, so that $0 \leq \eta \leq \pi$. The Friedel sum rule is then written as :

$$\eta_\sigma(\omega = 0) = \frac{\pi n_d}{2}. \tag{6.40}$$

This theorem is proven for the AIM at finite U Ref. ([58]), by adapting the argument of Luttinger and Ward Ref. ([59]), with an implicit assumption of a non-singular evolution in

U from 0. We assume that the Friedel sum rule also holds in the extreme correlation limit $U \to \infty$. Using the Dyson Mori representation Eq. (6.21) to compute the phase shift in Eq. (6.39), we may rewrite this as

$$n_d = 1 - \frac{2}{\pi} \tan^{-1} \left[\frac{\epsilon_d + \Re e \Sigma_{DM}(0)}{\Gamma_0 (1 - \frac{n_d}{2})} \right], \tag{6.41}$$

with $\epsilon_d + \Re e \Sigma_{DM}(0) > 0$, in the physical case of $0 \leq n_d \leq 1$. It is easily seen [61] that this form is equivalent to the standard statement of the Friedel sum rule(Ref. ([47])):

$$\rho_{\mathcal{G}}(0) = \frac{1}{\pi \Gamma_0} \ \sin^2(\frac{\pi n_d}{2}), \tag{6.42}$$

Within the approximation of the λ expansion, the Friedel sum rule implies a relationship between the values of the two self-energies at zero frequency.

$$n_d = 1 - \frac{2}{\pi} \tan^{-1} \left[\frac{\epsilon_d' - \frac{u_0}{2} \mu(0) + \chi(0)}{\Gamma_0 \mu(0)} \right], \tag{6.43}$$

This can be obtained by using the substitutions from Eq. (6.38) in Eq. (6.41), and using Eqs. (6.37),(6.36), and (6.30).

We can also record a result for the auxiliary density of states $\rho_{\mathbf{g}}(\omega = 0)$, analogous to Eq. (6.42) here. It follows from Eq. (6.47), with the Fermi liquid type assumption of vanishing of $\rho_\Psi(0)$ at $T = 0$, and reads

$$\rho_{\mathbf{g}}(0) = \frac{1}{\pi \Gamma_0 \mu(0)} \ \sin^2(\frac{\pi n_d}{2}) \tag{6.44}$$

We check the validity of the Friedel sum rule within the λ expansion in both the forms Eq. (6.42) and Eq. (6.43). In doing so, we are thus testing if the strategy of the two ECFL sum rules Eq. (6.23) enforces the Friedel sum rule, in a situation that is essentially different from that in finite U theories so that the central result of Luttinger and Ward Ref. ([59]) is not applicable in any obvious way.

6.5 Computation of Spectral function

In computing the spectral function, we follow the approach taken in Ref. ([6]), in which the spectral function is calculated for the $O(\lambda^2)$ ECFL theory of the t−J model. Our calculation is made simpler due to the absence of any spatial degrees of freedom, but more complicated by the presence of the frequency dependent factor $\Delta(i\omega_n)$. We define the various spectral functions and the relationships between them. These expressions are analogous to those in sec.III A of Ref. ([6]).

$$Q(i\omega_n) = \int_{-\infty}^{\infty} d\nu \frac{\rho_Q(\nu)}{i\omega_n - \nu} \tag{6.45}$$

Where Q can stand for any object such as $\mathcal{G}$, $\mathbf{g}$, χ, Σ_{DM} or Ψ. Therefore after analytic continuation $i\omega_n \to \omega + i0^+$

$$\rho_Q(\omega) \equiv -\frac{\Im m}{\pi} Q(\omega + i0^+) \text{ and } \Re e\ Q(\omega) = \mathcal{H}[\rho_Q](\omega), \tag{6.46}$$

where for any real density $\rho_Q(\omega)$ the Hilbert transform is denoted as $\mathcal{H}[\rho_Q](\omega) = P\int_{-\infty}^{\infty} d\nu \frac{\rho_Q(\nu)}{\omega-\nu}$. From Eq. (6.33), we find that

$$\rho_{\mathcal{G}}(\omega) = \rho_{\mathbf{g}}(\omega)[a_{\mathcal{G}} + \Re e\ \Psi(\omega)] + \rho_{\Psi}(\omega)\Re e\ \mathbf{g}(\omega) \tag{6.47}$$

With $f(\omega) = \frac{1}{1+e^{\beta\omega}}$ and $\bar{f}(\omega) = 1 - f(\omega)$, the two sum rules Eq. (6.23) read

$$\int_{-\infty}^{\infty} f(\omega)\ \rho_{\mathbf{g}}(\omega)\ d\omega = \frac{n_d}{2}\ ,\ \int_{-\infty}^{\infty} f(\omega)\ \rho_{\mathcal{G}}(\omega)\ d\omega = \frac{n_d}{2}. \tag{6.48}$$

We also note $\rho_{\Delta}(\omega) = \frac{\Gamma(\omega)}{\pi}$. It is useful to define a mixed (composite) density

$$\rho_M(x) = \rho_{\mathbf{g}}(x)(\Delta_R(x) - \frac{u_0}{2}) + \rho_{\Delta}(x)\Re e\ \mathbf{g}(x), \tag{6.49}$$

so that we can integrate (or sum) the internal frequencies in Eq. (6.33) efficiently (see Appendix B), and write the two relevant complex self-energies (with $\omega \equiv \omega + i0^+$) as

$$\begin{aligned}
\Psi(\omega) &= -2\lambda \int_{u,v,w} \frac{\rho_M(u)\rho_{\mathbf{g}}(v)\rho_{\mathbf{g}}(w)}{\omega - u - v + w} \\
&\quad \times \left[f(u)f(v)\bar{f}(w) + \bar{f}(u)\bar{f}(v)f(w)\right] \\
\chi(\omega) &= -2\lambda \int_{u,v,w} \frac{\rho_M(u)\rho_{\mathbf{g}}(v)\rho_M(w)}{\omega - u - v + w} \\
&\quad \times \left[f(u)f(v)\bar{f}(w) + \bar{f}(u)\bar{f}(v)f(w)\right]
\end{aligned} \tag{6.50}$$

In these expressions u, v, w are understood to be real variables, and using Eq. (6.46) we can extract the real and imaginary parts of Ψ and χ in terms of the spectral functions.

n_d	$\rho_{G,ECFL}(0)$	$\epsilon_{d,ECFL}$	$\epsilon_{d,NRG}$	z_{ECFL}	z_{NRG}
0.35	8.69 + 1.8 %	-0.003	-0.003	0.753	0.697
0.441	13.0 + 1.1 %	-0.010	-0.009	0.661	0.567
0.536	17.7 + 0.73%	-0.015	-0.015	0.559	0.416
0.6	20.8 + 0.41 %	-0.019	-0.018	0.489	0.312
0.7	25.3 + 0.62%	-0.024	-0.024	0.388	0.169
0.777	28.1 + 0.26%	-0.031	-0.029	0.314	0.081
0.834	29.7 + 0.20 %	-0.037	-0.035	0.265	0.035

Table 6.1: The bare impurity level ϵ_d as well as the quasiparticle weight z are displayed for the ECFL and the NRG calculations for all values of the density. Additionally, the theoretical value for the Friedel sum rule as well as the ECFL deviation from it are displayed.

Chapter 7

Results

The following explicit results were obtained after setting $\lambda = 1$ in the equations noted above. We calculated the spectral functions ρ_G , ρ_Σ , ρ_χ , and ρ_Ψ using the values $D = 1$, $\Gamma_0 = 0.01$, and $T = 0$. The zero temperature limit is easily achieved in the ECFL theory by setting all of the Fermi functions to step functions. We expect that the spectral function calculated within the ECFL $O(\lambda^2)$ theory will be accurate through a density of approximately $n_d = 0.6$, or perhaps at best $n_d \sim 0.7$. As discussed in [3, 6], this is the main limitation of the low order λ results, the theory begins to have substantial corrections as we increase n_d towards unity. The source of this error estimate is the high frequency behaviour within the λ expansion of the Green's function Eq. (6.33) $\mathcal{G} \sim \frac{a_\mathcal{G}}{i\omega}$, this deviates from the known exact behaviour $\mathcal{G} \sim \frac{1-n_d/2}{i\omega}$. The error grows with increasing density, but we expect to have reasonable results even at $n_d = 0.7$.

In Table (I), we show the results for the spectral function at zero energy in terms of the percentage deviation from the Friedel sum rule Eq. (6.42), demonstrating that the

ECFL satisfies the Friedel sum rule to a high degree of accuracy. We specify the occupation number n_d and show the values of the energy level ϵ_d and quasiparticle weight z calculated within the ECFL and NRG calculations. The values of ϵ_d are in good agreement between the two calculations, while there is a discrepancy in z which becomes more pronounced at higher densities. While the error in the scale of z as $n_d \to 1$ is expected from the low order in λ aspect of the theory, we should keep in mind that the *shape* of the spectral function, and also the imaginary part of the self energy is another matter altogether. We display below these objects after scaling the frequency with z, this captures the *shape* of the spectra, and isolates the discrepancy to a single number, namely the magnitude of z. The admittedly non trivial problem of the magnitude of z must await a more satisfactory resolution involving the treatment of higher order terms in λ.

In Fig. (7.1) we display the spectral functions at the indicated densities- indicating a smooth evolution with density. The Kondo or Abrikosov-Suhl resonance at positive frequencies becomes sharper as we increase density and moves closer to $\omega = 0$. If the raw ECFL and NRG spectral functions are compared (as in right panel of Fig. (7.2) for $n_d = 0.536$), one finds that the peak in the ECFL spectral function is too broad. This over-broadening becomes worse at larger densities and better at lower densities. However, it can be understood well in terms of the elevated value of z for ECFL at higher densities. Hence, before doing the comparison, as in Fig. (7.1), we first rescale the ω axis for both the ECFL and NRG spectral functions by the appropriate z (as in the left panel of Fig. (7.2) for $n_d = 0.536$ and in Fig. (7.1) for the other densities). They are then found to be in good agreement up to surprisingly high values of n_d, suggesting that the ECFL theory captures

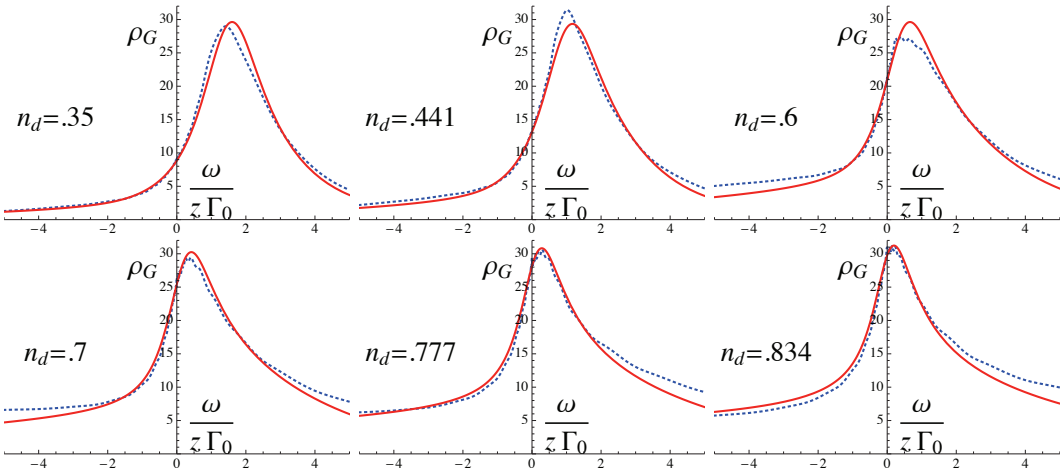

Figure 7.1: The spectral density for the physical Green's function versus $\frac{\omega}{\Gamma_0 z}$ for densities of $n_d = 0.35, 0.441, 0.6, 0.7, 0.777, 0.834$. The red curve is the ECFL calculation, while the blue curve is the NRG calculation.

the *shape* (but not the scale) of the spectral functions and their asymmetry in a very natural fashion. We also found good agreement with the NRG spectral functions in Ref. ([54]). The ECFL spectral function ρ_G is constructed out of the two spectral functions ρ_χ and ρ_Ψ that are shown at various densities in Fig. (7.3) and Fig. (7.4), exhibiting Fermi liquid type quadratic frequency dependence at low ω.

In Fig. (7.5) we present the density evolution of the spectral function for the Dyson Mori self-energy (see Eq. (6.22)). This exhibits a remarkable similarity to the analogous spectral density for the t-J model in the limit of high dimensions Ref. ([9]) and the Hubbard model at large U Ref. ([16]).

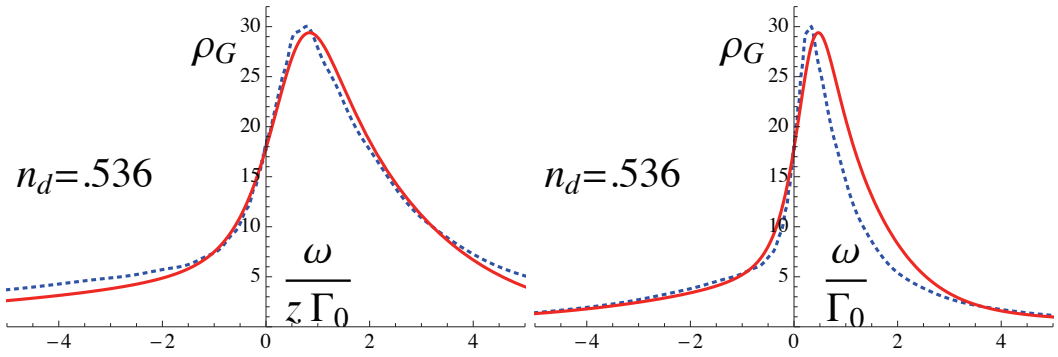

Figure 7.2: The spectral density for the physical Green's function for the density of $n_d = 0.536$. For the plot on the left, both the ECFL and NRG curves are plotted versus $\frac{\omega}{\Gamma_0 z}$. Since ECFL has a larger z value, the absolute scale of the ω axis differs for the two curves. For the plot on the right, both ECFL and NRG are plotted versus $\frac{\omega}{\Gamma_0}$ and hence the ECFL peak is too wide.

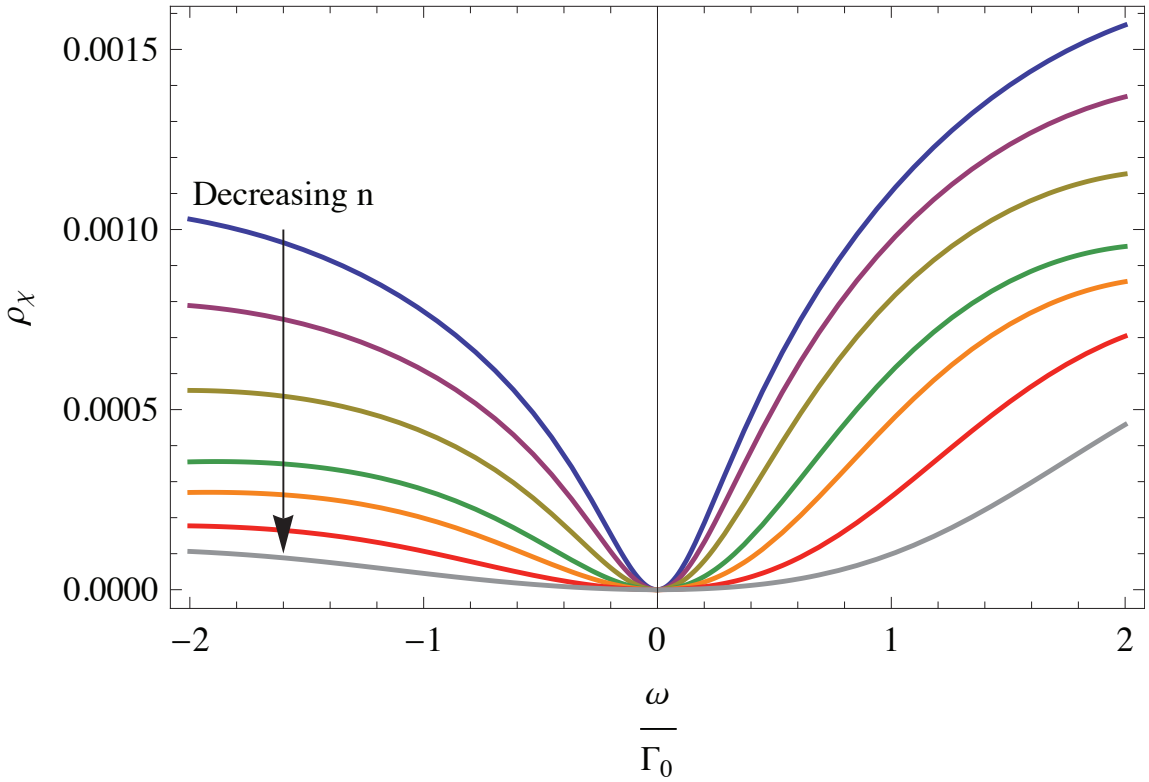

Figure 7.3: The spectral function for χ for densities of $n_d = 0.834, 0.777, 0.7, 0.6, 0.536, 0.441, 0.35$.

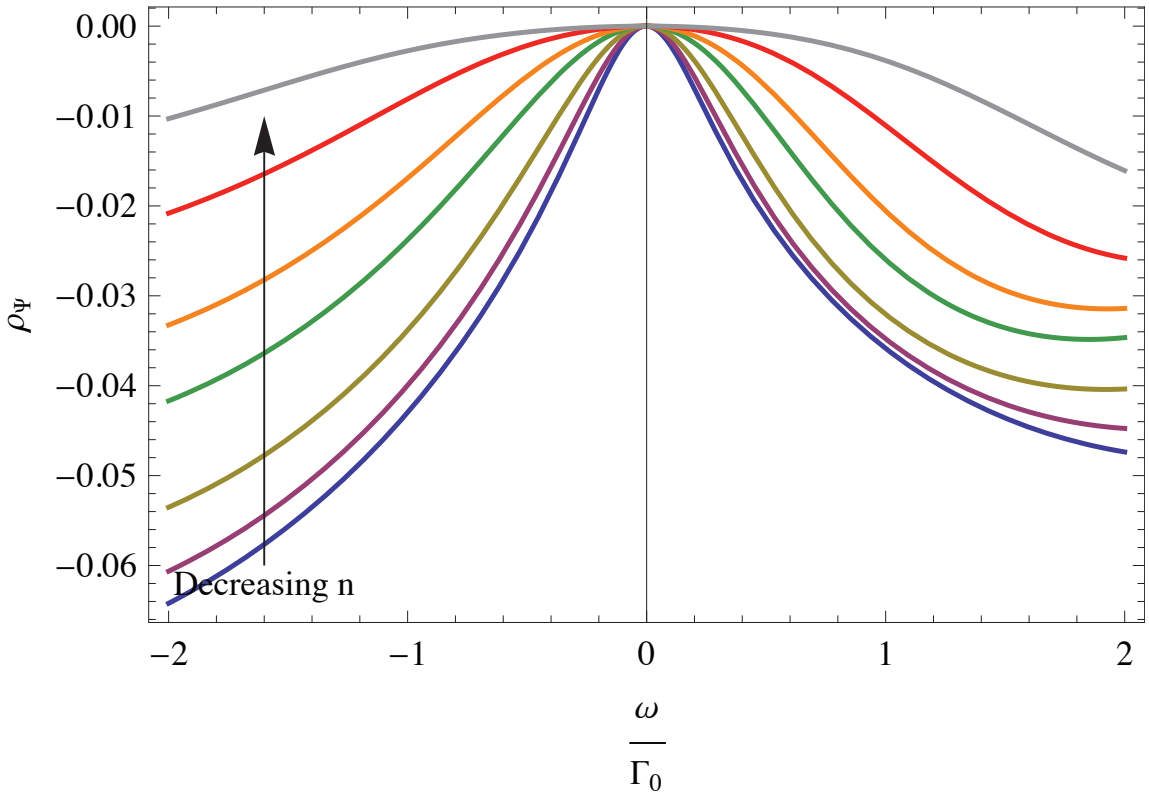

Figure 7.4: The spectral function for Ψ for densities of $n_d = 0.834, 0.777, 0.7, 0.6, 0.536, 0.441, 0.35$.

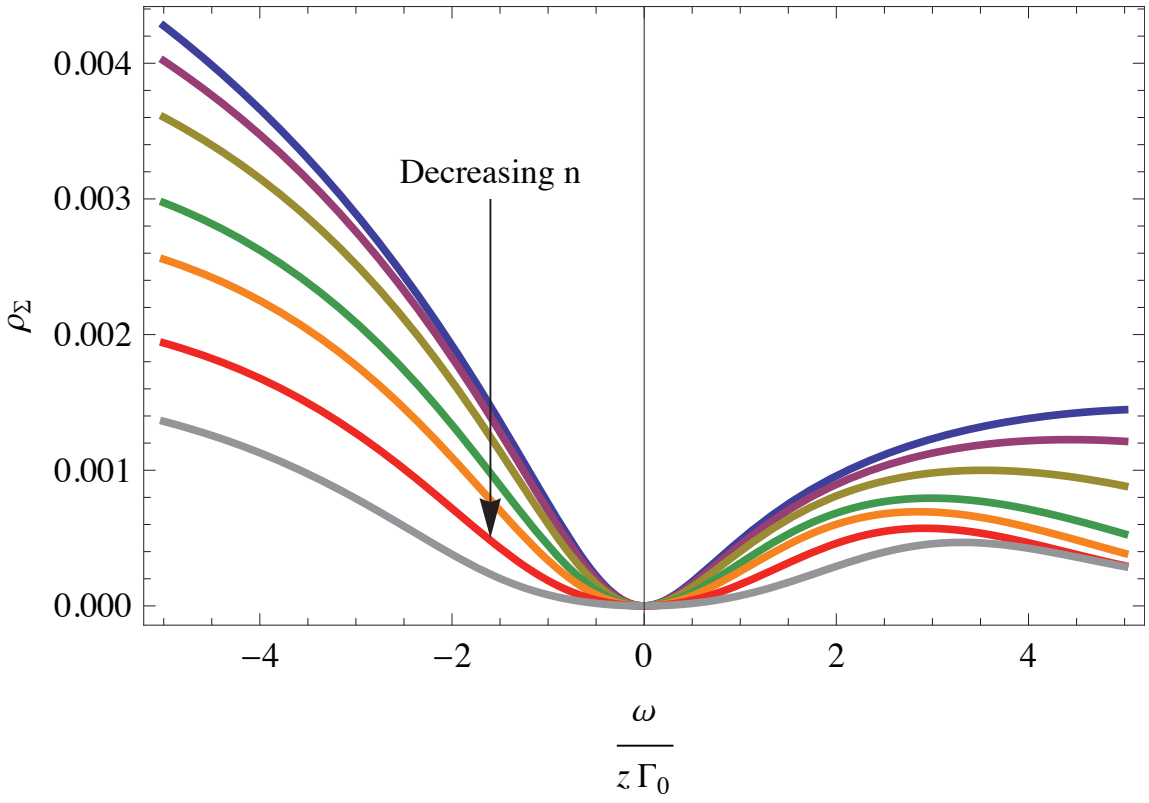

Figure 7.5: The spectral function for the Dyson-Mori self-energy for densities of $n_d = 0.874, 0.777, 0.7, 0.6, 0.536, 0.441, 0.35$. The curvature of the quadratic minimum becomes larger with increasing density.

Chapter 8

Conclusion

In this chapter we have applied the ECFL formalism at the simplest level, using the $O(\lambda^2)$ equations, to the Anderson impurity model with $U \to \infty$. In this formalism, the two self-energies of the ECFL theory Ψ and χ are calculated using a skeleton expansion in the auxiliary Green's function $\mathbf{g}$. This is analogous to the skeleton expansion for the Dyson self-energy Σ, in standard Feynman-Dyson perturbation theory applicable to the case of finite U. These two self-energies determine $\mathbf{g}$ as well as the physical $\mathcal{G}$, leading to a self-consistent solution. We obtained the equations to second order and solved them numerically at $T = 0$. We found that at low enough ω, the ECFL self-energies have symmetric spectra of the type predicted by Fermi-Liquid theory (see Fig. (7.3) and Fig. (7.4)). Combining them through the ECFL functional form Eq. (6.22) generates a non-trivial self-energy with an asymmetric spectrum displayed in Fig. (7.5). It therefore appears that functional form Eq. (6.22) has the potential to generate realistic and non trivial spectral densities, starting with rather simple components. The availability of convenient and natural analytical expressions is

seen to provide a distinct advantage of the ECFL formalism. Formally exact techniques such as the NRG involve steps that are not not automatically endowed with these, but rather rely on analytic continuation or other equivalent techniques.

The physical spectral function for the impurity site is obtained from the above pair of ECFL self energies, and displays a Kondo or Abrikosov-Suhl resonance. This feature becomes more narrow and the spectrum becomes more skewed towards the occupied side of the peak with increasing density. However, the computed quasiparticle z in the present calculation is considerably larger than the exact value $z \propto e^{-1/2(1-n_d)}$, as $n_d \to 1$ Ref. ([60]) , i.e. into the Kondo regime. This large z makes it impossible for the $O(\lambda^2)$ version of ECFL presented here, to address the Kondo regime $n_d \to 1$. It results in the the masking of a small (and broad) peak at $\omega \sim \epsilon_d$, found in our NRG spectral functions, as we approach the Kondo limit. Both real and imaginary parts of the computed $\Sigma_{DM}(\omega)$ are larger than their NRG counterparts in that regime, thereby precluding a peak.

To place this result in context, we observe that the same level of approximation of ECFL, applied to the lattice problem of the $d \to \infty,\ U \to \infty$ Hubbard model in Ref. ([9]) (see Fig (12)), *does* show a lower Hubbard band peak in the spectral function. This difference presumably arises from the robust value of $z \sim (1-n)$ in the lattice model, arising from Gutzwiller physics, it is much larger than the exponentially small value $z \propto e^{-1/2(1-n_d)}$ in the AIM. Therefore the fractional error made by the $O(\lambda^2)$ ECFL calculation is smaller in the lattice model compared to the AIM.

The location of the peak is set by $\epsilon_d + \Sigma_{DM}(0)$ (Eq. (6.21)). Using Eq. (6.41), we can see that this quantity must decrease with increasing density. This is consistent with

the expectation that the location of the peak will approach $\omega = 0$ as $n_d \to 1$. This can also be understood from the need to have more spectral weight when $\omega \leq 0$, to yield a higher value of n_d. We found that the ECFL spectrum satisfies the Friedel sum rule (Eq. (6.42)) to a high degree of accuracy, and that ECFL yields values of ϵ_d in good agreement with the NRG values at all densities (See Table (I).)

As mentioned above the ECFL calculation to $O(\lambda^2)$ overestimates the value of the quasiparticle weight z as compared with the NRG and the exact asymptotic result $z \propto e^{-1/2(1-n_d)}$ as $n_d \to 1$ Ref. ([60]), the difference becoming more significant with increasing density. This also leads to an over broadening of the peak in the ECFL spectrum at higher densities. This is consistent with the fact that the λ expansion of the ECFL is a low-density expansion and the current calculation has only been carried out to $O(\lambda^2)$. Nevertheless, after rescaling the ω axis for both the ECFL and NRG spectra by their respective values of z, we find good quantitative agreement between the two as in Fig. (7.1). In Fig. (7.2) we illustrate the comparison between scaled and unscaled spectral functions at a typical density. We find similarly good agreement with the NRG calculation from Ref. ([54]). This implies that the ECFL theory has the correct *shape* of the spectra built into it quite naturally.

Finally we note that the computed spectral functions exhibit a remarkable similarity to the analogous spectral density for the t-J model in the limit of high dimensions Ref. ([9]) and the Hubbard model at large U Ref. ([16]).

Chapter 9

Appendix A: Calculating the self-energies in the $O(\lambda^2)$ theory

The calculation follows the procedure given in Ref. ([6]). A few comments are provided to make the connections explicit- the zeroeth order vertices are common to Ref. ([6]) Eqs. (B3, B14), and the first order $\mathcal{U}$ is common to Eq. (B15). The first order vertex $[\Lambda]_1$ can be found parallel to Eq-(B23- B28) from differentiating

$$[\mathbf{g}^{-1}(i,f)]_1 = \Delta(i,f).\mathbf{g}^{(k)}(i,i) + \delta(i,f)\Delta(i,\mathbf{a}).\mathbf{g}^{(k)}(\mathbf{a},f), \tag{9.1}$$

as

$$[\Lambda^{(a)}(i,m;j)]_1 = -2\Delta(i,m).\mathbf{g}(i,j).\mathbf{g}(j,i)$$
$$-2\delta(i,m)\Delta(i,\mathbf{k}).\mathbf{g}(\mathbf{k},j).\mathbf{g}(j,i). \tag{9.2}$$

Here the bold labels are integrated over. From this we construct the time domain self-energies

$$\Psi(i,f) = -2\lambda\Delta(i,\mathbf{k}).\mathbf{g}(\mathbf{k},f).\mathbf{g}(i,f).\mathbf{g}(f,i), \tag{9.3}$$

and

$$\begin{aligned}\Phi(i,f) &= -\delta(i,f)\Delta(i\mathbf{k}).\mathbf{g}(\mathbf{k}i)\\ &-2\lambda\Delta(i\mathbf{j}).\mathbf{g}(\mathbf{jk}).\Delta(\mathbf{k}f).\mathbf{g}(\mathbf{k}i).\mathbf{g}(i\mathbf{k})\\ &-2\lambda\Delta(i\mathbf{j}).\mathbf{g}(\mathbf{j}f).\Delta(f\mathbf{k}).\mathbf{g}(\mathbf{k}i).\mathbf{g}(if).\end{aligned} \tag{9.4}$$

After shifting $\Delta(i,f) \rightarrow \Delta(i,f) - \frac{u_0}{2}\delta(i,f)$ and Fourier transforming these we obtain Eq. (6.33) and Eq. (6.34). These expressions for the self-energies are correct to $O(\lambda)$ and lead to expression for $\mathbf{g}^{-1}$ and μ which are correct to $O(\lambda^2)$. χ can be extracted from Φ as indicated in the text.

Chapter 10

Appendix B: Frequency summations

An efficient method to perform the frequency sums is to work with the time domain formulas Eq. (9.3) and Eq. (9.4) until the final step where Fourier transforms are taken. We note the representation for the Green's function

$$\mathbf{g}(\tau) = \int_x \rho_{\mathbf{g}}(x) e^{-\tau x} \left[\theta(-\tau) f(x) - \theta(\tau) \bar{f}(x) \right], \tag{10.1}$$

so that we can easily compound any pair that arises by dropping the cross products $\theta(\tau)\theta(-\tau)$ and using $\theta(\tau)^2 = \theta(\tau)$. An example illustrates this procedure:

$$\begin{aligned} \mathbf{g}(\tau)\mathbf{g}(-\tau) &= -\int_{x,y} \rho_{\mathbf{g}}(x)\rho_{\mathbf{g}}(y) e^{-\tau(x-y)} \times \\ &\quad \left[\theta(-\tau) f(x)\bar{f}(y) + \theta(\tau)\bar{f}(x) f(y) \right]. \end{aligned} \tag{10.2}$$

We also need to deal with the convolution of pairs of functions.

$$\begin{aligned} X(\tau) &= \int_{-\beta}^{\beta} d\bar{\tau}\ \mathbf{g}(\bar{\tau}) \left[\Delta(\tau-\bar{\tau}) - \frac{u_0}{2}\delta(\tau-\bar{\tau})\right] \\ &= \int_x \rho_M(x) e^{-\tau x} \left[\theta(-\tau) f(x) - \theta(\tau)\bar{f}(x)\right], \end{aligned} \tag{10.3}$$

where the density $\rho_M(x)$ is defined in Eq. (6.49). This equation in turn is easiest to prove by transforming into a product in the Matsubara frequency space, simplifying using partial fractions, and then transforming back to time domain. We next note that Eq. (9.3) and Eq. (9.4) imply

$$\begin{aligned} \Psi(\tau) &= -2\lambda\ X(\tau)\mathbf{g}(\tau)\mathbf{g}(-\tau), \\ \chi(\tau) &= -2\lambda\ X(\tau)X(-\tau)\mathbf{g}(\tau), \end{aligned} \tag{10.4}$$

so that taking Fourier transforms is simplest if first multiply out as in Eq. (10.2), leading to Eq. (6.50).

Part IV

High-temperature expansion for dynamic correlation functions

Chapter 11

Introduction

11.1 Previous work

An important tool in the study of the Hamiltonian in Eq. (0.3) is the high temperature expansion. In this expansion, various static and dynamic quantities such as the thermodynamic potential, the electron Green's function, and the (time-dependent) density-density and spin-spin correlation functions are expanded in the parameter βt, where β is the inverse temperature. Some recent examples of the use of the high temperature expansion can be found in Refs. [12] and [67], in which it is used synergistically with ECFL and DMFT respectively. In Ref. [12], the high-temperature expansion for the electron Green's function in the infinite-U Hubbard model is used to benchmark ECFL calculations. Furthermore, combined with insight gained from the asymmetric shape of the ECFL spectral function, it is used to study the evolution of the Fermi surface in the limit $n \to 1$. In [67], the high temperature expansion and DMFT are used to study the thermodynamic properties of the Hubbard Model and its implications for cold atomic gases in optical lattices.

In the 1970's and 1980's, Plischke[65], Kubo and Tada[66] extended the methods of Betts et. al.[64] (for the XY model) to the study the thermodynamic and ferromagnetic properties of the infinite-U Hubbard model, through the calculation of the high temperature expansion of the thermodynamic potential and static correlation functions. Although series expansions usually seek to remove disconnected diagrams using the linked-cluster theorem [62, 63], their approach contains disconnected diagrams and relies on the use of restricted lattice sums, in which distinct vertices of a diagram represent distinct sites on the lattice. In 1991, Metzner formulated the linked-cluster expansion around the atomic limit of the Hubbard model[21], in which the lattice sums are unrestricted, and disconnected diagrams are explicitly eliminated from the formalism. Metzner's expansion applies to both static and dynamic quantities, such as the single particle Green's function, and higher order dynamic correlation functions. In spite of this, there have not been many numerical results for the high-temperature series for dynamic correlation functions. Some notable exceptions are presented in Refs. [69] and [68], in which the Green's function is calculated to 8^{th} order for the infinite-U Hubbard model, and 5^{th} order for the finite-U Hubbard model respectively, using the Metzner (or similar) formalism.

11.2 Results

In this chapter, we extend the method of Kubo et. al. to the calculation of **dynamic correlation functions** for the infinite-U Hubbard model. We introduce an improvement in the evaluation of the spin sum and signature of a diagram, which permits us to make this evaluation with greater ease and for an arbitrary number of spin species m.

We also introduce a novel approach for dealing with the problem of disconnected diagrams, this is the main achievement of our work. Although this problem has been addressed in various ways in the context of high-temperature expansions of the Ising and Heisenberg models[63], and the methods adapted to the infinite-U Hubbard model by Kubo et. al., our approach is distinct from those taken previously. It has the advantage that it can be easily generalized to the case of dynamic correlation functions, as we do here. In our approach, first the connected diagrams are evaluated. Their contribution feeds into a temporal part and a spatial part, the latter consisting of the lattice sum of the diagram. Then, an arbitrary number of the connected diagrams are chosen to create a "generalized connected diagram". The temporal contribution of this generalized connected diagram consists of the product of the temporal contributions of the constituent diagrams, and its spatial contribution consists of the lattice sum of all the ways that one can partially or fully overlap these constituent diagrams on the lattice. The linked cluster theorem is then proved to be valid with respect to the generalized connected components. Our method is computationally more efficient than any used previously, and we are therefore able to calculate the Green's function to fourth order in βt by hand. Taking the $m \to \infty$ limit, we obtain expressions for the Dyson-Mori self-energy valid in the limit of infinite spin species, which may be interesting in the context of slave boson techniques [44, 71, 72]. Numerical high order calculations for both the Green's function and the time-dependent density-density and spin-spin correlation functions shall be presented in a separate paper[70].

11.3 Outline of the chapter

In sections 12.1 and 12.2, we develop diagrammatic rules for the partition function, and give examples of their use. In section 12.3 we discuss the linked-cluster theorem with respect to "generalized connected components". In sections 12.4 and 12.5 we derive a formula for the restricted lattice sum of a disconnected diagram with n of the original components and use this formula to prove the aforementioned linked-cluster theorem. We are thus able to write the thermodynamic potential as a sum of the contributions of the generalized connected components. In sections 13.1 and 13.2, we extend the methods developed for the thermodynamic potential to derive diagrammatic rules for the Green's function. In particular, the linked-theorem is used to show that the partition function in the denominator of the Green's function cancels the disconnected diagrams consisting of several generalized connected components in the numerator. Hence, the Green's function is written as a sum of generalized connected components. In section 13.3, we give results for the Green's function to 4^{th} order in βt for m spin species on a d-dimensional hypercube. In section 13.4, we give the 4^{th} order results for the Dyson-Mori self-energy in the limit of infinite spin species i.e. $m \to \infty$. Finally, in section 13.5, we extend the formalism to the calculation of time-dependent density-density and spin-spin correlation functions.

Chapter 12

Expansion for the thermodynamic potential

12.1 Diagrams for the partition function

The partition function and thermodynamic potential are defined as

$$Z = Tr(e^{-\beta \hat{H}}); \qquad \Omega = -T \ln Z. \tag{12.1}$$

We write the Hamiltonian as

$$\hat{H} = \hat{T} - \mu \hat{N}, \tag{12.2}$$

where $\hat{T}$ is the kinetic energy operator, and $\hat{N}$ is the number operator. Comparison with Eq. (0.3) shows that

$$\hat{T} = -\sum_{ij\sigma} t_{ij} X_i^{\sigma 0} X_j^{0\sigma}; \quad \hat{N} = \sum_{i\sigma} X_i^{\sigma\sigma}. \tag{12.3}$$

The partition function (Eq. (12.1)) is then written as

$$Z = Tr(e^{\beta\mu\hat{N}} e^{-\beta\hat{T}}), \tag{12.4}$$

where we have used the fact that the kinetic energy operator commutes with the number operator. Expanding $e^{-\beta\hat{T}}$, we obtain

$$\frac{Z}{Z_0} = \sum_{n=0}^{\infty} \frac{\beta^n}{n!} \sum_{\substack{j_1 j_1' \ldots j_n j_n' \\ \sigma_1 \ldots \sigma_n}} t_{j_1 j_1'} \ldots t_{j_n j_n'} \langle X_{j_1'}^{\sigma_1 0} X_{j_1}^{0\sigma_1} \ldots X_{j_n'}^{\sigma_n 0} X_{j_n}^{0\sigma_n} \rangle_0, \tag{12.5}$$

where we have used the definitions

$$Z_0 \equiv Tr(e^{\beta\mu\hat{N}}); \quad \langle \hat{O} \rangle_0 \equiv \frac{Tr(e^{\beta\mu\hat{N}}\hat{O})}{Z_0}. \tag{12.6}$$

The creation and destruction operators in the expectation value in Eq. (12.5) will distribute amongst the various sites of the lattice with the following restrictions. For a given site, creation and destruction must alternate. There must be an even number acting on each site. In addition, $X_{j_p'}^{\sigma_p 0}$ and $X_{j_p}^{0\sigma_p}$ operate on neighboring sites. Within the expectation value, the operators must be permuted from their current order so that all operators acting on a given site are next to each other. The sign of the diagram is determined by whether

the necessary permutation is even or odd. Once this permutation is done, the expectation value factors into a product of single site expectation values for each of the sites being acted on. Suppose there are p operators acting on a given site. Then, the expectation value for this site must have one of the 2 following forms:

$$\langle X^{\sigma_1 0} X^{0\sigma_2} X^{\sigma_3 0} X^{0\sigma_4} \dots X^{\sigma_{p-1} 0} X^{0\sigma_p} \rangle_0 = \frac{\rho}{m} \delta_{\sigma_p \sigma_1} \delta_{\sigma_{p-1} \sigma_{p-2}} \dots \delta_{\sigma_3 \sigma_2}, \tag{12.7}$$

or

$$\langle X^{0\sigma_1} X^{\sigma_2 0} X^{0\sigma_3} X^{\sigma_4 0} \dots X^{0\sigma_{p-1}} X^{\sigma_p 0} \rangle_0 = (1-\rho) \delta_{\sigma_p \sigma_{p-1}} \delta_{\sigma_{p-2} \sigma_{p-3}} \dots \delta_{\sigma_2 \sigma_1}, \tag{12.8}$$

where $\rho \equiv \frac{me^{\beta\mu}}{1+me^{\beta\mu}}$. This observation allows us to write down the rules for calculating the n^{th} order contribution to $\frac{Z}{Z_0}$:

1 Using lines labeled by σ_i starting from σ_n and going down to σ_1, draw all topologically distinct diagrams, such that each line emerges from one vertex and enters into another one. Each vertex can be one of 2 types, a filled circle $\bigotimes$ or an empty one $\bigcirc$. Every time a line is drawn, it can be attached to two existing vertices, or one may create new vertices for it to attach to. Multiple lines can go into the same vertex. However, the following rules must be satisfied at each step $i : n \to 1$ of the diagram process.

[a] For a filled circle with an odd number of lines attached to it, there must be one more coming out than going in. The opposite is true for an empty circle, one more going in than coming out.

[b] For an empty or filled circle with an even number of lines, as many must go

out as come in.

[c] In the final diagram, all circles must have an even number of lines.

2 Insert a factor of $\frac{\rho}{m}$ for each filled circle, and $1-\rho$ for each empty circle.

3 Each vertex is a distinct site on the lattice with lines connecting nearest neighbors. Compute the multiplicity of each diagram over the entire lattice (with the restriction that vertices are distinct sites and their relative positions are as indicated by the lines of the graph). Insert a factor of t^n.

4 Insert a factor of $\frac{\beta^n}{n!}$.

5 Determine the spin sum and the sign of the diagram as follows. At each site, pair the lines in the following way. For a full site with p lines,

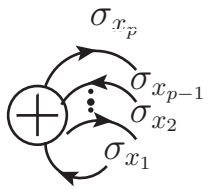

$$x_1 < x_2 \ldots < x_{p-1} < x_p$$

the pairings are $(x_1, x_p)(x_2, x_3)\ldots(x_{p-2}, x_{p-1})$. For an empty site with p lines,

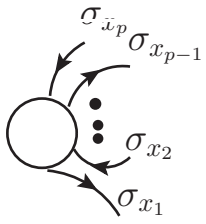

$$x_1 < x_2 < \ldots < x_{p-1} < x_p$$

the pairings are $(x_1, x_2)(x_3, x_4)\ldots(x_{p-1}, x_p)$.

Split the diagram into loops in the following way. Find the filled site with the line labeled by σ_n coming out of it. Find the line that this line is paired to on this site, and follow it to a neighboring site. Find the line that this new line is paired to on that site, and follow that line to a neighboring site, etc. Do this until you complete a loop. Now, find the highest remaining spin, call it σ_q, which will also come out of a full site. Repeat the above process to get another loop. Make loops until you run out of lines. Let l be the number of loops, and x be the number of full sites in the diagram. Insert a factor of $m^l(-1)^{x-l}$.

12.2 Derivation of sign and spin sum rule

Rules 1-4 follow from the expression for $\frac{Z}{Z_0}$ by inspection. We now derive rule 5. We will first show why it works for some examples and then prove that it works for all diagrams. The examples will also illustrate the other rules.

12.2.1 Examples

Consider the following example from fourth order.

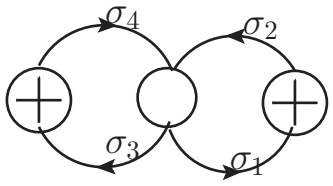

$(\frac{\rho}{m})^2(1-\rho)t^4L(2d)(2d-1)\frac{\beta^4}{24}m^2$

The original ordering of operators in the expectation value is $\langle X_{j_1'}^{\sigma_1 0} X_{j_1}^{0\sigma_1} X_{j_2'}^{\sigma_2 0} X_{j_2}^{0\sigma_2} X_{j_3'}^{\sigma_3 0} X_{j_3}^{0\sigma_3} X_{j_4'}^{\sigma_4 0} X_{j_4}^{0\sigma_4} \rangle_0$. Let us label the diagram by writing the indices of the operators acting on a given site above the site.

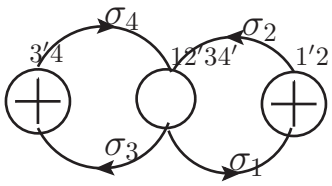

$(\frac{\rho}{m})^2(1-\rho)t^4L(2d)(2d-1)\frac{\beta^4}{24}m^2$

Let us now determine the sign of the diagram. This is the number of transpositions it takes to get between the following 2 orderings: 3'412'34'1'2 and 1'12'23'34'4. We can move a number past 2 numbers without changing the sign. We can also move a pair of numbers anywhere we want without changing the sign. Let us pair the numbers as indicated in rule 5 above: (3',4)(1,2')(3,4')(1',2). Let us now move the (3,4') pair inside the (3',4) pair to obtain (3'34'4)(1,2')(1',2). Let us now move the (1,2') pair inside the (1',2) pair to obtain (3'34'4)(1'12'2). Now we can move x'x pairs to get the desired order 1'12'23'34'4. Hence, the sign of the diagram is (+). Now we determine the contribution from the spin sum. For empty sites, we must first create a particle. For filled sites, we must first destroy a particle. Hence, recalling Eqs. (12.7) and (12.8), we see that the pairings in rule 5 correspond to the Kronecker deltas in these formulas. In addition, x' and x share the same spin label σ_x. Hence, in our expression (3'34'4)(1'12'2), all numbers within a given parenthesis share the same spin. Hence, the spin sum is m^2.

Alternatively, if we go back to the diagram and make loops by the process indicated in step 5 of the rules, we will see that the first loop corresponds to (3'34'4), while the second one corresponds to (1'12'2). Since there are 2 full sites in the diagram and 2 loops, rule 5 says that the sign and spin sum give a factor of $(-1)^{2-2}m^2 = +\ m^2$, which is exactly what we found. Using the other rules as well, the contribution of the diagram can be found and is written next to the diagram. We have assumed that the lattice is a d-dimensional

hypercube. Let us consider another example.

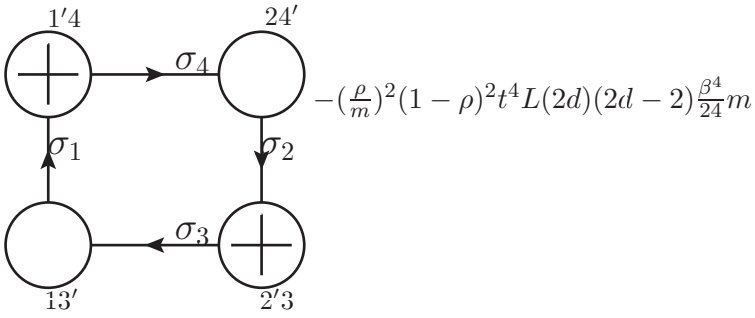

The initial ordering is 1'424'2'313'. Again, pair the numbers according to rule 5: (1',4)(2,4')(2',3)(1,3'). Move the (1,3') pair into (1',4) pair to obtain: (1'13'4)(2,4')(2',3). Now move the (2',3) pair inside the loop to obtain: (1'13'2'34)(2,4'). Now we need a transposition to get 3 to the right of 3'. This gives a (-) sign. We obtain: -(1'13'32'4)(2,4'). Now put (2,4') into the loop to obtain: -(1'1'3'32'24'4) = -(1'1'2'23'34'4). The reason that we got an overall (-) sign for this diagram was because the (2',3) pair was in the "wrong" order with the primed number to the left of the unprimed one instead of the other way around. Both (1,3') and (2,4') were in the "right" order and hence generated no (-) sign. The wrong order came about because (2',3) was on a full site rather than an empty site. The full site pair (1',4) did not generate a (-) sign because it started the loop. Hence, full sites generate (-) signs except when they start loops. This is the reason for the factor $(-1)^{x-l}$ in rule 5. Since we put everything into one parenthesis this time, the spin sum gives a factor of m.

Alternatively, using step 5 of the rules we would break the diagram into one loop. In addition, it has 2 full sites. So the factor from the sign and the spin sum should be $(-1)^{2-1}m^1 = -m$ as we have already found. Using the other rules as well, the contribution

of the diagram can be found and is written next to the diagram.

The only case we have yet to consider is when full sites have multiple pairs on them. Let us consider a full site which has the numbers $x'_1 x_2 x'_3 x_4 \dots x'_{p-1} x_p$ on it. In this case, the pairings should be made according to rule 5: $(x'_1, x_p)(x_2, x'_3) \dots (x_{p-2}, x'_{p-1})$. Making the pairings in this way does not generate a (-) sign because x_p has to move past a certain number of pairs to get to the right of x'_1. We see that only the (x'_1, x_p) pair is in the "wrong" order while the other pairs are in the "right" order. Hence, only this pair has the potential to generate a (-) sign and will do so unless it is used to start a loop. Let us consider a concrete example from sixth order which illustrates this.

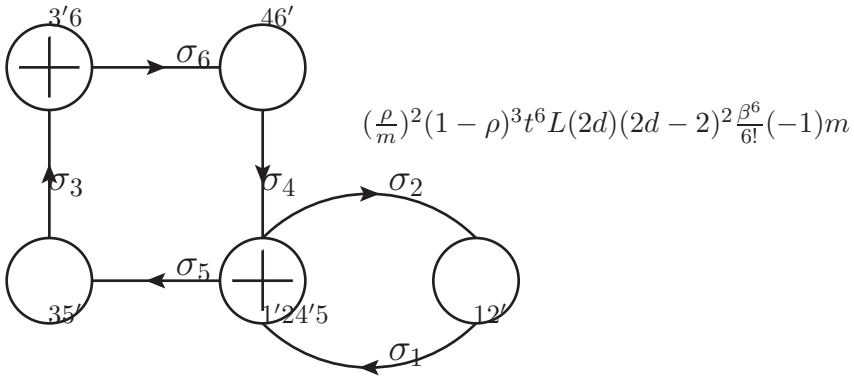

The initial ordering is 3'646'12'1'24'535'. Now we pair the numbers:

(3',6)(4,6')(1,2')(1',5)(2,4')(3,5'), and perform the necessary steps to bring them into the

desired order.

$$(3',6)(4,6')(1,2')(1',5)(2,4')(3,5') = (3'35'6)(4,6')(1,2')(1',5)(2,4')$$
$$= (3'35'1'56)(4,6')(1,2')(2,4') = -(3'35'51'6)(4,6')(1,2')(2,4')$$
$$= -(3'35'51'12'6)(4,6')(2,4') = -(3'35'51'12'24'6)(4,6')$$
$$= -(3'35'51'12'24'46'6) = -(1'12'23'34'45'56'6). \tag{12.9}$$

Note that the full site on the bottom right corner of the square generated a (-) sign from its "wrong" pair (1',5), which was not used to start a loop. The "wrong" pair (3',6) on the full site at the top left corner of the square was used to start a loop, and hence did not generate a (-) sign. Therefore, the overall sign of the diagram is (-). All of the pairs were put into one parenthesis, and hence the spin sum gave a factor of m.

Alternatively, we could use rule 5 according to which we find that the diagram has 1 loop. We also see that it has 2 full sites. Hence, the sign and spin sum give the contribution $(-1)^{2-1}(m)^1 = -m$, which matches our previous result. The total contribution of the diagram is again written next to the diagram.

12.2.2 Proof of the general case

We can now write down a rigorous proof for rule 5 for an n^{th} order diagram. For a given vertex, we indicate an incoming line with a prime, and an outgoing line with no prime. In the notation of rule 5, empty sites have the pairs $(x_1, x_2')(x_3, x_4') \dots (x_{p-1}, x_p')$ on them, while full sites have the pairs $(x_1', x_p)(x_2, x_3') \dots (x_{p-2}, x_{p-1}')$ on them. The loop starts with the pair (x', n) on a full site. This corresponds to the (x_1', x_p) pair on this site.

The next pair in this loop is either (x, y') or (y', x), where the latter can only correspond to the (x'_1, x_p) pair on a full site. The loop now becomes $\pm(x'xy'n)$ where (x, y') yields + and (y', x) yields $-$. This process continues until we come across n' at which point we complete the first loop.

Suppose that the first loop has not exhausted all of the lines in the diagram. Of the lines not used in the first loop, find the one with the highest spin label, σ_q. We now show that q must occur in a pair of the form (u', q), corresponding to the (x'_1, x_p) pair on a full site. The number q must be on some vertex. Remove the pairs that were used in the first loop from this vertex. q must be the biggest number of those still left on this vertex. However, we see that this could only occur if $x_p = q$ for a full site in the original diagram.

The pair (u', q) will start the second loop, which will be formed in exactly the same way as the first loop. We repeat the same reasoning to show that all of the loops are started by pairs of the form (x'_1, x_p) on full sites. Those (x'_1, x_p) pairs on full sites which do not start loops will generate (-) signs. This means that of the x full sites, $x - l$ generate $(-)$ signs. Hence, the overall sign of the diagram is $(-1)^{x-l}$. Furthermore, the lines in a loop must share the same spin, independent of the other loops. Hence, the spin sum is m^l. Thus, the overall factor from the sign and spin sum is $(-1)^{x-l}m^l$ as stated in rule 5.

12.3 Loss and recovery of the linked cluster theorem

In the case of Feynman diagrams or the Meyer cluster expansion of the classical gas, disconnected diagrams arise in the expression for the partition function, but are eliminated from the thermodynamic potential upon taking the log of the partition function. This so-

called "linked cluster theorem" [62, 63] is a consequence of two properties of the disconnected diagrams. a) The contribution of a disconnected diagram is the product of the contributions of the connected components from which it is formed. b) The combinatorial factors involved in permuting the labels work out in just the right way for the cancellation to occur. In the case of the expansion at hand, property b) continues to hold. However, property a) breaks down due to the restricted lattice sum in which the distinct vertices of the diagram represent distinct sites on the lattice. This is illustrated below by the simplest disconnected diagrams in the calculation of $\frac{Z}{Z_0}$, which appear in 4th order.

$\rho^2(1-\rho)^2\frac{\beta^4}{24}t^4L(2d)[2dL-4(2d-1)-2]$

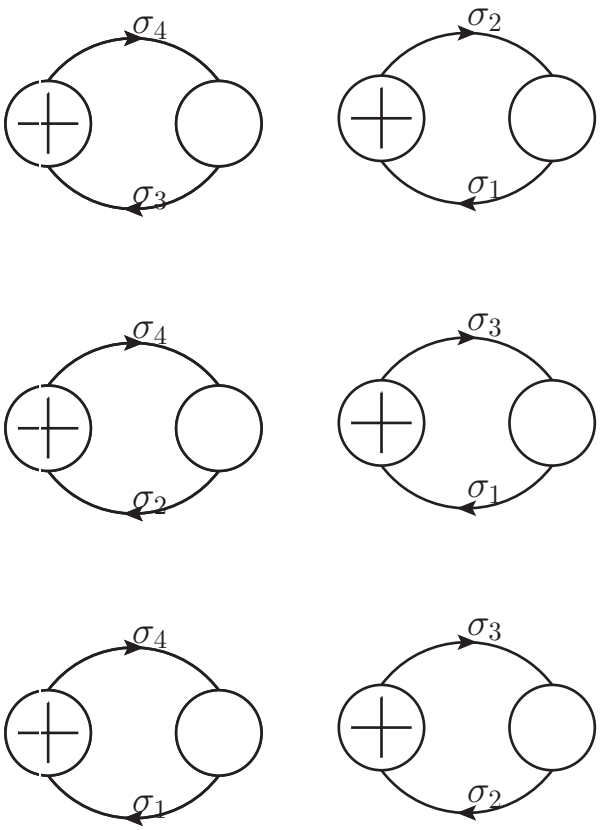

Applying the rules for $\frac{Z}{Z_0}$, we see that they all have an identical contribution which is written above the diagrams. The permutation of line labels leads to $\binom{4}{2}\frac{1}{2!}=3$ diagrams.

There are 4 lines, 2 of which must be chosen for the connected component on the left. However, since the 2 components are identical, exchanging all of the labels between them does not lead to a new labeling.

The lattice sum for each of these disconnected diagrams is $(2dL)[2dL-4(2d-1)-2]$. This lattice sum comes about because the vertices are restricted to being distinct sites on the lattice. For a second, let us suppose that this is not the case, and that the lattice sum is unrestricted. The lattice sum would then simply be $(2dL)^2$. In this case, the total contribution from the three disconnected diagrams would be $(\frac{Z}{Z_0})^{(4)}_{disconnected} = \rho^2(1-\rho)^2\frac{\beta^4}{8}t^4(2dL)^2$. We relate this contribution to the contribution of the only second order diagram, from which these disconnected diagram are formed.

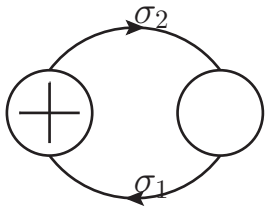

$$\rho(1-\rho)\frac{\beta^2}{2}t^2L(2d)$$

We find that $(\frac{Z}{Z_0})^{(4)}_{disconnected} = \frac{[(\frac{Z}{Z_0})^{(2)}]^2}{2!}$. This is exactly the factor we need for the linked-cluster theorem to work.

Let us return to the actual situation, in which the vertices are in fact restricted to being distinct sites on the lattice. In this case, the lattice sum of each diagram is $(2dL)[2dL-4(2d-1)-2]$. This lattice sum contains a term proportional to L and one proportional to L^2. However, we have just shown that the one proportional to L^2 is cancelled upon taking the log of the partition function, leaving only the one proportional to L. We expect this to be the case since the thermodynamic potential is an extensive quantity.

Therefore, we see that the linked cluster theorem may yet be possible, but with a generalized definition of the "connected components" which go into making a diagram. These generalized connected components will involve overlappings of the original connected components. A disconnected diagram for the partition function involving a number of these generalized connected components will in fact now satisfy both properties a) and b), necessary for the linked cluster theorem to work. Taking the log of the partition function will eliminate all disconnected diagrams leaving only the generalized connected components. This will also provide a rigorous proof for the observation just made, that the thermodynamic potential corresponds to the term proportional to L in the partition function. The proof of the linked cluster theorem in terms of generalized connected components will hinge upon a formula for the restricted lattice sum of a disconnected diagram with n of the original components, which we shall now derive.

12.4 Formula for the restricted lattice sum of disconnected diagrams

12.4.1 Restricted lattice sum of disconnected diagrams with 3 components

The simplest instance of a disconnected diagram is one of the 4th order disconnected diagrams considered above. One of the connected components can be placed anywhere on the lattice, hence the factor $(2dL)$. The other component can be placed anywhere on the lattice such that none of its sites overlap any of the sites of the first one. The number

of ways it can overlap the first one with just one site is $4(2d-1)$. The number of ways it can overlap it with both sites is 2. Hence the factor $[2dL - 4(2d-1) - 2]$. The lattice sum is thus $(2dL)[2dL - 4(2d-1) - 2]$.

In the case where there are more than two disconnected components, it will be difficult to calculate the lattice sum by adding on one component at a time, because for the third one, its options depend on how far apart the first two are on the lattice. Hence, we need a systematic way of calculating the lattice sums. Consider a disconnected diagram with 2 components.

$$LS[A\ dc\ B] = LS[AB] - LS[(A \cap B)]. \tag{12.10}$$

Here, $LS[A\ dc\ B]$ indicates the lattice sum of A disconnected from B, and is what we are trying to calculate for a disconnected diagram. $LS[AB]$ indicates the lattice sum where A and B ignore each other, and can each be placed anywhere on the lattice. Hence, $LS[AB] = LS[A]LS[B]$. $LS[(A \cap B)]$ indicates the lattice sum where A and B somehow overlap. We generalize this notation. $LS[D_1\ dc\ D_2\ dc \ldots dc\ D_n]$ indicates the lattice sum of the components $D_1 \ldots D_n$ in which they are not allowed to overlap each other in any way, and is the object that we need a systematic way of calculating. $LS[D_1 D_2 \ldots D_n] = LS[D_1]LS[D_2] \ldots LS[D_n]$. Finally, $LS[(D_1 \cap D_2 \cap \ldots \cap D_n)]$ indicates the lattice sum of the components $D_1 \ldots D_n$ in which they must overlap to form one connected component, but no two of the $D_1 \ldots D_n$ are required to overlap each other.

Consider a disconnected diagram with 3 components.

$$\begin{aligned} LS[A\ dc\ B\ dc\ C] &= LS[ABC] - LS[(A \cap B \cap C)] - LS[(A \cap B)\ dc\ C] \\ &\quad -LS[(A \cap C)\ dc\ B] - LS[(B \cap C)\ dc\ A]. \end{aligned} \tag{12.11}$$

Here, $LS[(A \cap B)\ dc\ C]$ indicates the lattice sum where A and B overlap to form a connected component, which is then not allowed to overlap the component C. This formula states that to obtain the lattice sum of A, B, and C not overlapping in any way, we take the lattice sum of them ignoring each other, and subtract the lattice sums of all of the possible ways in which they can overlap (either overlapping to form one connected component or two, which are then not allowed to overlap each other). According to the formula for two components, we have

$$LS[(A \cap B)\ dc\ C] = LS[(A \cap B)C] - LS[((A \cap B) \cap C)]. \tag{12.12}$$

Here, $LS[((A \cap B) \cap C)]$ indicates the lattice sum in which first A and B must overlap to form a connected component, and then the resulting connected component must overlap C. This is not the same as the term $LS[(A \cap B \cap C)]$ in which A, B, and C must overlap to form a connected component, but may do so without A overlapping B. In general, we use the notation $(D_1 \cap D_2 \cap \ldots \cap D_n)$ to indicate that first $D_1 \ldots D_n$ must overlap to form a

connected component. Combining Eq. (12.11) with Eq. (12.12), we see that

$$LS[A\ dc\ B\ dc\ C] = LS[ABC] - LS[(A \cap B \cap C)] - LS[(A \cap B)C] + LS[((A \cap B) \cap C)]$$
$$-LS[(A \cap C)B] + LS[((A \cap C) \cap B)] - LS[(B \cap C)A] + LS[((B \cap C) \cap A)]. \quad (12.13)$$

12.4.2 Restricted lattice sum of disconnected diagrams with n components

Consider a disconnected diagram with n components $D_1 \dots D_n$. The object we wish to calculate is $LS[D_1\ dc\ D_2\ dc \dots dc\ D_n]$. We think of each term in Eq. (12.13) as coming from a particular "configuration". For example, the term $LS[((B \cap C) \cap A)]$ comes from the configuration $((B \cap C) \cap A)$. We call $D_1 D_2 \dots D_n$ the initial configuration. $LS[D_1\ dc\ D_2\ dc \dots dc\ D_n]$ is a sum of terms, which are generated by the following set of rules:

1 Starting from the initial configuration, arbitrarily group the components $D_1 \dots D_n$. Enclose each group with a parenthesis and place intersection symbols between the members of a single group. For a component not grouped with any of the other ones we imagine that there is a parenthesis around it but we do not draw it in.

2 Identify the **outer parentheses**. These are the parentheses not enclosed in any other parenthesis. Arbitrarily group the outer parentheses. Enclose each group with a parenthesis and place intersection symbols between the members of a single group.

3 We denote each time you group objects as a step. Take anywhere from 0 to $n-1$ steps, each time grouping the outer parentheses, to get from the initial configu-

ration to the final configuration associated with this sequence of steps. The final configuration will have $p \leq n$ outer parentheses. Each outer parenthesis represents an overlapping of some subset of the components present in the initial configuration. **Let us number the outer parentheses by the index i, and denote the overlapping of components represented by each outer parenthesis as w_i.** Let s denote the number of steps taken. Then, the contribution of this sequence of steps to $LS[D_1\ dc\ D_2\ dc \ldots dc\ D_n]$ is given by $(-1)^s LS[w_1 w_2 \ldots w_p] = (-1)^s LS[w_1]LS[w_2]\ldots LS[w_p]$.

4 $LS[D_1\ dc\ D_2\ dc \ldots dc\ D_n]$ is given by the sum of all terms generated by a distinct sequence of steps.

We illustrate these rules with a couple of examples from the case $n = 3$ (Eq. (12.13)). Consider the configuration $(A \cap B)C$. It is reached from the initial configuration by grouping A and B in the first step. Hence, $s = 1$, $w_1 = (A \cap B)$, and $w_2 = C$. The contribution of this sequence of steps is therefore $(-1)^1 LS[(A \cap B)C] = -LS[A \cap B]LS[C]$. Consider the configuration $((A \cap B) \cap C)$. It is reached from the initial configuration by grouping A and B in the first step. The second step consists of grouping $(A \cap B)$ with C. Hence, $s = 2$, and $w_1 = ((A \cap B) \cap C)$. The contribution of this sequence of steps is therefore $(-1)^2 LS[((A \cap B) \cap C)] = LS[((A \cap B) \cap C)]$.

For $n \leq 3$ components, each final configuration must be reached by a unique sequence of steps starting from the initial configuration. However, this is not the case for $n \geq 4$. For $n = 4$, consider the configuration $(D_1 \cap D_2)(D_3 \cap D_4)$. There are three distinct sequences of steps to get from the initial configuration to this configuration. One sequence

involves only one step in which D_1 and D_2 are grouped together and D_3 and D_4 are grouped together. Another sequence involves two steps. In the first step, D_1 and D_2 are grouped together, while in the second one D_3 and D_4 are grouped together. The third sequence also involves two steps. In the first step, D_3 and D_4 are grouped together, while in the second one D_1 and D_2 are grouped together. Since all of these sequences end in the same final configuration, their contribution differs only in the number of steps it takes to get from the initial configuration to this final configuration. The first sequence involves only one step and hence has a contribution of $-LS[(D_1 \cap D_2)]LS[(D_3 \cap D_4)]$. The other two sequences each involve 2 steps and hence each have a contribution of $LS[(D_1 \cap D_2)]LS[(D_3 \cap D_4)]$. Hence, the overall contribution of this configuration is $-LS[(D_1 \cap D_2)]LS[(D_3 \cap D_4)] + 2LS[(D_1 \cap D_2)]LS[(D_3 \cap D_4)] = LS[(D_1 \cap D_2)]LS[(D_3 \cap D_4)]$.

12.4.3 Classification of configurations

We now want to isolate a particular final configuration, and add all of the contributions from the distinct sequences of steps which lead to this final configuration from the initial configuration. This will give us the contribution of this final configuration. If we can do this for any final configuration, then instead of adding contributions from sequences of steps to determine $LS[D_1\ dc\ D_2\ dc \ldots dc\ D_n]$, we can add contributions from final configurations. Let us denote an arbitrary final configuration by κ. Suppose κ has p outer parentheses. Then each distinct sequence of steps leading to κ will have the contribution $\pm LS[w_1]LS[w_2] \ldots LS[w_p]$, where the choice of plus or minus depends on how many steps there are in that sequence. Hence, the overall contribution from κ will be

$C_\kappa LS[w_1]LS[w_2]\dots LS[w_p]$ where $C_\kappa = \sum_{sequences} (-1)^{s(sequence)}$, where the sum is over all sequences leading to κ from the initial configuration. We want to find C_κ for all κ. To this end, we classify the different κ into types that will share the same value of C_κ.

First, we classify the parentheses appearing in the various configurations. A type 0 parenthesis is the invisible parenthesis enclosing any one of the n components present in the initial configuration. A type 1 parenthesis is a parenthesis which encloses only type 0 parentheses. A type 2 parenthesis encloses at least 1 type 1 parenthesis and zero or more parentheses of lower type. A type 3 parenthesis encloses at least 1 type 2 parenthesis and zero or more parentheses of lower type. A type k parenthesis encloses at least 1 type $k-1$ parenthesis and zero or more parentheses of lower type. We give some examples to illustrate the different types of parentheses. In the following examples, the very outer parenthesis is of the specified type. Type 1 parenthesis: $(D_1 \cap D_2)$. Type 2 parenthesis: $((D_1 \cap D_2) \cap D_3)$. Type 3 parenthesis: $(((D_1 \cap D_2) \cap D_3) \cap (D_4 \cap D_5))$.

We are now in a position to classify all of the final configurations. A type $m_{(i_1,i_2,\dots,i_m)}$ configuration is a configuration which has i_1 type 1 parentheses, i_2 type 2 parantheses, $\dots i_m$ type m parentheses. Every possible final configuration falls into one of these types. We shall see that all final configurations of a given type have equal C_κ. For a configuration κ of type $m_{(i_1,i_2,\dots,i_m)}$, we shall denote C_κ by $C_{m_{(i_1,i_2,\dots,i_m)}}$. The following are examples of different types of configurations. $1_{(1)}$: $(D_1 \cap D_2)D_3D_4$, $1_{(2)}$: $(D_1 \cap D_2)(D_3 \cap D_4)$, $2_{(1,1)}$: $((D_1 \cap D_2) \cap D_3 \cap D_4)$, $2_{(2,1)}$: $((D_1 \cap D_2) \cap (D_3 \cap D_4))$, $2_{(1,2)}$: not possible, $2_{(2,2)}$: $((D_1 \cap D_2) \cap D_3)((D_4 \cap D_5) \cap D_6)$, $3_{(1,1,1)}$: $(((D_1 \cap D_2) \cap D_3) \cap D_4)$, etc.

12.4.4 Calculation of $C_{1_{(i_1)}}$

We now calculate $C_{m_{(i_1,i_2,\ldots,i_m)}}$ for a few simple cases before stating and proving the general result. We start with C_0. This is just the initial configuration, reached by making 0 steps.

$$C_0 = 1. \tag{12.14}$$

Consider one of the type $1_{(1)}$ configurations. The only sequence of steps by which one can get to this configuration is to form the single type 1 parenthesis on the first step.

$$C_{1_{(1)}} = -1. \tag{12.15}$$

Consider one of the type $1_{(2)}$ configurations. As already discussed, there are 3 distinct sequences of steps by which this configuration can be reached. One consists of forming both type 1 parentheses in one step from the initial configuration, while the other two consist of forming one of the type 1 parentheses as the first step and forming the other one as the second step.

$$C_{1_{(2)}} = -1 + 2 \times 1 = 1. \tag{12.16}$$

The way in which we shall calculate $C_{1_{(3)}}$ illustrates the way in which we shall calculate $C_{m_{(i_1,i_2,\ldots,i_m)}}$ for all m. Consider a particular type $1_{(3)}$ configuration. In all of the sequences of steps which lead to this configuration, the configuration reached right before

the last step in the sequence must be either of type 0, $1_{(1)}$, or $1_{(2)}$. Hence, we have the following formula for $C_{1_{(3)}}$.

$$C_{1_{(3)}} = C_0(-1) + (\#\text{ of type } 1_{(1)}\text{configs. 1 step away from type } 1_{(3)}\text{config.})C_{1_{(1)}}(-1)$$
$$+(\#\text{ of type } 1_{(2)}\text{configs. 1 step away from type } 1_{(3)}\text{config.})C_{1_{(2)}}(-1). \tag{12.17}$$

Thus, our strategy in calculating $C_{m_{(i_1,i_2,\ldots,i_m)}}$ is to calculate these coefficients in the correct order, so that by the time we are calculating the coefficient for a particular type of configuration, we have already calculated the coefficients for all configurations that are within one step of it. This makes the initially daunting task of calculating $C_{m_{(i_1,i_2,\ldots,i_m)}}$ very manageable.

Returning to our calculation of $C_{1_{(3)}}$, a type $1_{(3)}$ configuration can be reached in one step from the initial configuration by forming all three of the type 1 parentheses in this single step. It can be reached in one step from $\binom{3}{1} = 3$ distinct type $1_{(1)}$ configurations, one for each of the type 1 parentheses that define the $1_{(3)}$ configuration. This is done by forming the other two type 1 parentheses in that step. It can be reached in one step from $\binom{3}{2} = 3$ distinct type $1_{(2)}$ configurations, one for each choice of 2 of the type 1 parentheses that define it. This is done by forming the other type 1 parenthesis in that step. Therefore,

$$C_{1_{(3)}} = C_0(-1) + 3C_{1_{(1)}}(-1) + 3C_{1_{(2)}}(-1) = 1(-1) + 3(-1)(-1) + 3(1)(-1) = -1. \tag{12.18}$$

Similarly, we can calculate $C_{1_{(4)}}$.

$$C_{1_{(4)}} = -1 + \binom{4}{1}(-1)(-1) + \binom{4}{2}(1)(-1) + \binom{4}{3}(-1)(-1) = -1 + 4 - 6 + 4 = 1. \tag{12.19}$$

We can now calculate $C_{1_{(i_1)}}$.

$$C_{1_{(i_1)}} = -1 + \binom{i_1}{1} - \binom{i_1}{2} + \binom{i_1}{3} - \ldots + (-1)^{i_1}\binom{i_1}{i_1 - 1} = (-1)^{i_1}. \tag{12.20}$$

12.4.5 Calculation of $C_{m_{(i_1,i_2,\ldots,i_m)}}$ for all m

We are now ready to state and prove the general formula for $C_{m_{(i_1,i_2,\ldots,i_m)}}$

$$C_{m_{(i_1,i_2,\ldots,i_m)}} = (-1)^{i_1+i_2+\ldots+i_m}. \tag{12.21}$$

We prove this formula by induction. Before stating the inductive hypothesis, we order the coefficients $C_{m_{(i_1,i_2,\ldots,i_m)}}$. To compare the coefficients $C_{m_{(i_1,i_2,\ldots,i_m)}}$ and $C_{k_{(j_1,j_2,\ldots,j_k)}}$, find the leftmost entry where they differ, where from left to right the entries are $m, i_1, \ldots, i_m$ and $k, j_1, \ldots, j_k$. The one that has the bigger number in this entry is greater according to this ordering. We write the coefficients in order from least to greatest:

$$C_0, C_{1_{(1)}}, C_{1_{(2)}}, \ldots, C_{2_{(1,1)}}, C_{2_{(2,1)}}, C_{2_{(2,2)}}, C_{2_{(3,1)}}, C_{2_{(3,2)}}, C_{2_{(3,3)}}, \ldots, C_{3_{(1,1,1)}}, \ldots, C_{n-1_{(1,1,1,\ldots,1)}}.$$

Inductive hypothesis: $C_{m_{(i_1,i_2,\ldots,i_m)}} = (-1)^{i_1+i_2+\ldots+i_m}$ holds for all coefficients less than or equal to the r^{th} coefficient in the above sequence of coefficients. We have already proven

the base case, so we now prove the inductive step.

Suppose that the $r+1^{st}$ coefficient is $C_{m_{(i_1,i_2,\ldots,i_m)}}$. The inductive hypothesis implies that

$C_{k_{(j_1,j_2,\ldots,j_k)}} = (-1)^{j_1+j_2+\ldots+j_k}$ if all of the inequalities $k \leq m$, $j_1 \leq i_1$, $j_2 \leq i_2$, $\ldots$, $j_k \leq i_k$ are satisfied, except for the case where all of the inequalities are equalities. We now split the i_1 type 1 parentheses into 2 sets, α and β. In the α set, we put those type 1 parentheses which are enclosed by other (higher type) parentheses. We put the rest into the set β. We do the same for the type 2 parentheses, type 3 parentheses, $\ldots$ type $m-1$ parentheses. All of the type m parentheses are put into the set β since they can't be enclosed by other parentheses. Consider the configurations from which the type $m_{(i_1,i_2,\ldots,i_m)}$ configuration in question can be reached in one step. Any such configuration must have all of the parentheses in the set α, since these are enclosed by higher type parentheses, but we can only make one more step. In addition to these, it can have anywhere from zero to all but one of the parentheses from the set β, since any number of them can be formed in 1 step. Let x be the number of parentheses in the set α, and y be the number of parentheses in the set β. Then,

$$x + y = i_1 + i_2 + \ldots + i_m. \tag{12.22}$$

Consider a configuration κ with all x of the parentheses from the set α and $0 \leq z \leq y-1$ of the parentheses from the set β. Then, by the inductive hypothesis, $C_\kappa = (-1)^{x+z}$. Since one more step is required to reach the type $m_{(i_1,i_2,\ldots,i_m)}$ configuration in question, the contribution of κ to $C_{m_{(i_1,i_2,\ldots,i_m)}}$ is $C_\kappa(-1) = (-1)^{x+z+1}$. There are $\binom{y}{z}$ such configurations

since we have to choose z out of y parentheses from the set β. Therefore,

$$\begin{aligned} C_{m_{(i_1,i_2,\ldots,i_m)}} &= \binom{y}{0}(-1)^{x+1} + \binom{y}{1}(-1)^{x+2} + \binom{y}{2}(-1)^{x+3} \\ &\quad + \binom{y}{3}(-1)^{x+4} + \ldots + \binom{y}{y-1}(-1)^{x+y} \\ &= (-1)^x \left[-1 + \binom{y}{1} - \binom{y}{2} + \binom{y}{3} - \ldots + (-1)^y \binom{y}{y-1} \right] \\ &= (-1)^x (-1)^y = (-1)^{x+y} = (-1)^{i_1+i_2+\ldots+i_m}. \end{aligned} \tag{12.23}$$

Thus we have proven the claim and shown that $C_{m_{(i_1,i_2,\ldots,i_m)}} = (-1)^{i_1+i_2+\ldots+i_m}$.

We now have the following expression for the lattice sum of a disconnected diagram with components $D_1, D_2, \ldots D_n$.

$$LS[D_1\ dc\ D_2\ dc \ldots dc\ D_n] = \sum_{\kappa} (-1)^{i_1+i_2+\ldots+i_m} LS[w_1]LS[w_2]\ldots LS[w_p]. \tag{12.24}$$

Here, the sum is over the configurations κ that one can make from the components $D_1, D_2, \ldots D_n$. Each configuration κ has p outer parentheses, i_1 type 1 parentheses, $\ldots$ i_m type m parentheses. $LS[w_i]$ represents the lattice sum of the overlapping of components inside the i^{th} outer parenthesis.

12.5 Calculation of the thermodynamic potential

12.5.1 Partition function as a sum over configurations

We return to our calculation of $\frac{Z}{Z_0}$ via the diagrammatic rules presented in section 12.1. Let z_D denote the contribution to $\frac{Z}{Z_0}$ of a connected diagram D. Let $z_{(D_1 \ldots D_p)}$ denote

the contribution to $\frac{Z}{Z_0}$ of a disconnected diagram with components $D_1, D_2, \ldots D_p$. Let us recall that such a disconnected diagram will have a certain multiplicity which we denote by $\eta_{(D_1 \ldots D_p)}$. Suppose the components $D_1, D_2, \ldots D_p$ are of orders $n_1, n_2, \ldots n_p$ in t respectively. Then, the whole diagram is of order n in t, where $n = n_1 + n_2 + \ldots + n_p$. In addition, out of the p components $D_1, D_2, \ldots D_p$, let us suppose that $k \leq p$ are distinct, with degeneracies $g_1, g_2, \ldots, g_k$, where $g_1 + g_2 + \ldots + g_k = p$. Then, we find that

$$\eta_{(D_1 \ldots D_p)} = \frac{n!}{n_1! n_2! \ldots n_p!} \frac{1}{g_1! g_2! \ldots g_k!}. \tag{12.25}$$

This factor comes about because we must distribute n labelled lines among p components with n_i lines going to component D_i, but exchanging all of the lines of two identical components does not give a new distribution of lines. Now, instead of drawing $\eta_{(D_1 \ldots D_p)}$ diagrams with different distributions of lines, we draw only one such diagram with contribution

$$\eta_{(D_1 \ldots D_p)} z_{(D_1 \ldots D_p)} = \frac{n!}{n_1! n_2! \ldots n_p!} \frac{1}{g_1! g_2! \ldots g_k!} \frac{\beta^n}{n!} z_{B(D_1 \ldots D_p)} LS[D_1 \; dc \; D_2 \; dc \ldots dc \; D_p]. \tag{12.26}$$

Here, $z_{B(D_1 \ldots D_p)}$ indicates that we have dropped the factors $\frac{\beta^n}{n!}$ and $LS[D_1 \; dc \; D_2 \; dc \ldots dc \; D_p]$ from $z_{(D_1 \ldots D_p)}$. Now, let l denote the number of loops and x denote the number of full sites in the disconnected diagram with components $D_1, D_2, \ldots D_p$. Let l_i denote the number of loops and x_i denote the number of full sites in the component

D_i. Then, we have that

$$\begin{aligned} t^n m^l (-1)^{x-l} &= t^{n_1} m^{l_1} (-1)^{x_1 - l_1} t^{n_2} m^{l_2} (-1)^{x_2 - l_2} \dots t^{n_p} m^{l_p} (-1)^{x_p - l_p}, \\ z_{B(D_1 \dots D_p)} &= z_{BD_1} z_{BD_2} \dots z_{BD_p}. \end{aligned} \tag{12.27}$$

Therefore,

$$\eta_{(D_1 \dots D_p)} z_{(D_1 \dots D_p)} = \frac{1}{g_1! g_2! \dots g_k!} z_{nLD_1} z_{nLD_2} \dots z_{nLD_p} LS[D_1 \ dc \ D_2 \ dc \dots dc \ D_p]. \tag{12.28}$$

Here, z_{nLD} indicates that we have dropped the lattice sum from z_D . The partition function can now be expressed as

$$\frac{Z}{Z_0} = 1 + \sum_{p=1}^{\infty} \sum_{(D_1 \dots D_p)} \frac{1}{g_1! g_2! \dots g_k!} z_{nLD_1} z_{nLD_2} \dots z_{nLD_p} LS[D_1 \ dc \ D_2 \ dc \dots dc \ D_p]. \tag{12.29}$$

Here, the sum over $(D_1 \dots D_p)$ includes only one term for each set of connected components since the multiplicity from the different distributions of lines has already been taken into account. Plugging in our expression for $LS[D_1 \ dc \ D_2 \ dc \dots dc \ D_p]$ from Eq. (12.24), we obtain

$$\begin{aligned} \frac{Z}{Z_0} = 1 \ + \ & \sum_{p=1}^{\infty} \sum_{(D_1 \dots D_p)} \frac{1}{g_1! g_2! \dots g_k!} z_{nLD_1} z_{nLD_2} \dots z_{nLD_p} \\ & \times \sum_{\kappa} (-1)^{i_1 + i_2 + \dots + i_m} LS[w_1] LS[w_2] \dots LS[w_q]. \end{aligned} \tag{12.30}$$

Here, the sum over κ runs over all configurations that arise from the components $(D_1 \dots D_p)$.

However, a given configuration κ can only come from a unique set of components $(D_1 \dots D_p)$. Hence, we can sum over all possible κ directly, where in each term of the sum, by specifying κ, we automatically specify the $(D_1 \dots D_p)$ that it came from.

$$\frac{Z}{Z_0} = 1 + \sum_{\kappa} \frac{1}{g_1! g_2! \dots g_k!} z_{nLD_1} z_{nLD_2} \dots z_{nLD_p} (-1)^{i_1+i_2+\dots+i_m} LS[w_1] LS[w_2] \dots LS[w_q]. \tag{12.31}$$

12.5.2 Linked cluster theorem w.r.t. generalized connected components

For each configuration κ, we relabel the components $(D_1 \dots D_p)$ according to which ones are contained in w_i. Those in w_1 are now labeled $(D_{w_1 1} D_{w_1 2} \dots D_{w_1 r_1}) \dots$ those in w_q are now labeled $(D_{w_q 1} D_{w_q 2} \dots D_{w_q r_q})$, where r_1 is the number of components in w_1, etc. We also count the number of different types of parentheses in the w_j. We denote the highest type of parenthesis (which is the outer parenthesis) in a given w_j by m_{w_j}. We denote the number of type 1 parentheses in w_j by $i_1(w_j)$, ... the number of type m_{w_j} parentheses in w_j by $i_{m_{w_j}}(w_j)$. Note that $i_{m_{w_j}}(w_j) = 1$, unless $w_j = D_i$ (i.e. $m_{w_j} = 0$), in which case $i_{m_{w_j}}(w_j) \equiv 0$. Then, we have that

$$i_1 + i_2 + \dots + i_m = i_1(w_1) + \dots + i_{m_{w_1}}(w_1) + \dots + i_1(w_q) + \dots + i_{m_{w_q}}(w_q). \tag{12.32}$$

We also make the following definition. For a particular w,

$$z_w \equiv z_{nLD_{w1}} z_{nLD_{w2}} \dots z_{nLD_{wr_w}} (-1)^{i_1(w)+i_2(w)+\dots+i_{m_w}(w)} LS[w]. \tag{12.33}$$

Eq. (12.31) now becomes

$$\frac{Z}{Z_0} = 1 + \sum_{\kappa} \frac{1}{g_1! g_2! \dots g_k!} z_{w_1} z_{w_2} \dots z_{w_q}. \tag{12.34}$$

In a given configuration κ, all of the p components that go into making κ are given the distinct labels $D_1 \dots D_p$, regardless of whether they are identical or not. However, there are distinct configurations which would be identical if we gave identical components the same label. As an example, consider configurations with three components which are all identical, but given the labels D_1, D_2, D_3. Then, the configuration $((D_1 \cap D_2) \cap D_3)$ is distinct from the configuration $((D_1 \cap D_3) \cap D_2)$. However, if all 3 components had the same label, the 2 configurations would be the same. All such configurations clearly have equal contributions to $\frac{Z}{Z_0}$. We therefore only consider configurations κ^*, in which identical components are given identical labels.

$$\sum_{\kappa} Z(\kappa) = \sum_{\kappa^*} H(\kappa^*) Z(\kappa^*). \tag{12.35}$$

Here, $H(\kappa^*)$ is equal to the number of configurations κ which collapse into κ^* once identical components are given the same label.

Consider an arbitrary configuration κ. It consists of $w_1, w_2, \dots w_q$. Transform it to a κ^* by giving identical components the same label. Then κ^* consists of $w_1^*, w_2^*, \dots w_q^*$, where w_j is transformed to w_j^* in the process of transforming κ to κ^*. After the transformation, there may be some degeneracy among the w_j^*. Suppose there are u distinct w^*:$w_1^*, w_2^*, \dots w_u^*$

with degeneracies $s_1, s_2, \ldots, s_u$ respectively. Then,

$$H(\kappa^*) = \frac{g_1! g_2! \ldots g_k!}{s_1! s_2! \ldots s_u! [\gamma(w_1^*)]^{s_1} [\gamma(w_2^*)]^{s_2} \ldots [\gamma(w_u^*)]^{s_u}}, \tag{12.36}$$

where $\gamma(w_j^*)$ is the symmetry factor of w_j^*. By this we mean that if we momentarily give distinct labels to the identical components in w_j^*, it is the number of ways to permute labels amongst **identical** components and return to the same labeling. For example, if $w_j^* = ((D_1 \cap D_1) \cap (D_1 \cap D_1))$, then $\gamma(w_j^*) = 8$. If $w_j^* = ((D_1 \cap D_1) \cap (D_2 \cap D_2))$, then $\gamma(w_j^*) = 4$. Plugging the expression for $H(\kappa^*)$ into Eq. (12.34), we obtain

$$\frac{Z}{Z_0} = 1 + \sum_{\kappa^*} \frac{[z_{w_1^*}]^{s_1} [z_{w_2^*}]^{s_2} \ldots [z_{w_u^*}]^{s_u}}{s_1! s_2! \ldots s_u! [\gamma(w_1^*)]^{s_1} [\gamma(w_2^*)]^{s_2} \ldots [\gamma(w_u^*)]^{s_u}}. \tag{12.37}$$

An arbitrary κ^* has an arbitrary number (from 0 to ∞) of each of the different possible w^*, except there has to be at least 1 w^* of some kind for κ^* to exist. However, the term in which there are zero of all of the possible w^* is 1 and is therefore accounted for in the expression for $\frac{Z}{Z_0}$. Therefore,

$$\frac{Z}{Z_0} = \exp\left[\sum_{w^*} \frac{z_{w^*}}{\gamma(w^*)}\right], \tag{12.38}$$

$$\ln\left(\frac{Z}{Z_0}\right) = \sum_{w^*} \frac{z_{w^*}}{\gamma(w^*)}. \tag{12.39}$$

We see that the w^* are the "generalized components" alluded to in section 12.3.

12.5.3 Diagrammatic rules for calculating the thermodynamic potential

We now have the following set of rules for the n^{th} order contribution to $\ln(\frac{Z}{Z_0})$:

1 Choose $p \geq 1$ connected diagrams (not necessarily distinct) whose orders add up to n. If $p = 1$, the overall diagram is connected and evaluated according to the rules for $\frac{Z}{Z_0}$.

2 If $p > 1$, the overall diagram is disconnected. The p connected diagrams are now components in this disconnected diagram.

3 Denote the contribution of a connected diagram D to $\frac{Z}{Z_0}$ by z_D. If one removes the lattice sum factor from z_D, denote this by z_{nLD}. Multiply together the factors z_{nLD} from the individual components.

4 Create all distinct w^* from the components by forming $i_1(w^*)$ type 1 parentheses, ..., $i_{m_{w^*}}(w^*) = 1$ type m_{w^*} parentheses. There is only one outer parenthesis in each w^* which encloses all p components. The contribution of each w^* is $\frac{(-1)^{i_1(w^*)+\ldots+i_{m_{w^*}}(w^*)} LS[w^*]}{\gamma(w^*)}$, where $\gamma(w^*)$ is the symmetry factor of w^* as explained below Eq. (12.36), and $LS[w^*]$ is the lattice sum of the overlapping of components represented by w^*. Sum the contributions over all w^*.

5 Multiply the factor from 4 by the factor from 3.

In addition to proving the above rules, the derivation shows that $\ln \frac{Z}{Z_0}$ is indeed the term in $\frac{Z}{Z_0}$ proportional to L. From Eq. (12.33), we see that z_{w*} is proportional to L. Therefore, the term proportional to L on the RHS of Eq. (12.37) corresponds to $s_i = 1$ for some i and $s_j = 0$ for $j \neq i$. Comparing this with Eq. (12.39), we see that it is equal to

$\ln \frac{Z}{Z_0}$. Therefore, an alternative to the above set of rules for $\ln \frac{Z}{Z_0}$ is to use the rules for $\frac{Z}{Z_0}$ from section 12.1, but to keep only the term proportional to L in the lattice sum of a disconnected diagram.

Chapter 13

Expansion for time dependent correlation functions

13.1 Diagrams for the numerator of the Green's function

The Green's function is defined as

$$G_{jj'\sigma}(\tau) = -\langle X_j^{0\sigma}(\tau) X_{j'}^{\sigma 0}\rangle, \tag{13.1}$$

where

$$\langle O\rangle = \frac{Tr(e^{-\beta H}O)}{Z}, \tag{13.2}$$

and the time dependence is given by the Heisenberg representation. Furthermore, $0 \leq \tau \leq \beta$, where β is the inverse temperature. From Eq. (13.1), the Green's function is written as

$$G_{jj'\sigma}(\tau) = -\frac{Tr(e^{-\beta H} X_j^{0\sigma}(\tau) X_{j'}^{\sigma 0})}{Z}. \tag{13.3}$$

Plugging in Eq. (12.2),

$$G_{jj'\sigma}(\tau) = -\frac{e^{\mu\tau}\langle e^{(\tau-\beta)\hat{T}} X_j^{0\sigma} e^{-\tau\hat{T}} X_{j'}^{\sigma 0}\rangle_0}{\frac{Z}{Z_0}}. \tag{13.4}$$

Finally, expanding the exponentials, we obtain

$$G_{jj'\sigma}(\tau)(\tfrac{Z}{Z_0}) = -e^{\mu\tau} \sum_{a=0b=0}^{\infty} \tfrac{(\beta-\tau)^a}{a!}\tfrac{\tau^b}{b!} \sum_{\substack{j_1 j'_1 \ldots j_n j'_n \\ \sigma_1 \ldots \sigma_n}} t_{j_1 j'_1} \ldots t_{j_n j'_n} \langle X_{j'_1}^{\sigma_1 0} X_{j_1}^{0\sigma_1} \ldots X_{j'_a}^{\sigma_a 0} X_{j_a}^{0\sigma_a} X_j^{0\sigma} X_{j'_{a+1}}^{\sigma_{a+1} 0} X_{j_{a+1}}^{0\sigma_{a+1}} \ldots X_{j'_n}^{\sigma_n 0} X_{j_n}^{0\sigma_n} X_{j'}^{\sigma 0}\rangle_0, \tag{13.5}$$

where $n = a + b$. This leads to the following rules for calculating the n^{th} order contribution to $G_{jj'\sigma}(\tau)(\frac{Z}{Z_0})$:

1 Choose $0 \leq a \leq n$. Set $b = n - a$. Draw the diagram as you would for $\frac{Z}{Z_0}$, except for the following changes. Begin drawing the diagram with a line labeled by $\sigma_{n.6}$ going into an empty site labeled by j'. The line does not come out of any site, it only goes into j'. In addition to this, after drawing the line labeled by σ_{a+1}, and before drawing the line labeled by σ_a, draw a line labeled by $\sigma_{a.5}$ going out of a site labeled j. The line does not go into any site, it only comes out of j. j and j' may label the same site.

2 Insert a factor of $\frac{-e^{\mu\tau}}{a!b!}(\beta - \tau)^a \tau^b$.

3 Insert a factor of $\frac{\rho}{m}$ for each filled circle, and $(1-\rho)$ for each empty circle.

4 Compute the multiplicity of the diagram, keeping in mind that j and j' are fixed sites on the lattice. Insert a factor of t^n.

5 Pair the lines at each site in the same way as for $\frac{Z}{Z_0}$, including the $\sigma_{n.6}$ and $\sigma_{a.5}$ lines. Now, find the line which is paired with the $\sigma_{n.6}$ line on the site j'. Follow the same process as for $\frac{Z}{Z_0}$ until you reach the $\sigma_{a.5}$ line. This completes the loop started by the $\sigma_{n.6}$ line. Find the line with the highest remaining spin label, and continue to the break the diagram into loops just as for $\frac{Z}{Z_0}$. Let l be the number of loops. Let x be the number of full sites in the diagram. Insert a factor of $(-1)^{x+1-l}m^{l-1}$.

13.1.1 Proof of the rules for the numerator of the Green's function

The rules for calculating $G_{jj'\sigma}(\tau)(\frac{Z}{Z_0})$ are modified from those for calculating $\frac{Z}{Z_0}$ by introducing the external line $\sigma_{n.6}$ on the site j' to account for $X^{\sigma 0}_{j'}$, and the external line $\sigma_{a.5}$ on the site j to account for $X^{0\sigma}_{j}$. We now state the proof of rule 5 for $G_{jj'\sigma}(\tau)(\frac{Z}{Z_0})$, which is similar to the proof of rule 5 for $\frac{Z}{Z_0}$, given in section 12.2.2.

The order of the numbers in the expectation value in Eq. (13.5) is $1'12'2\ldots a'aa_{.5}(a+1)'(a+1)\ldots n'nn'_{.6}$. This is equivalent to the order $1'12'2\ldots a'a(a+1)'(a+1)\ldots n'na_{.5}n'_{.6}$, since $a_{.5}$ has to be moved past a certain number of pairs to get to the left of $n'_{.6}$. The first loop is started by the pair $(x, n'_{.6})$ on an empty site. This corresponds to the (x_{p-1}, x'_p) pair on this site. The next pair in this loop is either (y, x') or (x', y), where the latter can only correspond to the (x'_1, x_p) pair on a full site. The loop now becomes $\pm(x'xyn'_{.6})$ where

(y, x') gives + and (x', y) gives $-$. This process continues until we come across $a_{.5}$, at which point we complete the first loop.

The subsequent loops are made in the same way as for $\frac{Z}{Z_0}$. We make the same arguments to show that each subsequent loop is started by the (x'_1, x_p) pair on a full site. However, in the case of $G_{jj'\sigma}(\tau)(\frac{Z}{Z_0})$, this does not apply to the first loop. Therefore, only $l-1$ full sites don't contribute a minus sign, and the sign of the diagram is $(-1)^{x-(l-1)} = (-1)^{x-l+1}$.

For the spin sum we note that $\sigma_{n.6} = \sigma_{a.5} = \sigma$. Thus, the spin of the first loop is fixed to be σ. Hence, this loop does not give a factor of m. Therefore, the spin sum is m^{l-1}. The overall factor from the sign and spin sum is $(-1)^{x-l+1}m^{l-1}$ as stated in rule 5.

13.2 Calculation of the Green's function

13.2.1 Numerator of the Green's function as a sum over configurations

To proceed further with our calculation of the Green's function, we need to address the issue of disconnected diagrams in $G_{jj'\sigma}(\tau)(\frac{Z}{Z_0})$. In a disconnected diagram, there will be one component, which we denote by D_G, which will contain the external lines. The other components will be the same as those in the diagrams for $\frac{Z}{Z_0}$. Let G_{D_G} be the contribution of D_G as calculated by the rules for $G_{jj'\sigma}(\tau)(\frac{Z}{Z_0})$. Let $G_{(D_G D_1 \ldots D_p)}$ be the contribution of a disconnected diagram with components $D_G D_1 \ldots D_p$ as calculated by these rules. Consider a disconnected diagram of order n, with $0 \leq a \leq n$, comprised of components $D_G D_1 \ldots D_p$, where D_G is of order c, and $D_1 \ldots D_p$ are of orders $n_1 \ldots n_p$ respectively. Let $f \equiv n_1 + n_2 + \ldots + n_p$. Then, $f = n - c$. In general, D_G has α lines

numbered lower than $\sigma_{a.5}$, and $\delta \equiv c - \alpha$ lines numbered higher than $\sigma_{a.5}$(excluding $\sigma_{n.6}$). Additionally, there could be some degeneracy among the components $D_1 \ldots D_p$. Assume that out of these, k are distinct, with degeneracy $g_1 \ldots g_k$. Then, the number of different ways to distribute lines among the components $D_G D_1 \ldots D_p$ is:

$$\eta_{a(D_G D_1 \ldots D_p)} = \binom{a}{\alpha}\binom{b}{\delta}\frac{f!}{n_1! \ldots n_p!}\frac{1}{g_1! \ldots g_k!}. \tag{13.6}$$

Hence, for a given choice of a, the components $D_G D_1 \ldots D_p$

make the following contribution to $G_{jj'\sigma}(\tau)(\frac{Z}{Z_0})$:

$$\begin{aligned}\eta_{a(D_G D_1 \ldots D_p)} G_{(D_G D_1 \ldots D_p)} &= \binom{a}{\alpha}\binom{b}{\delta}\frac{f!}{n_1! \ldots n_p!}\frac{1}{g_1! \ldots g_k!}\frac{(-e^{\mu\tau})}{a!b!}(\beta - \tau)^a \tau^b \\ &\quad \times G_{B(D_G D_1 \ldots D_p)} LS[D_G\ dc\ D_1\ dc \ldots dc\ D_p], \end{aligned} \tag{13.7}$$

where $G_{B(D_G D_1 \ldots D_p)}$ is $G_{(D_G D_1 \ldots D_p)}$ without the factors

$\frac{(-e^{\mu\tau})}{a!b!}(\beta - \tau)^a \tau^b$ and $LS[D_G\ dc\ D_1\ dc \ldots dc\ D_p]$. However, there are multiple values of $0 \leq a \leq n$ for which a disconnected diagram can have the components $D_G D_1 \ldots D_p$. The values of a are restricted by the values of α and δ for the given D_G. In particular, $\alpha \leq a$ and $\delta \leq n - a$. Therefore, we have

$$\alpha \leq a \leq n - \delta. \tag{13.8}$$

Hence, the total contribution of the components $D_G D_1 \dots D_p$ to $G_{jj'\sigma}(\tau)(\frac{Z}{Z_0})$ is:

$$\eta_{(D_G D_1 \dots D_p)} G_{(D_G D_1 \dots D_p)} = \sum_{a=\alpha}^{n-\delta} \quad \frac{1}{\alpha!(a-\alpha)!} \frac{1}{\delta!(b-\delta)!} \frac{f!}{n_1! \dots n_p!} \frac{1}{g_1! \dots g_k!} \times(-e^{\mu\tau})(\beta-\tau)^{a-\alpha}\tau^{b-\delta}(\beta-\tau)^{\alpha}\tau^{\delta} \times G_{B(D_G D_1 \dots D_p)} LS[D_G\ dc\ D_1 dc \dots dc\ D_p]. \tag{13.9}$$

We also have the following equalities:

$$G_{B(D_G D_1 \dots D_p)} = G_{BD_G} z_{B(D_1 \dots D_p)}, \tag{13.10}$$

$$G_{nLD_G} = \frac{(-e^{\mu\tau})}{\alpha!\delta!}(\beta-\tau)^{\alpha}\tau^{\delta} G_{BD_G}. \tag{13.11}$$

Furthermore, using the definitions of b, δ, and f, one can show that

$$\sum_{a=\alpha}^{n-\delta} \frac{1}{(a-\alpha)!} \frac{1}{(b-\delta)!}(\beta-\tau)^{a-\alpha}\tau^{b-\delta} = \sum_{a=0}^{f} \frac{1}{a!} \frac{1}{(f-a)!}(\beta-\tau)^{a}\tau^{f-a} = \frac{\beta^f}{f!}. \tag{13.12}$$

Hence, Eq. (13.9) simplifies to:

$$\eta_{(D_G D_1 \dots D_p)} G_{(D_G D_1 \dots D_p)} = \frac{1}{g_1! \dots g_k!} G_{nLD_G} z_{nLD_1} \dots z_{nLD_p} LS[D_G\ dc\ D_1\ dc \dots dc\ D_p]. \tag{13.13}$$

Therefore,

$$G_{jj'\sigma}(\tau)\left(\frac{Z}{Z_0}\right) = \sum_{D_G}\sum_{p=0}^{\infty}\sum_{(D_1\ldots D_p)}\frac{1}{g_1!\ldots g_k!}G_{nLD_G}z_{nLD_1}\ldots z_{nLD_p} LS[D_G\ dc\ D_1\ dc\ldots dc\ D_p]. \quad (13.14)$$

$LS[D_G\ dc\ D_1\ dc\ldots dc\ D_p]$ is evaluated in terms of configurations in the same way as $LS[D_1\ dc\ldots dc\ D_p]$ from $\frac{Z}{Z_0}$ was, except that now in each κ, there will be one w which contains D_G. We shall denote it by w_G. The other w will be the same as those found in the calculation of $\frac{Z}{Z_0}$. Thus, we obtain

$$G_{jj'\sigma}(\tau)\left(\frac{Z}{Z_0}\right) = \sum_{D_G}\sum_{p=0}^{\infty}\sum_{(D_1\ldots D_p)}\frac{1}{g_1!\ldots g_k!}G_{nLD_G}z_{nLD_1}\ldots z_{nLD_p} \times\sum_{\kappa}(-1)^{i_1+\ldots+i_m}LS[w_G]LS[w_1]\ldots LS[w_q]. \quad (13.15)$$

A given κ can only come from a unique $(D_GD_1\ldots D_p)$. Therefore,

$$G_{jj'\sigma}(\tau)\left(\frac{Z}{Z_0}\right) = \sum_{\kappa}\frac{1}{g_1!\ldots g_k!}G_{nLD_G}z_{nLD_1}\ldots z_{nLD_p}(-1)^{i_1+\ldots+i_m} \times LS[w_G]LS[w_1]\ldots LS[w_q]. \quad (13.16)$$

13.2.2 Cancellation of the denominator of the Green's function

We define

$$G_{w_G}\equiv G_{nLD_G(w_G)}z_{nLD_{w_G1}}z_{nLD_{w_G2}}\ldots z_{nLD_{w_Gr_{w_G}}}(-1)^{i_1(w_G)+i_2(w_G)+\ldots+i_{m_{w_G}}(w_G)}LS[w_G]. \quad (13.17)$$

Then, Eq. (13.16) simplifies to

$$G_{jj'\sigma}(\tau)\left(\frac{Z}{Z_0}\right) = \sum_{\kappa} \frac{1}{g_1! \dots g_k!} G_{w_G z_{w_1}} \dots z_{w_q}. \tag{13.18}$$

Just as in the case of $\frac{Z}{Z_0}$, we perform the transformation $\kappa \to \kappa^*$ by giving identical components identical labels. In the process, $w_G \to w_G^*$ and $w_j \to w_j^*$. After the transformation, there may be some degeneracy in the $w_1^* \dots w_q^*$. Suppose there are u distinct w_j^*: $w_1^* \dots w_u^*$ with degeneracies $s_1 \dots s_u$ respectively. There can only be one w_G^* because there is only one D_G in any diagram. Therefore, the multiplicity factor for the number of configurations κ which correspond to a single κ^* is

$$H(\kappa^*) = \frac{g_1! g_2! \dots g_k!}{s_1! s_2! \dots s_u! [\gamma(w_1^*)]^{s_1} [\gamma(w_2^*)]^{s_2} \dots [\gamma(w_u^*)]^{s_u} \gamma(w_G^*)}, \tag{13.19}$$

and Eq. (13.18) becomes

$$G_{jj'\sigma}(\tau)\left(\frac{Z}{Z_0}\right) = \sum_{\kappa^*} \frac{G_{w_G^*} [z_{w_1^*}]^{s_1} [z_{w_2^*}]^{s_2} \dots [z_{w_u^*}]^{s_u}}{s_1! s_2! \dots s_u! [\gamma(w_1^*)]^{s_1} [\gamma(w_2^*)]^{s_2} \dots [\gamma(w_u^*)]^{s_u} \gamma(w_G^*)}. \tag{13.20}$$

An arbitrary κ^* has one of the w_G^* and an arbitrary number from 0 to ∞ of each of the w^*. Therefore,

$$G_{jj'\sigma}(\tau)\left(\frac{Z}{Z_0}\right) = \sum_{w_G^*} \frac{G_{w_G^*}}{\gamma(w_G^*)} \exp\left[\sum_{w^*} \frac{z_{w^*}}{\gamma(w^*)}\right]. \tag{13.21}$$

Recalling that $\frac{Z}{Z_0} = \exp[\sum_{w^*} \frac{z_{w^*}}{\gamma(w^*)}]$, we have that

$$G_{jj'\sigma}(\tau) = \sum_{w_G^*} \frac{G_{w_G^*}}{\gamma(w_G^*)}. \tag{13.22}$$

13.2.3 Diagrammatic rules for the calculation of the Green's function

This leads to the following set of rules for the n^{th} order contribution to $G_{jj'\sigma}(\tau)$:

1 Choose one connected diagram from $G_{jj'\sigma}(\tau)(\frac{Z}{Z_0})$ and $p \geq 0$ connected diagrams (not necessarily distinct) from $\frac{Z}{Z_0}$. The orders of the $p+1$ diagrams must add up to n. If $p = 0$, then the overall diagram is connected and must be evaluated according to the rules for $G_{jj'\sigma}(\tau)(\frac{Z}{Z_0})$.

2 If $p > 0$, the overall diagram is disconnected. The $p+1$ connected diagrams are now components in this disconnected diagram.

3 Denote the contribution of a connected diagram D_G to $G_{jj'\sigma}(\tau)(\frac{Z}{Z_0})$ by G_{D_G}. If one removes the lattice sum factor from G_{D_G}, denote this by G_{nLD_G}. Multiply G_{nLD_G} from the component D_G together with $z_{nLD_1} \ldots z_{nLD_p}$ from the p components $D_1 \ldots D_p$.

4 Create all distinct w^* from the components by forming $i_1(w^*)$ type 1 parentheses, ..., $i_{m_{w^*}}(w^*) = 1$ type m_{w^*} parentheses. There is only one outer parenthesis in each w^* which encloses all $p+1$ components. The contribution of each w^* is $\frac{(-1)^{i_1(w^*)+\ldots+i_{m_{w^*}}(w^*)} LS[w^*]}{\gamma(w^*)}$, where $\gamma(w^*)$ is the symmetry factor of w^*, and $LS[w^*]$ is the lattice sum of the overlapping of components represented by w^*. Sum the contributions over all w^*.

5 Multiply the factor from 4 by the factor from 3.

In addition to proving the above rules, the derivation shows that $G_{jj'\sigma}(\tau)$ is indeed the term in $G_{jj'\sigma}(\tau)(\frac{Z}{Z_0})$ independent to L. From Eq. (12.33), we see that z_{w*} is proportional to L. Therefore, the term independent L on the RHS of Eq. (13.20) corresponds to $s_i = 0$ for all i. Comparing this with Eq. (13.22), we see that it is equal to $G_{jj'\sigma}(\tau)$. Therefore, an alternative to the above set of rules for $G_{jj'\sigma}(\tau)$ is to use the rules for $G_{jj'\sigma}(\tau)(\frac{Z}{Z_0})$ from section 13.1, but to keep only the term independent of L in the lattice sum of a disconnected diagram.

13.3 Examples and results for the Green's function

13.3.1 Examples from 0^{th} to 2^{nd} order

We now show some examples of diagrams for $G_{jj'\sigma}(\tau)$, with the contribution written next to the diagram. In zeroth order, there is only one diagram:

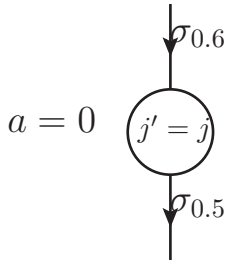

$$-e^{\mu\tau}(1-\rho)\delta_{jj'}$$

In first order, there are 2 diagrams:

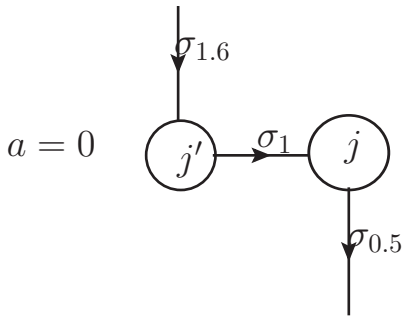

$a = 0$ $\quad -e^{\mu\tau}\tau(1-\rho)^{c_i}t_{jj'}$

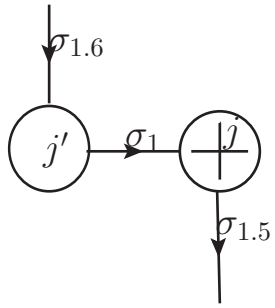

$a = 1$ $\quad e^{\mu\tau}(\beta-\tau)\frac{\rho}{m}(1-\rho)t_{jj'}$

In second order, one can have a disconnected diagram:

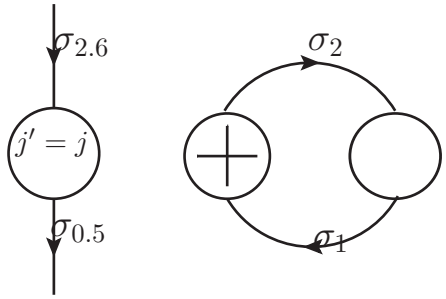

$a = 0$ $\quad \frac{-e^{\mu\tau}}{2}\tau^2(1-\rho)^2\rho\delta_{jj'}(-2\cdot 2d)t^2$

13.3.2 Green's function to fourth order in βt

We have used the above rules to calculate the Green's function to 4th order in t on a hypercube in d dimensions with m spin species:

$$
\begin{aligned}
G_\sigma^{(0)}(\vec{k},\omega_k) &= \frac{m(-\rho)+m+\rho}{mz},\\
G_\sigma^{(1)}(\vec{k},\omega_k) &= \frac{\epsilon_k(m(-\rho)+m+\rho)^2}{m^2z^2},\\
G_\sigma^{(2)}(\vec{k},\omega_k) &= \frac{2d(m-1)t^2\rho(m(\rho-2)-\rho)(m(\rho-1)-\rho)}{m^3z^3} - \frac{2d(m-1)t^2\beta(\rho-1)\rho}{mz^2}\\
&-\frac{d(m-1)t^2\beta^2(\rho-1)\rho(2\rho-1)}{mz} + \frac{\epsilon_k^2(m(-\rho)+m+\rho)^3}{m^3z^3},\\
G_\sigma^{(3)}(\vec{k},\omega_k) &= -\frac{(4d-1)(m-1)t^2\rho\epsilon_k(m(\rho-2)-\rho)(m(-\rho)+m+\rho)^2}{m^4z^4}\\
&+\frac{2(2d-1)(m-1)t^2\beta(\rho-1)\rho\epsilon_k(m(\rho-1)-\rho)}{m^2z^3}\\
&+\frac{(m-1)t^2\beta^2(\rho-1)\rho\epsilon_k((d(4\rho-2)-\rho)(m(\rho-1)-\rho)-\rho)}{m^2z^2} + \frac{\epsilon_k^3(m(-\rho)+m+\rho)^4}{m^4z^4},\\
G_\sigma^{(4)}(\vec{k},\omega_k) &= -\frac{2(3d-1)(m-1)t^2\rho\epsilon_k^2(m(\rho-2)-\rho)(m(-\rho)+m+\rho)^3}{m^5z^5}\\
&-\frac{2(3d-2)(m-1)t^2\beta(\rho-1)\rho\epsilon_k^2(m(-\rho)+m+\rho)^2}{m^3z^4}\\
&-\frac{(m-1)t^2\beta^2(\rho-1)\rho\epsilon_k^2(m(\rho-1)-\rho)((d(6\rho-3)-2\rho)(m(\rho-1)-\rho)-2\rho)}{m^3z^3}\\
&+\frac{2d(m-1)t^4\beta(\rho-1)\rho\left(-4dm^2+2(3d-2)(m-1)^2\rho^2+m\rho(-6d(m-3)+5m-11)\right)}{m^3z^4}\\
&+\frac{d(m-1)t^4\beta^2(\rho-1)\rho\left(-4dm^2+4(3d-1)(m-1)^2\rho^3-2(m-1)\rho^2(3d(5m-1)-4m+2)+m\rho(2d(9m-7)-3m+5)\right)}{m^3z^3}\\
&-\frac{d(m-1)t^4\beta^3(\rho-1)\rho\left(m^2\left(d\left(26\rho^2-28\rho+6\right)+2(5-4\rho)\rho-3\right)+8(d-1)m(\rho-1)\rho+2(d-1)\rho^2\right)}{3m^3z^2}\\
&-\frac{d(m-1)t^4\beta^4(\rho-1)\rho\left(m^2(2d(\rho(52\rho-81)+34)-3)-2\rho(\rho(16\rho-27)+13)+3)+16(d-1)m(\rho-1)\rho(2\rho-1)+2(d-1)\rho^2(4\rho-3)\right)}{12m^3z}\\
&+\frac{2d(m-1)t^4\rho(m(\rho-1)-\rho)\left(10(1-2d)m^3+2m^2\rho(d(8m-2)-6m+3)-(m-1)^3\rho^3+4(m-1)^2m\rho^2\right)}{m^5z^5}\\
&+\frac{\epsilon_k^4(m(-\rho)+m+\rho)^5}{m^5z^5}. \qquad (13.23)
\end{aligned}
$$

$$z \equiv i\omega_k + \mu. \tag{13.24}$$

In the case where $m = 1$, this should reduce to the answer for a single species free Fermi gas. We can see that this is indeed the case as all the terms but the free propagator vanish. When we set $m = 2$ and $d = 2$, we recover the expressions obtained from the Metzner expansion [69]. Using the formula

$$n - 1 = G_{jj\sigma}(\tau = 0), \tag{13.25}$$

we can convert to expressions where n is the independent parameter and hence t-independent.

$$G_\sigma^{(0)}(\vec{k},\omega_k) = \frac{m(-n)+m+n}{mz},$$

$$G_\sigma^{(1)}(\vec{k},\omega_k) = \frac{\epsilon_k(m(-n)+m+n)^2}{m^2z^2},$$

$$G_\sigma^{(2)}(\vec{k},\omega_k) = \frac{2d(m-1)nt^2(m(n-2)-n)(m(n-1)-n)}{m^3z^3}$$
$$-\frac{dt^2\beta(m(n-1)+n)}{mz^2} + \frac{\epsilon_k^2(m(-n)+m+n)^3}{m^3z^3},$$

$$G_\sigma^{(3)}(\vec{k},\omega_k) = -\frac{(4d-1)(m-1)nt^2\epsilon_k(m(n-2)-n)(m(-n)+m+n)^2}{m^4z^4}$$
$$-\frac{2t^2\beta\epsilon_k(m(n-1)-n)(d(m-(m+1)n)+(m-1)(n-1)n)}{m^2z^3}$$
$$+\frac{\epsilon_k^3(m(-n)+m+n)^4}{m^4z^4} - \frac{(m-1)^2(n-1)^2n^2t^2\beta^2\epsilon_k}{m^2z^2},$$

$$G_\sigma^{(4)}(\vec{k},\omega_k) = \frac{2(3d-1)(m-1)nt^2\epsilon_k^2(m(n-2)-n)(m(n-1)-n)^3}{m^5z^5}$$
$$+\frac{t^2\beta\epsilon_k^2(m(-n)+m+n)^2(4(m-1)(n-1)n-3d(m(n-1)+n))}{m^3z^4}$$
$$+\frac{2d(m-1)nt^4\beta\big(d\big(m^2(n-1)(9n-10)+3mn(2n-3)-3n^2\big)+(1-n)n\big(4(m-1)^2n+(11-5m)m\big)\big)}{m^3z^4}$$
$$+\frac{dt^4\beta^2\big(dm\big(m^2+2(m-1)^2n^3-2((m-4)m+1)n^2-m(m+3)n\big)+(1-m)(n-1)n^2\big(4(m-1)^2n^2-4(m-1)(2m-1)n+m(3m-5)\big)\big)}{m^3z^3}$$
$$+\frac{dt^4\beta^3\big(-2(m+1)n^3\big((d-7)m^2+10(d-1)m+d-1\big)+m^2n(-8d(m+2)+17m+25)+2mn^2(d(5m(m+4)+11)+(-2m-1)(7m+11))-3m^3\big)}{12m^3z^2}$$
$$+\frac{2d(m-1)nt^4(m(n-1)-n)\big(10(1-2d)m^3+2m^2n(d(8m-2)-6m+3)-(m-1)^3n^3+4(m-1)^2mn^2\big)}{m^5z^5}$$
$$+\frac{\epsilon_k^4(m(-n)+m+n)^5}{m^5z^5} + \frac{2(m-1)^2(n-1)^2n^2t^2\beta^2\epsilon_k^2(m(n-1)-n)}{m^3z^3}. \tag{13.26}$$

$$z \equiv i\omega_k + \mu^{(0)}. \tag{13.27}$$

$$\rho(\mu^{(0)}) \equiv n. \tag{13.28}$$

13.4 The infinite spin species limit.

It is interesting to see how the above expressions simplify in the limit of infinite spin species, i.e. as $m \to \infty$. In this case, the Green's function may be written in the form

$$G(k) = \frac{1-n}{z-(1-n)\epsilon_k - \Sigma_{DM}(k)}, \tag{13.29}$$

where $\Sigma_{DM}(k)$ is the Dyson-Mori self energy [4], which has a finite value as $i\omega_k \to \infty$. The high frequency limit of the Green's function is therefore $\lim_{i\omega_k \to \infty} G(k) = \frac{1-n}{i\omega_k}$, as can be seen explicitly from the anti-commutation relations of the Hubbard X operators:

$$\langle \{X_i^{0\sigma}, X_j^{\sigma 0}\} \rangle = \delta_{ij} \langle X_i^{00} + X_i^{\sigma\sigma} \rangle = \delta_{ij} \langle 1 - \sum_{\sigma' \neq \sigma} X_i^{\sigma'\sigma'} \rangle = \delta_{ij}[1-(m-1)\frac{n}{m}]. \tag{13.30}$$

Taking the $m \to \infty$ limit of the above equation gives the high frequency coefficient $1-n$, while $m=2$ gives the usual coefficient of $1-\frac{n}{2}$ [15]. Using Eq. (13.26), we derive a high temperature expansion for $\Sigma_{DM}(k)$ in the $m \to \infty$ limit:

$$\begin{aligned}
&\Sigma_{DM}^{(0)}(\vec{k},\omega_k) = 0, \\
&\Sigma_{DM}^{(1)}(\vec{k},\omega_k) = 0, \\
&\Sigma_{DM}^{(2)}(\vec{k},\omega_k) = dt^2\beta - \frac{2d(n-2)nt^2}{z}, \\
&\Sigma_{DM}^{(3)}(\vec{k},\omega_k) = (n-1)n^2t^2\beta^2\epsilon_k - \frac{(n-2)(n-1)nt^2\epsilon_k}{z^2} + \frac{2(n-1)nt^2\beta\epsilon_k}{z}, \\
&\Sigma_{DM}^{(4)}(\vec{k},\omega_k) = \frac{dn^2t^4\beta^2(-2d+4(n-2)n+3)}{z} - \frac{2d(2d-1)n(n((n-4)n+12)-10)t^4}{z^3} \\
&-\frac{2dnt^4\beta(d(7n-6)+(5-4n)n)}{z^2} + \frac{1}{12}dt^4\beta^3(2n(d(n-4)-7n+7)-3).
\end{aligned} \tag{13.31}$$

The connection between this high temperature expansion for the Dyson-Mori self-energy in the $m \to \infty$ limit and slave boson techniques [44, 71, 72] is an interesting direction for further study.

13.5 Time-dependent density-density and spin-spin correlation functions

13.5.1 The density-density correlation function

The density-density correlation function is defined to be

$$\Pi_{jj'}(\tau) = \langle \widetilde{n}_j(\tau)\widetilde{n}_{j'}\rangle = \frac{Tr(e^{-\beta H}\widetilde{n}_j(\tau)\widetilde{n}_{j'})}{Z}, \tag{13.32}$$

where

$$\widetilde{n}_j(\tau) \equiv n_j(\tau) - \langle n_j\rangle; \quad n_j \equiv \sum_\sigma X_j^{\sigma\sigma}. \tag{13.33}$$

Expanding the exponentials in the density matrix and the time dependence of the number operator, we obtain

$$(\Pi_{jj'}(\tau) + n^2)(\tfrac{Z}{Z_0}) = \sum_{a=0b=0}^{\infty} \tfrac{(\beta-\tau)^a}{a!}\tfrac{\tau^b}{b!} \sum_{\substack{j_1 j'_1 \ldots j_n j'_n \\ \sigma_1 \ldots \sigma_n}} t_{j_1 j'_1} \ldots t_{j_n j'_n} \langle X_{j'_1}^{\sigma_1 0} X_{j_1}^{0\sigma_1} \ldots X_{j'_a}^{\sigma_a 0} X_{j_a}^{0\sigma_a} n_j X_{j'_{a+1}}^{\sigma_{a+1} 0} X_{j_{a+1}}^{0\sigma_{a+1}} \ldots X_{j'_n}^{\sigma_n 0} X_{j_n}^{0\sigma_n} n_{j'}\rangle_0, \tag{13.34}$$

where $n = a + b$. We shall now state the rules for calculating the n^{th} order contribution to $\Pi_{jj'}(\tau)$. The proof of these rules runs along the same lines as the ones given for the

thermodynamic potential and the Green's function. We will not give the full proof, but will merely point out a few key points particular to this case. First, we give the rules for drawing the diagrams D_Π, and evaluating their contributions Π_{D_Π}. The rules for $\Pi_{jj'}(\tau)$ will be given in terms of these diagrams and the partition function diagrams D_i. Rules for drawing and evaluating the n^{th} order diagram D_Π:

1 If $n > 0$, draw the diagram D_Π in the same way as you would a connected diagram for $\frac{Z}{Z_0}$. Mark a site on this diagram to distinguish it from the other sites. If $n = 0$, the only diagram is a single full site whose contribution is ρ. The single full site is then the site marked.

2 Insert a factor of $\frac{\rho}{m}$ for each filled circle, and $1 - \rho$ for each empty circle. Insert a factor of t^n.

3 Define the time $\tau_{a.5}$ for $0 \leq a \leq n$ to lie between τ_a and τ_{a+1} (recall also that higher numbers correspond to "earlier" times when drawing the diagram). Then, insert a factor of $\sum_{a=0}^{n} \frac{(\beta-\tau)^a}{a!} \frac{\tau^b}{b!} f(\tau_{a.5})$, where $b = n - a$, $f(\tau_{a.5}) = 1$ if the site marked in rule 1 is full **at time** $\tau_{a.5}$, and $f(\tau_{a.5}) = 0$ otherwise. The site being full at a certain time means that either the last line on this site before this time entered the site, or it is a filled vertex whose earliest line occurs after this time.

4 The sign and spin sum of the diagram are determined in the same way as for $\frac{Z}{Z_0}$.

The n^{th} order contribution to $\Pi_{jj'}(\tau)$ is split into 2 pieces, $\Pi^{(n)}_{jj'}(\tau) = \Pi^{(n)}_{jj',a}(\tau) + \Pi^{(n)}_{jj',b}(\tau)$. Rules for calculating $\Pi^{(n)}_{jj',a}(\tau)$:

1 Choose one diagram D_Π, and $p \geq 0$ connected diagrams (not necessarily distinct)

from $\frac{Z}{Z_0}$. The orders of the $p+1$ diagrams must add up to n. The $p+1$ diagrams are now components in this diagram.

2 Multiply the contribution Π_{D_Π} from D_Π with the contributions $z_{nLD_1} \ldots z_{nLD_p}$ from the p components $D_1 \ldots D_p$.

3 Fix any full site in the diagram D_Π to be j' on the lattice. Fix the marked site in the diagram D_Π (from rule 1 of the rules for D_Π) to be j on the lattice. Create all distinct w^* from the components by forming $i_1(w^*)$ type 1 parentheses, $\ldots$, $i_{m_{w^*}}(w^*) = 1$ type m_{w^*} parentheses. There is only one outer parenthesis in each w^* which encloses all $p+1$ components. The contribution of each w^* is $\frac{(-1)^{i_1(w^*)+\ldots+i_{m_{w^*}}(w^*)} LS[w^*]}{\gamma(w^*)}$, where $\gamma(w^*)$ is the symmetry factor of w^*, and $LS[w^*]$ is the lattice sum of the overlapping of components represented by w^*. Note that in calculating $\gamma(w^*)$, D_Π **should not** be considered identical to any of the $D_1 \ldots D_p$. Sum the contributions over all w^*.

4 Multiply the factor from 3 with the factor from 2.

Rules for calculating $\Pi^{(n)}_{jj',b}(\tau)$:

1 Choose one diagram D_Π, one connected diagram from $\frac{Z}{Z_0}$ (or the single full site with contribution ρ) denoted by $\widetilde{D}$, and $p \geq 0$ connected diagrams (not necessarily distinct) from $\frac{Z}{Z_0}$. The orders of the $p+2$ diagrams must add up to n. The $p+2$ diagrams are now components in this diagram.

2 Multiply the contribution Π_{D_Π} from D_Π with the contribution $z_{nL\widetilde{D}}$ from $\widetilde{D}$, and the contributions $z_{nLD_1} \ldots z_{nLD_p}$ from the p components $D_1 \ldots D_p$.

3 Fix any full site in the diagram $\widetilde{D}$ to be j' on the lattice. Fix the marked site in the diagram D_Π to be j on the lattice. Create all distinct w^* from the components by forming $i_1(w^*)$ type 1 parentheses, ..., $i_{m_{w^*}}(w^*) = 1$ type m_{w^*} parentheses. There is only one outer parenthesis in each w^* which encloses all $p+2$ components. The contribution of each w^* is $\frac{(-1)^{i_1(w^*)+\ldots+i_{m_{w^*}}(w^*)} LS[w^*]}{\gamma(w^*)}$, where $\gamma(w^*)$ is the symmetry factor of w^*, and $LS[w^*]$ is the lattice sum of the overlapping of components represented by w^*. Note that in calculating $\gamma(w^*)$, **neither** D_Π **nor** $\widetilde{D}$ should be considered identical to any of the $D_1 \ldots D_p$. Sum the contributions over all w^*.

4 Multiply the factor from 3 with the factor from 2.

The following observations went into deriving these rules.

a Number operators commute with all other operators (on different sites), and accommodate all spin species with equal coefficient. Therefore, they don't affect the sign or spin sum of a diagram.

b Since the number operators don't create or destroy particles, n_j and $n_{j'}$ don't have to occur in the same connected component. When they do appear in the same connected component, this is the component D_Π. When they appear in different connected components, n_j appears in D_Π while $n_{j'}$ appears in $\widetilde{D}$.

c For the density-density correlation function, D_Π plays the same role as D_G plays in the Green's function. For $\Pi_{jj',a}(\tau)$, the combinatorial factors involved in distributing lines work out exactly as they do in Eq. (13.6). For $\Pi_{jj',b}(\tau)$, the presence of $\widetilde{D}$ does not complicate matters since the operator $n_{j'}$ occurs to the right of all other

operators in the expectation value in Eq. (13.34). Hence, any combination of lines in the disconnected diagram can go into making $\widetilde{D}$, as is the case for the diagrams $D_1 \ldots D_p$ (but in contrast to D_Π). Therefore, $\widetilde{D}$ of order $\widetilde{n}$ gets the usual factor of $\frac{\beta^{\widetilde{n}}}{\widetilde{n}!}$.

d Below Eq. (12.31), we explain that the different components originally present in the diagram go into making the various "generalized components" w. In the case when both D_Π and $\widetilde{D}$ are present, they can either both go into making the same w or go into different w's. The former is accounted for by $\Pi_{jj',b}(\tau)$, while the latter is cancelled by $(-)n^2$.

13.5.2 The spin-spin correlation function

The spin-spin correlation function is defined to be

$$\Pi^s_{jj'}(\tau) = \langle \widetilde{s^z_j}(\tau) \widetilde{s^z_{j'}} \rangle, \tag{13.35}$$

where

$$\widetilde{s^z_j}(\tau) \equiv s^z_j(\tau) - \langle s^z_j \rangle; \quad s^z_j \equiv \sum_\sigma s(\sigma) X^{\sigma\sigma}_j. \tag{13.36}$$

By $s(\sigma)$ we mean the spin corresponding to σ. For example, for spin-half particles, $s(\pm 1) = \pm\frac{1}{2}$. We note that for spin l particles ($m = 2l+1$):

$$\sum_\sigma s(\sigma) = 0; \quad \sum_\sigma s^2(\sigma) = \frac{1}{3} l(l+1)m. \tag{13.37}$$

The first of these two equations tells us that s^z_j and $s^z_{j'}$ must occur in the same "loop" of the diagram. Therefore, the rules for the spin-spin correlation function can be obtained from those for the density-density correlation function by making the following simple changes.

1 $\Pi^s_{jj',b}(\tau) = 0$

2 In the calculation of D_{Π^s}, mark any site j and a full site j' (see rule 1 for D_Π for comparison). This is in contrast to D_Π in which the choice of j' did not affect the evaluation of D_Π (or occurred in $\widetilde{D}$ rather than D_Π), and hence only came when calculating the lattice sum in rule 3 for $\Pi_{jj',a}(\tau)$ or $\Pi_{jj',b}(\tau)$.

3 Rule 3 for the contribution of D_{Π^s} is modified from that of D_Π, so that there are now additional requirements for $f(\tau_{a.5}) = 1$. In the case that the last line on the site j before the time $\tau_{a.5}$ enters j, this line must be in the same loop as the earliest line on the site marked j'. In the case that the site j is full and its earliest line occurs after the time $\tau_{a.5}$, then this line must be in the same loop as the earliest line on the site marked j'. Otherwise, $f(\tau_{a.5}) = 0$.

4 Insert a factor of $\frac{1}{3}l(l+1) = \frac{1}{12}(m^2-1)$ into the contribution of the diagram D_{Π^s}.

We note that the above rules imply that there will only be even order contributions to the density-density and spin-spin correlation functions, since this is the case for the partition function. This was expected, since the number operator and spin operator conserve particle number.

Chapter 14

Conclusion

In conclusion, we have developed a high-temperature series for the thermodynamic potential, the Green's function, and the time-dependent density-density and spin-spin correlation functions in the infinite-U Hubbard model. The n^{th} order contribution in βt is given in terms of diagrams consisting of n lines connecting vertices that can either be empty or full, corresponding to unoccupied and occupied sites on the lattice. The signature and spin sum of the diagram are evaluated with the help of a simple rule that increases the efficiency of computation, and enables results to be obtained for any number of spin species with no additional difficulty. The contribution of a diagram factors into a temporal part and a spatial part. The computation proceeds in two stages. In the first stage, the temporal part is evaluated for all of the connected diagrams. In the second stage, an arbitrary number of connected diagrams are combined into a "generalized connected diagram". Its temporal part is the product of the temporal parts of its constituent connected diagrams, while its spatial part is the lattice sum corresponding to overlapping its constituent connected

diagrams on the lattice. The linked cluster theorem is proved, enabling one to express the thermodynamic potential and the dynamical correlation functions as a sum over the generalized connected diagrams.

This is an especially efficient way of doing the calculation because the temporal part of each constituent connected diagram, which is by far the most time-consuming part of the calculation, is evaluated only once. The rest of the complexity is taken care of by calculating lattice sums of overlappings of constituent connected diagrams. This should be contrasted with the Metzner approach [21], in which a "generalized connected diagram" (referred to in [21] as a connected diagram) is broken into constituent connected diagrams through the use of cumulants. The temporal contributions of the constituent connected diagrams are then evaluated and multiplied together **every time** a generalized connected diagram is broken up. Therefore, the temporal contribution of a given constituent connected diagram is evaluated many times. What is gained by this is extreme simplicity in evaluating lattice sums. However, although complex, the lattice sum part of our calculation takes very little computation time, and even in high order calculations, can be done for a few minutes on a computer [70]. This is the essential reason why our method constitutes an improvement over those employed previously for the Green's function, and especially for the time-dependent density-density and spin-spin correlation functions. We have used our method to calculate the Green's function to fourth order in βt valid for m spin species on a d-dimensional hypercube. Taking the $m \to \infty$ limit, we obtained expressions for the Dyson-Mori self-energy to fourth order in βt, valid for the case of an infinite number of spin species. This may have interesting connections to slave Boson techniques [44, 71, 72] used

for the study of this model.

Bibliography

[1] L. D. Landau, Sov. Phys. JETP **3**, 920 (1957).

[2] L. D. Landau, Sov. Phys. JETP **5**, 101 (1957).

[3] B. S. Shastry, Phys. Rev. Letts. **107**, 056403 (2011).

[4] B. S. Shastry, Phys. Rev. **B 84**, 165112 (2011).

[5] B. S. Shastry, Phys. Rev. Letts. **109**, 067004 (2012).

[6] B. S. Shastry, Phys. Rev. **B 87** 125124 (2013).

[7] G.-H. Gweon, B. S. Shastry, and G. D. Gu, Phys. Rev. Lett. **107**, 056404 (2011).

[8] D. Hansen and B. S. Shastry, Phys. Rev. **B 87**, 245101 (2013).

[9] R. Zitko, D. Hansen, E. Perepelitsky, J.Mravlje, A. Georges, and B. S. Shastry, Phys. Rev. **B 88**, 235132 (2013).

[10] E. Perepelitsky and B. S. Shastry, Annals of Physics **338**, 283 (2013)

[11] B. S. Shastry , E. Perepelitsky, and A.C. Hewson, Phys. Rev. B **88**, 205108 (2013)

[12] E. Khatami, D. Hansen, E. Perepelitsky, M. Rigol, and B. S. Shastry, Phys. Rev. **B 87**, 161120 (2013).

[13] K.Matsuyama and G.-H. Gweon, Phys. Rev. Lett. **111**, 246401 (2013).

[14] B. S. Shastry, Phys. Rev. Lett. **108**, 029702 (2012).

[15] B. S. Shastry, Phys. Rev. **B 81**, 045121 (2010).

[16] X. Deng, J. Mravlje, R. Zitko, M. Ferrero, G. Kotliar, and A. Georges, Phys. Rev. Letts. **110**, 086401 (2013).

[17] J.Otsuki and D.Vollhardt, Phys. Rev. Lett. **110**, 196407 (2013).

[18] Y. Kuramoto and T. Watanabe, Physica **B 148**, 80 (1987).

[19] W. Metzner and D. Vollhardt, Phys. Rev. Lett. **62**, 324 (1989).

[20] E.Müller-Hartmann, Z Phys. **B 74**, 507 (1989);E.Müller-Hartmann, Z. Phys. **B 76**, 211 (1989);E.Müller-Hartmann, Int. J. Mod. Phys. **B 3**, 2169 (1989).

[21] W. Metzner, Phys. Rev. **B 43**, 8549 (1991).

[22] F.J. Ohkawa, J. Phys. Soc. Jpn. **60**, 3218 (1991);F.J. Ohkawa, Prog. Theor. Phys. (Suppl.) **106**, 95 (1991).

[23] A. Georges and G. Kotliar, Phys. Rev. **B 45**, 6479 (1992).

[24] A. Georges, G. Kotliar, W. Krauth, and M. J. Rozenberg, Rev. Mod. Phys. **68(1)**:13–125 (January 1996).

[25] A. Khurana, Phys. Rev. Lett. **64**, (1990).

[26] V. Zlatić and B. Horvatić, Solid State Commun. **75**, 263 (1990).

[27] Y. Nagaoka, Phys. Rev. **147**, 392 (1966).

[28] B. S. Shastry, H. R. Krishnamurthy, and P. W. Anderson, Phys. Rev. **B 41**, 2375 (1990).

[29] P. W. Anderson, Science **235**, 1196 (1987); The Theory of Superconductivity , Princeton University Press, Princeton, NJ,1997; arXiv:0709.0656 (unpublished).

[30] P. W. Anderson, P. A. Casey, Phys. Rev. **B 80**, 094508 (2009).

[31] M. R. Norman, D. Pines, C. Kallin, Advances in Physics, **Vol. 54**, No. 8 (2005).

[32] C. Varma, Nature **468**, 184-185 (2010).

[33] A. Shekhter et al., Nature **498**, 75-77 (2013).

[34] D. Hansen, E. Perepelitsky, and B. S. Shastry Phys. Rev. **B 83**, 205134 (2011).

[35] Aficionados will recognize this as the case for the virial expansion in statistical mechanics, where a low density expansion can often be found for very strongly interacting systems. The critical density (where a phase transition occurs) is a natural boundary for such an expansion. If one knows a priori, that there is no critical density in a given problem such the Anderson model, then this expansion can be pushed to arbitrarily high densities. In the very different context of the theory of integrable systems in 1-dimension, this is precisely the reason why the *asymptotic Bethe Ansatz* works very well, even yielding exact results in regimes where its validity seems *a-priori* only approx-

imate, as explained in Bill Sutherland, *Beautiful Models*, World Scientific Publishing Company, Singapore (2004).

[36] P. W. Anderson, Phys. Rev. **124**, 41 (1961).

[37] P. W. Anderson, Phys. Rev. **164**, 352 (1967); P. W. Anderson and G. Yuval, Phys. Rev. Lett. **23**, 89 (1969).

[38] F. D. M. Haldane, Phys. Rev. Letts. **40**, 416 (1978).

[39] K. G. Wilson, Rev. Mod. Phys. **47**, 773 (1975).

[40] H. R. Krishnamurthy, K. Wilson and J. Wilkins, Phys. Rev. **B 21**, 1003, 1044 (1980).

[41] A.C. Hewson, A. Oguri, and D. Meyer, Eur. Phys. J. **B. 40**, 177 (2004); K. Edwards, A. C. Hewson, and V. Pandis, Phys. Rev. **B 87**, 165128 (2013).

[42] D. E. Logan, M. P. Eastwood and M. A. Tusch, J. Phys. Condens. Matter **10**, 2673 (1998)., M. T. Glossop and D. E. Logan J. Phys.: Condens. Matter **14** 6737, (2002).

[43] N. Bickers, Rev. Mod. Phys. **59**, 845939 (1987).

[44] N. Read and D. M. Newns J. Phys. **C 16**, L1055 (1983); doi:10.1088/0022-3719/16/29/007; N. Read, J. Phys. **C 18**, 2651 (1985).

[45] P. Coleman, Phys. Rev. **B 29**, 3035 (1984); S. E. Barnes, J. Phys. **F 6** 1375 (1976).

[46] N. Andrei, Phys. Rev. Lett. **45**, 379 (1980); P.B. Wiegmann, Sov. Phys. JETP Lett. **31**, 392 (1980).

[47] A. C. Hewson, *The Kondo Problem to Heavy Fermions*, Cambridge University Press, Cambridge (1993).

[48] K. Yosida and K. Yamada, Prog. Theor. Phys. Suppl. **46**, 244 (1970).

[49] P. Nozières, J. Low. Temp. Phys. **17**, 31 (1974).

[50] A. C. Hewson, Phys. Rev. Letts. **70**, 4007 (1993).

[51] H. O. Frota and L. N. Olivera, Phys. Rev. **B 33**, 7871 (1986).

[52] O. Sakai, Y. Shimuzu and T. Kasuya, J. Phys. Soc. Japan, **58**, 162 (1989).

[53] T. A. Costi and A. C. Hewson, J.. Phys. Cond. Matter, **L 361** (1993).

[54] T. A. Costi, J. Kroha, and P. Wölfle, Phys. Rev. **B 53**, 1850 (1996). We thank the authors for providing us with the digital versions of their results.

[55] In the notation of Ref. ([3]) Eq. (58), this corresponds to writing $Y_1(\tau_i, \tau_f) = -\gamma(\tau_i).\ \Delta(\tau_i, \tau_f)$.

[56] J. Friedel, Can. Jour. Phys. **54**, 1190 (1956)

[57] J. S. Langer and V. Ambegaokar, Phys. Rev. **164**, 498 (1961).

[58] D. C. Langreth, Phys. Rev. **150**, 516 (1966).

[59] J. M. Luttinger and J. C. Ward, Phys. Rev. **118**, 1417 (1960).

[60] J. W. Rasul and A. C. Hewson, J. Phys. C: Solid State Phys. **17**, 3337 (1984).

[61] To recover Eq. (6.42), we may use Eq. (6.21) and the Fermi liquid assumption of $\Im m\ \Sigma_{DM}(0) = 0$ so that $\rho_{\mathcal{G}}(0) = \frac{1}{\pi}\frac{\Gamma_0(1-\frac{n_d}{2})^2}{\Gamma_0^2(1-\frac{n_d}{2})^2+(\epsilon_d+\Re e\Sigma_{DM}(0))^2}$, and combine with Eq. (6.41).

[62] P. Nozières, Theory of Interacting Fermi Systems (W. A. Benjamin, Amsterdam, 1964).

[63] Phase Transitions and Critical Phenomena, edited by C. Domb and M. S. Green (Academic, London, 1974), Vol. 3.

[64] Exact high temperature series expansions for the XY model, Canadian Journal of Physics, **48**, 1566 (1970).

[65] M. Plischke, J. Stat. Phys. **11**, 159 (1974).

[66] K. Kubo and M. Tada, Progr. Theor. Phys. **69**, 1345 (1983); **71**, 479 (1984).

[67] Lorenzo De Leo, Jean-Sbastien Bernier, Corinna Kollath, Antoine Georges, and Vito W. Scarola, Phys. Rev. **A 83**, 023606 (2011).

[68] Stephane Pairault, David Senechal, A.-M. S. Tremblay, Eur. Phys. J. **B 16**, 85 (2000).

[69] "Linked-Cluster Expansion of the Greens function of the infinite-U Hubbard Model", E. Khatami, E. Perepelitsky, M. Rigol, and B. S. Shastry, arXiv:1310.8029 (2013).

[70] "A study of the phase transitions of the infinite-U Hubbard Model", E. Khatami, E. Perepelitsky, M. Rigol, and B. S. Shastry, to be published (2014).

[71] P. Coleman, Phys. Rev. **B 28**, 5255 (1983).

[72] G. Kotliar and J. Liu, Phys. Rev. **B 38**, 5142 (1988).

[73] Diagrams in the paper created through the use of "JaxoDraw", D. Binosi, L. Theußl, Computer Physics Communications, **Volume 161**, Issues 1-2, 1 August 2004, Pages 76-86